A COMPARISON OF THE NEAL-SMITH AND $\omega_{sp} T_{\theta_2}$, ζ_{sp}, τ_θ FLYING QUALITIES CRITERIA

THESIS

Brian Andrew Kish
First Lieutenant, USAF

AFIT/GAE/ENY/94D-11

DEPARTMENT OF THE AIR FORCE
AIR UNIVERSITY
AIR FORCE INSTITUTE OF TECHNOLOGY

Wright-Patterson Air Force Base, Ohio

AFIT/GAE/ENY/94D-11

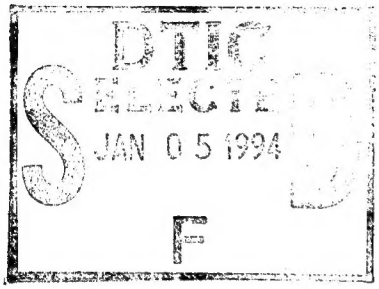

A COMPARISON OF THE NEAL-SMITH AND $\omega_{sp}T_{\theta_2}, \zeta_{sp}, \tau_\theta$ FLYING QUALITIES CRITERIA

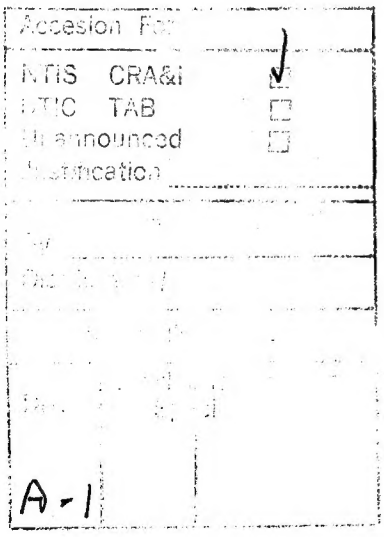

THESIS
Brian Andrew Kish
First Lieutenant, USAF

AFIT/GAE/ENY/94D-11

Approved for public release; distribution unlimited

AFIT/GAE/ENY/94D-11

A COMPARISON OF THE NEAL-SMITH AND $\omega_{sp}T_{\theta_2}, \zeta_{sp}, \tau_\theta$ FLYING QUALITIES CRITERIA

THESIS

Presented to the Faculty of the School of Engineering
of the Air Force Institute of Technology
Air Education and Training Command
In Partial Fulfillment of the
Requirements for the Degree of
Master of Science in Aeronautical Engineering

Brian Andrew Kish, B.S.
First Lieutenant, USAF

December, 1994

Acknowledgements

There have been many people who have influenced the completion of this work. While I cannot possibly thank everyone who has guided me, I would like to acknowledge some people who had a direct impact.

First and foremost, I want to thank Dr. Brian Jones who challenged me with this handling qualities problem. It was only with his insight and guidance throughout this endeavor that I was able to complete my research. In addition, his career counselling has helped me set new goals for my future.

I want to thank Mr. David Leggett and Mr. David Doman from the Flight Dynamics Lab for their explanation of the original Neal-Smith criteria. I also want to thank Dr. Brad Liebst who taught my handling qualities class and continually provided sources. Capt Richard Cobb helped me with special software to enhance the many plots shown in this thesis.

Most importantly, I could not have completed this thesis without the support and understanding of my loving wife Georgetta. She is the person who has sacrificed the most during the past 18 months, and I know that I will never be able to make up for it.

Brian Andrew Kish

Table of Contents

REPORT DOCUMENTATION PAGE

Form Approved
OMB No. 0704-0188

1. AGENCY USE ONLY (Leave blank)	2. REPORT DATE	3. REPORT TYPE AND DATES COVERED
	December 1994	Master's Thesis

4. TITLE AND SUBTITLE

A COMPARISON OF THE NEAL-SMITH AND $\omega_{sp}T_{\theta_2}, \zeta_{sp}, \tau_\theta$ FLYING QUALITIES CRITERIA

5. FUNDING NUMBERS

6. AUTHOR(S)

Brian Andrew Kish
1Lt, USAF

7. PERFORMING ORGANIZATION NAME(S) AND ADDRESS(ES)

Air Force Institute of Technology
Wright-Patterson AFB OH 45433-6583

8. PERFORMING ORGANIZATION REPORT NUMBER

AFIT/GAE/ENY/94D-11

9. SPONSORING / MONITORING AGENCY NAME(S) AND ADDRESS(ES)

D. Leggett
Flight Dynamics Directorate
Wright Laboratory
Wright Patterson AFB, OH 45433-7562

10. SPONSORING / MONITORING AGENCY REPORT NUMBER

11. SUPPLEMENTARY NOTES

12a. DISTRIBUTION / AVAILABILITY STATEMENT

Approved for public release; distribution unlimited

12b. DISTRIBUTION CODE

13. ABSTRACT *(Maximum 200 words)*

Aircraft pitch response is a vital element of piloted vehicle flying qualities. There has been controversy over both the form and the substance of the requirements for short-term pitch response. Currently, MIL-STD-1797A offers six different methods for evaluating short-term pitch response. These six methods often give conflicting results. Two methods are analyzed in this thesis – the Neal-Smith criteria and the $\omega_{sp}T_{\theta_2}, \zeta_{sp}, \tau_\theta$ criteria. Domains from both criteria are mapped into each other identifying regions of conflict and regions of agreement. Parametric studies are performed and evaluated for trends. Further, a real-time analysis tool for evaluating these methods is developed.

14. SUBJECT TERMS

Handling Qualities, Pilot Models,
Flying Qualities, Control Theory

15. NUMBER OF PAGES

145

16. PRICE CODE

17. SECURITY CLASSIFICATION OF REPORT	18. SECURITY CLASSIFICATION OF THIS PAGE	19. SECURITY CLASSIFICATION OF ABSTRACT	20. LIMITATION OF ABSTRACT
UNCLASSIFIED	UNCLASSIFIED	UNCLASSIFIED	UL

List of Figures

List of Tables

List of Symbols

Abstract

Aircraft pitch response is a vital element of piloted vehicle flying qualities. There has been controversy over both the form and the substance of the requirements for short-term pitch response. Currently, MIL-STD-1797A offers six different methods for evaluating short-term pitch response. These six methods often give conflicting results. Two methods are analyzed in this thesis – the Neal-Smith criteria and the $\omega_{sp}T_{\theta_2}, \zeta_{sp}, \tau_\theta$ criteria. Domains from both criteria are mapped into each other identifying regions of conflict and regions of agreement. Parametric studies are performed and evaluated for trends. Further, a real-time analysis tool for evaluating these methods is developed.

A COMPARISON OF THE NEAL-SMITH AND $\omega_{sp}T_{\theta_2}, \zeta_{sp}, \tau_\theta$ FLYING QUALITIES CRITERIA

I. Introduction

The short-term pitch response of an aircraft is a vital element of flying qualities (4:171). MIL-STD-1797A, *Flying Qualities of Piloted Aircraft*, offers six different methods for evaluating short-term pitch response. There are strengths and weaknesses for each method depending on aircraft classification and flight phase. All six methods have been maintained because the short-term pitch response characteristics are universally regarded to be extremely important– so important that controversy over both the form and the substance of requirements still exists (4:171). MIL-STD-1797A provides a large amount of guidance for determining the appropriate method. Still, one must decide which of the six methods to include in a specification. The simple answer of including all six leads to conflicting results.

Two methods are analyzed in this thesis — the $\omega_{sp}T_{\theta_2}, \zeta_{sp}, \tau_\theta$ criteria and the Neal-Smith Criteria. The $\omega_{sp}T_{\theta_2}, \zeta_{sp}, \tau_\theta$ criteria provides a relatively simple way to predict flying qualities. When the airplane data from (1) is used, the criteria has a confidence level of about 82 percent (4:206). Still, the $\omega_{sp}T_{\theta_2}, \zeta_{sp}, \tau_\theta$ criteria only deals with the aircraft as an open-loop system. A modified version of the Neal-Smith criteria uses a mathematical model of the pilot to determine the pilot-vehicle *system* response. This closed-loop criteria is known as the Pilot-in-the-Loop criteria. The original Neal-Smith criteria is more restrictive than the Pilot-in-the-Loop criteria in that pilot phase contribution is taken into consideration. Other than that, the two criteria are essentially equivalent. Both will be compared to the open-loop $\omega_{sp}T_{\theta_2}, \zeta_{sp}, \tau_\theta$ criteria.

One method for comparing the $\omega_{sp}T_{\theta_2}, \zeta_{sp}, \tau_\theta$ and Neal-Smith criteria is to map one criteria into the domain of the other criteria. This identifies regions of conflict and regions

of agreement. Ultimately, flight testing of various points from the regions of conflict could determine whether a criteria needs to be modified. The answer may be to combine the criteria somehow to form a new criteria. The motivation for this type of research comes directly from MIL-STD-1797A:

> The large amount of this guidance reflects the importance of short-term pitch response, the high attention it has been given, and the great need for further study to derive a clear-cut, generally applicable set of requirements. (4:172)

1.1 Background

Flying qualities is that discipline in aeronautical engineering that is concerned with basic aircraft stability and pilot-in-the-loop controllability. 'Flying qualities,' 'stability and control,' and 'handling qualities' are three terms which are generally considered synonymous (13). To prevent confusion, the following definitions will be used. Both the US Air Force and Navy agree that "*flying qualities* are those stability and control characteristics which influence the ease of safely flying an aircraft during steady and maneuvering flight in the execution of the total mission" (10). Edkins defines *stability* as "...the tendency or lack of it, of an airplane to fly with wings level" and *control* as "...steering an airplane on an arbitrary flight path" (5). Cooper and Harper define *handling qualities* as "...those qualities or characteristics of an aircraft that govern the ease and precision with which a pilot is able to perform the tasks required in support of an aircraft role" (2). Figure 1.1 shows how flying qualities, stability, control, and handling qualities are related.

Stability and control analysis deals with the interaction of the aerodynamic controls with the external forces and moments on the aircraft (3). That is, stability and control analysis primarily deals with open-loop systems that are still in the design phase. On the other hand, handling qualities assessment deals with the pilot and aircraft performing as a closed-loop system. This assumes the aircraft is already built. The six methods offered by MIL-STD-1797A are used to *predict* handling qualities while the aircraft is still in the design phase. If a mathematical model is used for the pilot, a closed-loop stability and control analysis is

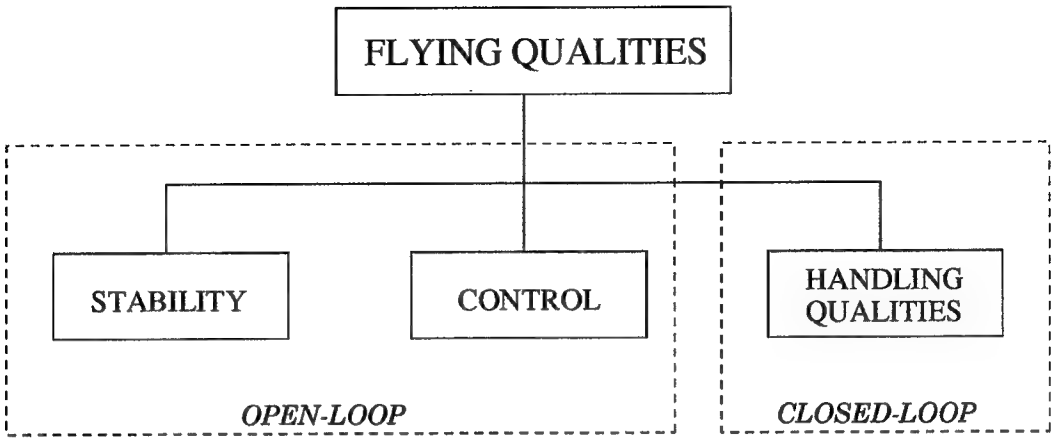

Figure 1.1 Flying Qualities Breakdown

possible (e.g. the Neal-Smith criteria). Since aircraft perform a wide variety of maneuvers and vary in size, some type of grouping is necessary before analysis can begin.

Aircraft are procured to perform defined missions. The class designation is used to help particularize the requirements according to broad categories of intended use (4:76). The intended use of an aircraft must be known before required configurations, loadings and operational flight envelopes can be defined (4:76). MIL-STD-1797A identifies four classes of aircraft as outlined in Table 1.1.

Table 1.1 Aircraft Classification

Class	*Description*	*Example*
I	small light aircraft	T-41
II	medium weight aircraft with low-to-medium maneuverability	C-21
III	large, heavy aircraft with low-to-medium maneuverability	KC-10
IV	highly maneuverable aircraft	F-16

This research examines two different aircraft. The first is Calspan Corporation's variable stability Lear jet 24 (Fig. 1.2). The second is the Variable Stability In-flight Simulator (VISTA) which uses the F-16D as its host aircraft (Fig. 1.3). The Lear jet can be considered a Class II aircraft. The F-16 VISTA can be considered a Class IV aircraft. Using variable stability

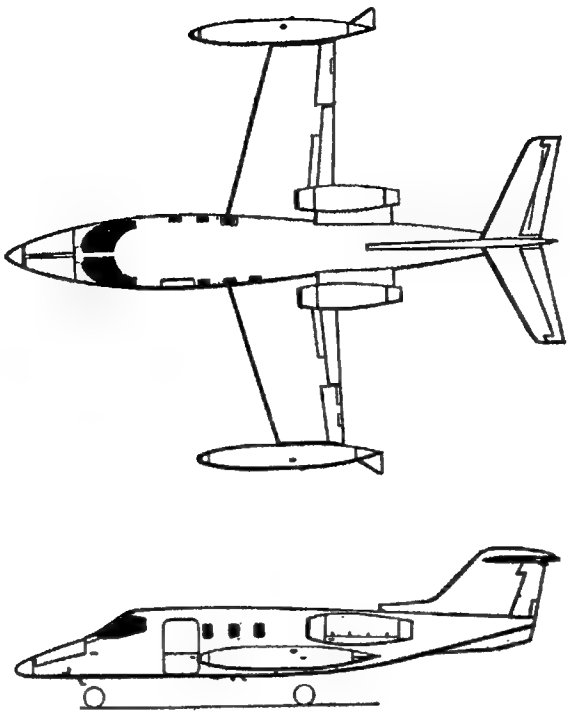

Figure 1.2 Picture of Lear jet (14)

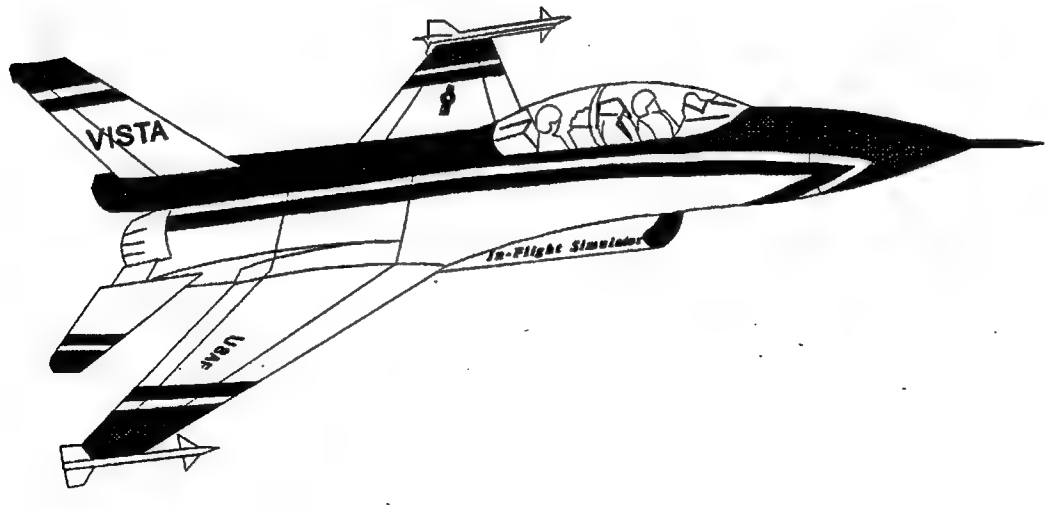

Figure 1.3 Picture of F-16 VISTA (17)

aircraft makes it possible to flight test the analytic results of this thesis in the future. The cockpit environment can be changed to match that of another aircraft. Since an actual aircraft is being flown, it provides a degree of realism not present in ground simulation. As the pilot moves the controls, he or she experiences the real flight motions, accelerations, and handling qualities of the simulated aircraft. This realism gives the pilot a higher level of confidence when determining a handling qualities level.

In this thesis, a mapping will be provided that will show regions of agreement and regions of conflict for two different methods used to predict handling qualities. Since every point in a region represents a different aircraft transfer function, a variable stability aircraft can be configured to one of these transfer functions. Table 1.2 shows the operating envelopes of some parameters for the F-16 VISTA (18). A point in the region of conflict could be 'dialed in' to the flight control system. A test pilot could then fly the simulated aircraft and determine what the real handling qualities level is. If enough cases are flight tested and the results show a trend, a decision could be made on whether one of the methods used to predict handling qualities needs to be modified or eliminated. This thesis lays the foundation for this type of future analysis.

Table 1.2 Operating Envelopes for the F-16 VISTA

Parameter	*Range*
Short Period Natural Frequency	0 to 12 rad/sec
Short Period Damping	-0.1 to 1.1
Aircraft Time Delay	0.01 to 0.5 sec

Experience with aircraft operations indicates that certain flight phases require more stringent values of flying qualities parameters (4:80). A given flight phase can have an aircraft normal state associated with it. For example, the flaps and gear are down for landing approaches and up for cruising flight. MIL-STD-1797A defines three categories of flight phases as outlined in Table 1.3.

Table 1.3 Flight Phase Categories

Category	*Description*	*Example*
A	nonterminal flight phases that require rapid maneuvering, precision tracking, or precise flight-path control	air-to-air combat
B	nonterminal flight phases that require gradual maneuvering without precision tracking	climb
C	terminal flight phases that require gradual maneuvering with accurate flight-path control	landing

This research only examines the Category C flight phase. However, the approach derived in Chapter III can handle any flight phase category. With aircraft classification and flight phase known, handling qualities levels can now be addressed.

MIL-STD-1797A defines three levels of handling qualities which are outlined in Table 1.4 (4:85). These definitions are based on the Cooper-Harper (2) rating scale shown in Fig. 1.4.

Table 1.4 Handling Qualities Levels

Level	*Meaning*	*Description*
1	satisfactory	Flying qualities clearly adequate for the mission flight phase. Desired performance is achievable with no more than minimal pilot compensation.
2	acceptable	Flying qualities adequate to accomplish the mission flight phase, but some increase in pilot workload and/or degradation in mission effectiveness exists.
3	controllable	Flying qualities are such that the aircraft can be controlled in the context of the mission flight phase, even though pilot workload is excessive and/or mission effectiveness is inadequate.

It is not uncommon to have feedback control systems of twentieth order or more. Writing a specification for such a system presents a problem. Considerable research has been devoted to reducing the order of these high-order feedback control systems by matching frequency

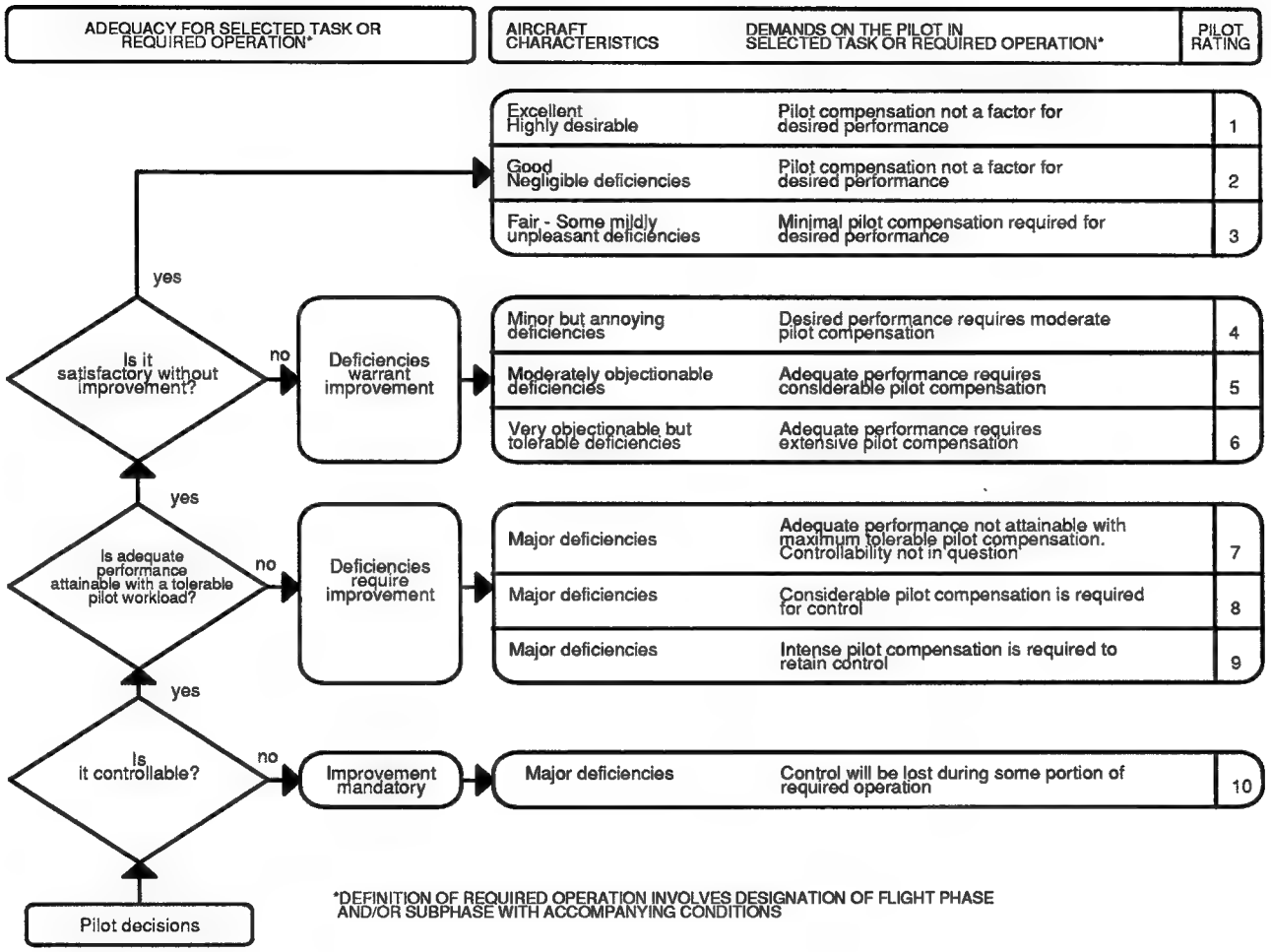

Figure 1.4 Cooper-Harper Scale

responses to obtain lower-order equivalent systems (4:175). Using lower-order equivalent systems allows the application of well-established boundaries generated by classical airplane data to be extended to many high order systems (4:175). With respect to pitch axis control requirements, boundaries have been established on the classical modal parameters in Eq. (1.1).

$$\frac{\theta(s)}{\delta(s)} = \frac{K_\theta \left(T_{\theta_1} \cdot s + 1\right)\left(T_{\theta_2} \cdot s + 1\right) e^{-\tau_\theta \cdot s}}{\left(s^2 + 2\zeta_p \omega_p \cdot s + \omega_p^2\right)\left(s^2 + 2\zeta_{sp} \omega_{sp} \cdot s + \omega_{sp}^2\right)} \tag{1.1}$$

where,

K_θ = aircraft gain
T_{θ_1} = low-frequency pitch attitude zero
T_{θ_2} = high-frequency pitch attitude zero
τ_θ = aircraft time delay
ζ_p = damping ratio of the phugoid mode
ω_p = undamped natural frequency of the phugoid mode
ζ_{sp} = damping ratio of the short period mode
ω_{sp} = undamped natural frequency of the short period mode
s = Laplace variable

Equation (1.1) is a linearized, reduced-order model of the actual aircraft response. The flight control system is also embedded in Eq. (1.1). In most cases, the phugoid and short-period modes are sufficiently separated that further order reduction is possible. Equation (1.2), universally recognized as the pitch model of short-period dynamics, may normally be used in place of Eq. (1.1) (4:175).

$$\frac{\theta(s)}{\delta(s)} = \frac{K_\theta (T_{\theta_2} \cdot s + 1) e^{-\tau_\theta \cdot s}}{s\left(s^2 + 2\zeta_{sp} \omega_{sp} \cdot s + \omega_{sp}^2\right)} \tag{1.2}$$

For example, the following pitch transfer function is for an A-4 aircraft with a feel system and actuators flying at Mach 0.85 (6:9).

$$\frac{\theta(s)}{\delta(s)} = \frac{1.07745 \cdot 10^4 (s + 2.085)(s + 0.0287)}{(s^2 + 36.4s + 676)(s^2 + 6.39s + 54.02)(s^2 + 0.00313s + 0.00484)} \tag{1.3}$$

Equation (1.4) is the short-period approximation of Eq. (1.3).

$$\frac{\theta(s)}{\delta(s)} = \frac{16.26(s+2.085)e^{-0.09471 \cdot s}}{s(s^2+6.98s+51.29)} \tag{1.4}$$

Figure 1.5 compares Bode plots of the original higher order system to the short-period approximation. For this example, the short-period approximation describes the aircraft pitch response fairly well for the frequency range given. Both the $\omega_{sp}T_{\theta_2}, \zeta_{sp}, \tau_\theta$ and Neal-Smith criteria are only valid for frequencies up to 10 radians per second (4:190,237).

1.2 Objectives

The overall goal of this thesis is to compare the $\omega_{sp}T_{\theta_2}, \zeta_{sp}, \tau_\theta$ and Neal-Smith criteria. The following objectives are needed to accomplish this goal. First, a computer program that calculates the pilot model parameters for the Neal-Smith criteria needs to be developed. Second, a computer program that maps areas from the $\omega_{sp}T_{\theta_2}, \zeta_{sp}, \tau_\theta$ criteria into the Neal-Smith criteria needs to be developed. Third, regions of agreement and regions of conflict need to be identified on the Neal-Smith criteria. Forth, a computer program that maps these regions back into the $\omega_{sp}T_{\theta_2}, \zeta_{sp}, \tau_\theta$ criteria needs to be developed. Finally, a parametric study to identify trends needs to be performed.

1.3 Assumptions

The first assumption is the aircraft transfer function for pitch control can be modeled by a short-period approximation which includes the flight control system. This assumption is only needed when the $\omega_{sp}T_{\theta_2}, \zeta_{sp}, \tau_\theta$ criteria is mapped into the Neal-Smith criteria. The algorithm developed in Chapter III for determining the Neal-Smith criteria can handle any aircraft transfer function.

The second assumption is the pilot can be modeled by a variable gain, a constant time delay, and a variable first-order compensation network. This assumption is needed for the Neal-Smith criteria.

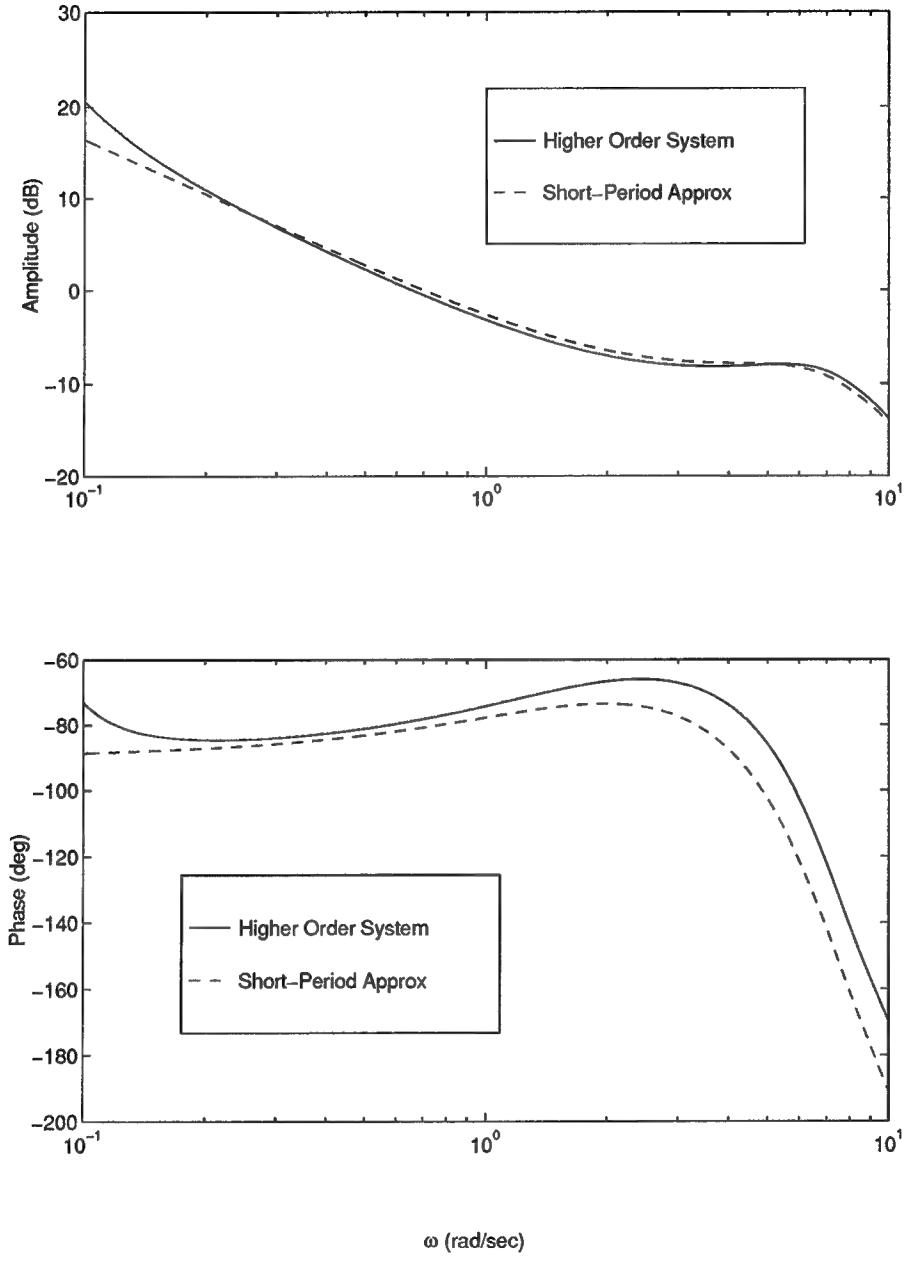

Figure 1.5 Bode Magnitude and Phase Plots for the A-4 Aircraft

1.4 General Approach

The $\omega_{sp}T_{\theta_2}, \zeta_{sp}, \tau_\theta$ criteria involves four parameters. Holding T_{θ_2} and τ_θ fixed while varying ω_{sp} and ζ_{sp} forms a two-dimensional region that can be mapped into the Neal-Smith criteria. For example, the region might be all points corresponding to level 1 handling qualities. The actual values of all four parameters completely define the aircraft transfer function. The remainder of the problem involves solving for the parameters of the pilot transfer function.

The assumed pilot transfer function has three unknowns. The resulting equations are complicated functions of frequency with no closed-form solution. The solution is found by posing the problem as a constrained optimization problem. Once all three unknowns are determined, the mapping of the original point used to define the aircraft transfer function can be accomplished. The procedure is repeated for any point contained by the two-dimensional region described above. Ultimately, a grid of points representing the region will be mapped.

The inverse mapping would be even more difficult. A point from the Neal-Smith criteria represents the pilot-aircraft system in the form of *one* transfer function. The individual pilot and aircraft parameters are not easily distinguished. Rather than trying to accomplish this for a grid of points, bookkeeping of the original mapping is used. When a point from the $\omega_{sp}T_{\theta_2}, \zeta_{sp}, \tau_\theta$ criteria is mapped into the Neal-Smith criteria, information on the Neal-Smith handling qualities level is stored and identified with that point. After the entire grid is mapped, every point from $\omega_{sp}T_{\theta_2}, \zeta_{sp}, \tau_\theta$ is assigned a handling qualities level from the Neal-Smith criteria. The same method can be applied to the Pilot-in-the-Loop criteria.

1.5 Sequence of Presentation

Chapter II contains an in-depth look at the $\omega_{sp}T_{\theta_2}, \zeta_{sp}, \tau_\theta$, Neal-Smith and Pilot-in-the-Loop criteria. Chapter III contains a detailed description of the approach used to perform the mappings. Chapter IV contains the results of the mappings of the Category C flight phase of the Class II and Class IV aircraft. Chapter V contains conclusions and recommendations for future research.

II. Pitch Response Criteria

2.1 The $\omega_{sp}T_{\theta_2}, \zeta_{sp}, \tau_\theta$ Criteria

Physically, $\omega_{sp}T_{\theta_2}$ represents the lag in phase (at ω_{sp}) or time between aircraft responses in pitch attitude and path. If T_{θ_2} is too small with respect to ω_{sp}, the path and attitude response may not be separated enough to give a pilot the additional cues he or she needs to control the slower path loop (4:192). $\omega_{sp}T_{\theta_2}$, in combination with ζ_{sp}, defines the shape of the attitude frequency response (4:192). If the aircraft transfer function in Eq. (1.2) is known, the handling qualities level can be read directly from Fig. 2.1 for a Category C flight phase. There is no upper limit placed on $\omega_{sp}T_{\theta_2}$. However, MIL-STD-1797A only plots $\omega_{sp}T_{\theta_2}$ up to ten. Therefore, the highest value of $\omega_{sp}T_{\theta_2}$ in this thesis is ten.

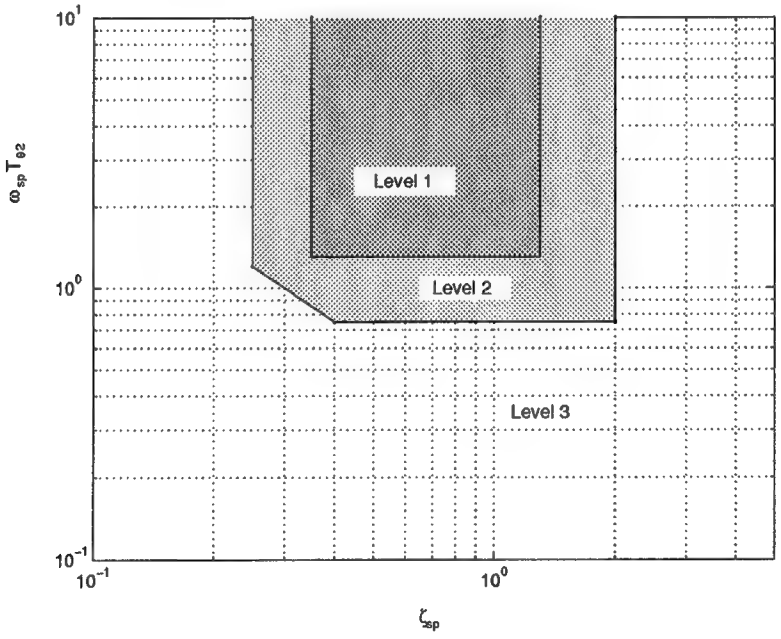

Figure 2.1 Handling Qualities Boundaries for the $\omega_{sp}T_{\theta_2}, \zeta_{sp}, \tau_\theta$ criteria

Table 2.1 Limits on τ_θ

LEVEL	$\tau_{\theta_{max}}$ (seconds)
1	0.10
2	0.20
3	0.30

Table 2.2 Minimum Values for ω_{sp} and Maximum values for T_{θ_2}

LEVEL	*CLASS*	$(\omega_{sp})_{min}$	$(T_{\theta_2})_{max}$
1	I, IV	0.87	2.63
	II, III	3.57	0.28
2	I, IV	0.60	4.17
	II, III	7.14	0.14

2.1.1 Maximum Values for τ_θ. In addition to satisfying the boundaries in Fig. 2.1, the aircraft equivalent time delay (τ_θ) must not be more than a certain value. MIL-STD-1797A maximum values for τ_θ with respect to handling qualities level are listed in Table 2.1.

2.1.2 Minimum Values for ω_{sp} and Maximum values for T_{θ_2}. MIL-STD-1797A places limits on ω_{sp} and T_{θ_2} as outlined in Table 2.2. These limits are dependent on aircraft classification as well as handling qualities level. Normal acceleration response to attitude changes is a primary factor affecting the pilot's perception of the minimum allowable ω_{sp} (4:192). The maximum values for T_{θ_2} are based on an approach speed of 135 kt (4:206).

2.2 *The Neal-Smith Criteria*

The Neal-Smith criteria is not as straight forward as the $\omega_{sp} T_{\theta_2}, \zeta_{sp}, \tau_\theta$ criteria. The main difference is the Neal-Smith criteria uses a closed-loop system that incorporates a pilot model. Figure 2.2 shows the block diagram of the pilot-aircraft system. The system is a single-input-single-output system that uses negative unity feedback. Understanding of the following terminology is needed for the remaining sections. Y_p is the pilot transfer function. $\frac{\theta}{\delta}$ is the *open-loop* transfer function of the airplane plus control system, Y_c. Equation 1.2 will be used for this. $\frac{\theta}{\theta_c}$ is the *open-loop* transfer function of the airplane plus control system plus

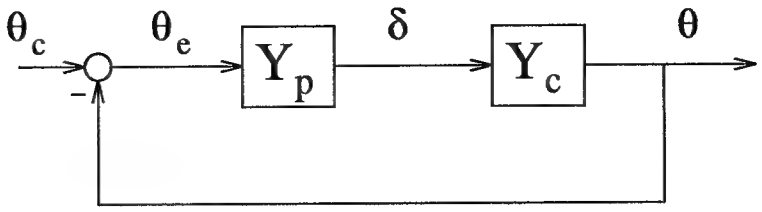

Figure 2.2 Block Diagram of the Pilot-Aircraft System used in the Neal-Smith Criteria

pilot which is given the symbol G.

$$G = Y_p Y_c \tag{2.1}$$

$\frac{\theta}{\theta_c}$ is the *closed-loop* transfer function of the airplane, control system, and pilot. Equation 2.2 represents this transfer function which is given the symbol T.

$$T = \frac{G}{1+G} \tag{2.2}$$

T is also known as the complimentary sensitivity (7). The magnitude of any transfer function will be designated $|\cdot|$, and the phase of any transfer function will be designated $\angle(\cdot)$.

2.2.1 A Pilot's View of Good Tracking Performance. What is a pilot trying to accomplish when he or she adapts to an aircraft configuration? Neal and Smith examined pilot comments and led to the following conclusion. The pilot wants to acquire the target quickly and predictably, with minimum of overshoot and oscillation (12:39). References (9) and (11) place the following mathematical relationships on pilot comments:

(1) The pilot tries to achieve a particular value of the open-loop gain crossover frequency, ω_c (the frequency at which $\left|\frac{\theta}{\theta_e}\right|$ is 0 dB).

(2) The pilot tries to minimize any closed-loop 'droop' (hold $\left|\frac{\theta}{\theta_e}\right|$ near 0 dB, for $\omega \leq \omega_c$).

(3) The pilot tries to maintain good high-frequency stability by keeping the damping ratio of any closed-loop oscillatory modes greater than 0.35, and by maintaining a phase margin of 60 to 110 degrees.

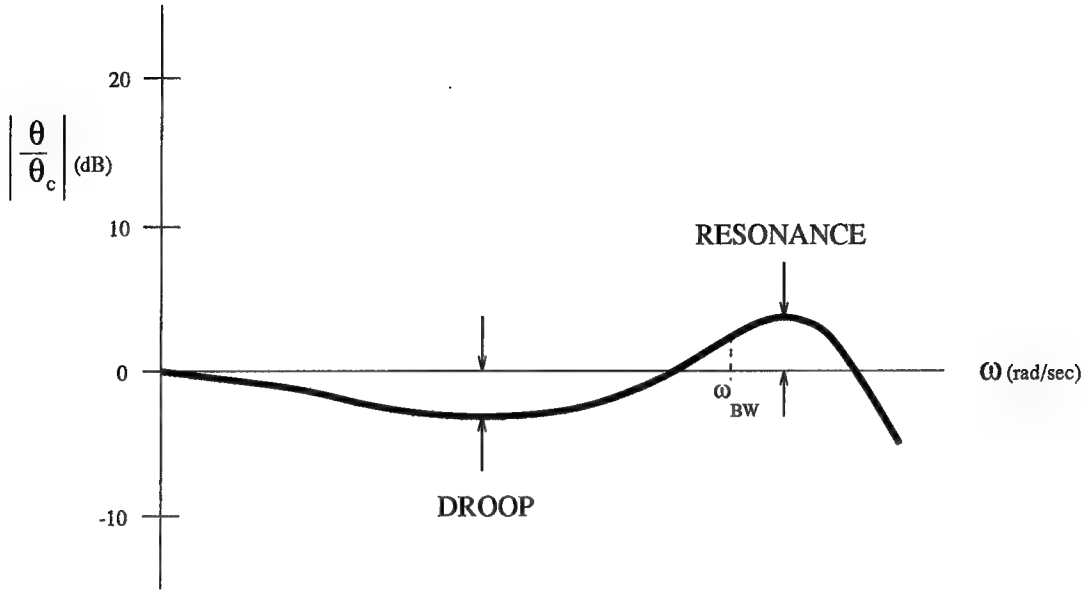

Figure 2.3 Designation of Droop and Resonance

Neal and Smith substituted another closed-loop relation in place of (1). First a closed-loop parameter similar to the crossover frequency, ω_c, needed to be defined. Neal and Smith defined a parameter called closed-loop bandwidth (ω_{BW}) to be the frequency at which the closed-loop phase ($\angle\frac{\theta}{\theta_c}$) is -90 degrees (12:41).

$$\angle\frac{\theta}{\theta_c} = -90° \quad \text{for} \quad \omega = \omega_{BW} \tag{2.3}$$

Neal and Smith determined that the pilot wants to minimize closed-loop droop for frequencies below ω_{BW}. For frequencies above ω_{BW}, the pilot wants to minimize the resonant peak (12:42). Figure 2.3 illustrates droop and resonance.

2.2.2 Tracking Performance Standards. Neal and Smith defined the minimum value for closed-loop droop to be -3 dB (12:43).

$$\left|\frac{\theta}{\theta_c}\right| \geq -3dB \quad \text{for} \quad \omega \leq \omega_{BW} \tag{2.4}$$

Figure 2.4 illustrates this constraint along with closed-loop bandwidth.

Another way to look at these constraints with regards to open-loop information is via a Nichol's chart. A Nichol's chart shows closed-loop boundaries overlaid on a plot of open-loop magnitude versus open-loop phase. Figure 2.5 illustrates the closed-loop bandwidth and droop requirements on a Nichol's Chart. Also shown on Fig. (2.5) are the upper boundaries according to MIL-STD-1797A. These upper boundaries will be discussed further in the section on the Pilot-in-the-Loop criteria. So far, only the aircraft transfer function has been discussed. The pilot transfer function will be the focus of the next section.

2.2.3 The Pilot Model. Neal and Smith require the pilot transfer function, Y_p, to be

$$Y_p = \frac{K_p(T_{p_1} \cdot s + 1)e^{-\tau_p \cdot s}}{(T_{p_2} \cdot s + 1)}. \tag{2.5}$$

The pilot includes a variable gain (K_p), a constant time delay (τ_p), and a variable first-order compensation network involving the parameters T_{p_1} and T_{p_2}. Past work suggests τ_p may vary with airplane dynamics and will usually lie between 0.2 and 0.4 seconds (12:38). Neal and Smith assumed τ_p to be fixed at 0.3 seconds (12:38).

$$\tau_p = 0.3 \quad (seconds) \tag{2.6}$$

This assumption will be used for this thesis. The remaining parameters K_p, T_{p_1}, and T_{p_2} will need to be solved. So far, no guidelines or criteria have been given for resonance limits. The closed-loop droop must be greater than -3 dB and the closed-loop phase must be $-90°$ when $\omega = \omega_{BW}$. The next section will examine closed-loop resonance and pilot phase contribution.

2.2.4 Neal-Smith Boundaries for Handling Qualities. Neal and Smith examined a great deal of pilot comments and grouped the comments as a function of closed-loop and open-loop parameters. Figure 2.6 is the result of this examination (12:94). Closed-loop

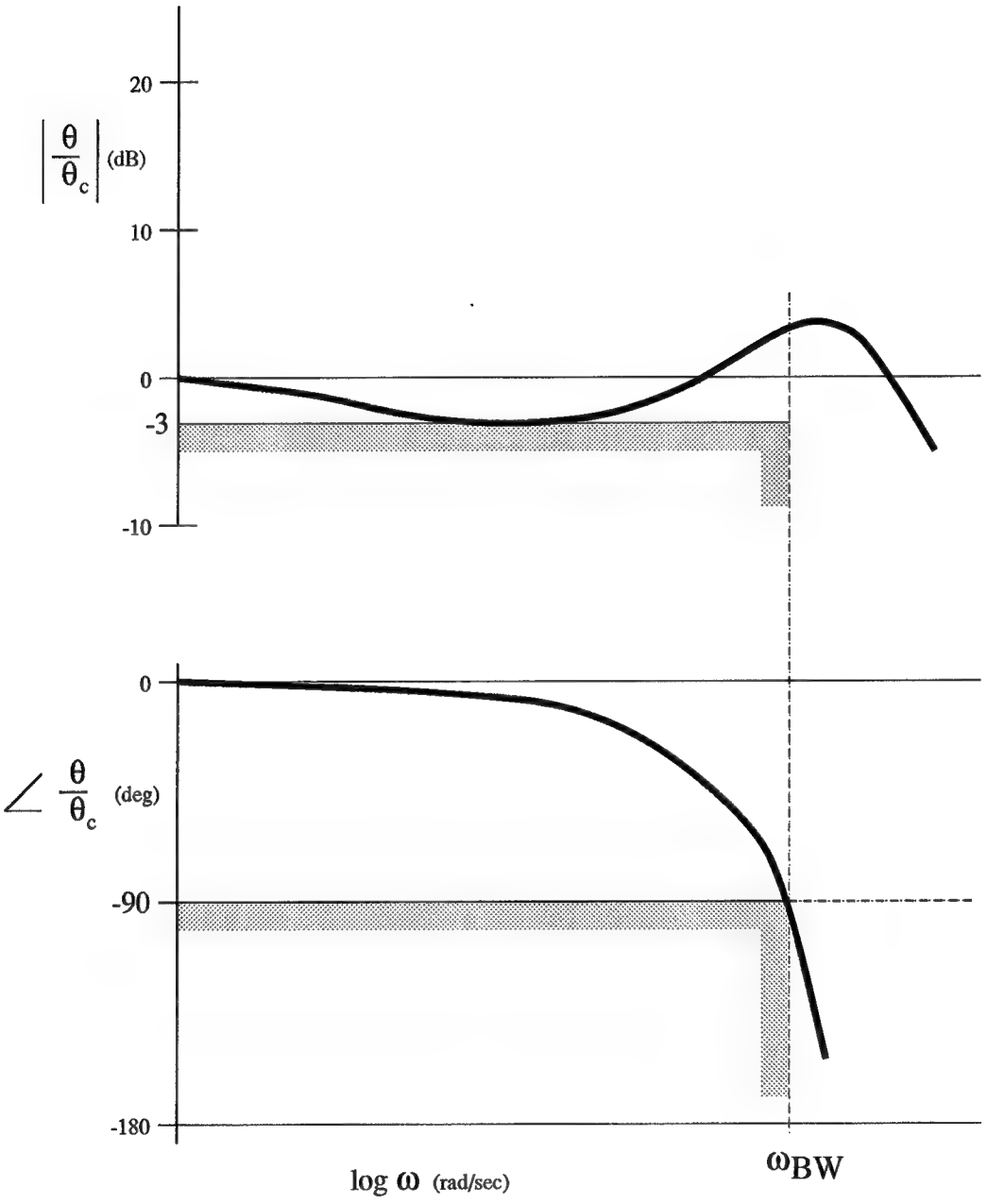

Figure 2.4 Neal-Smith Tracking Performance Standards

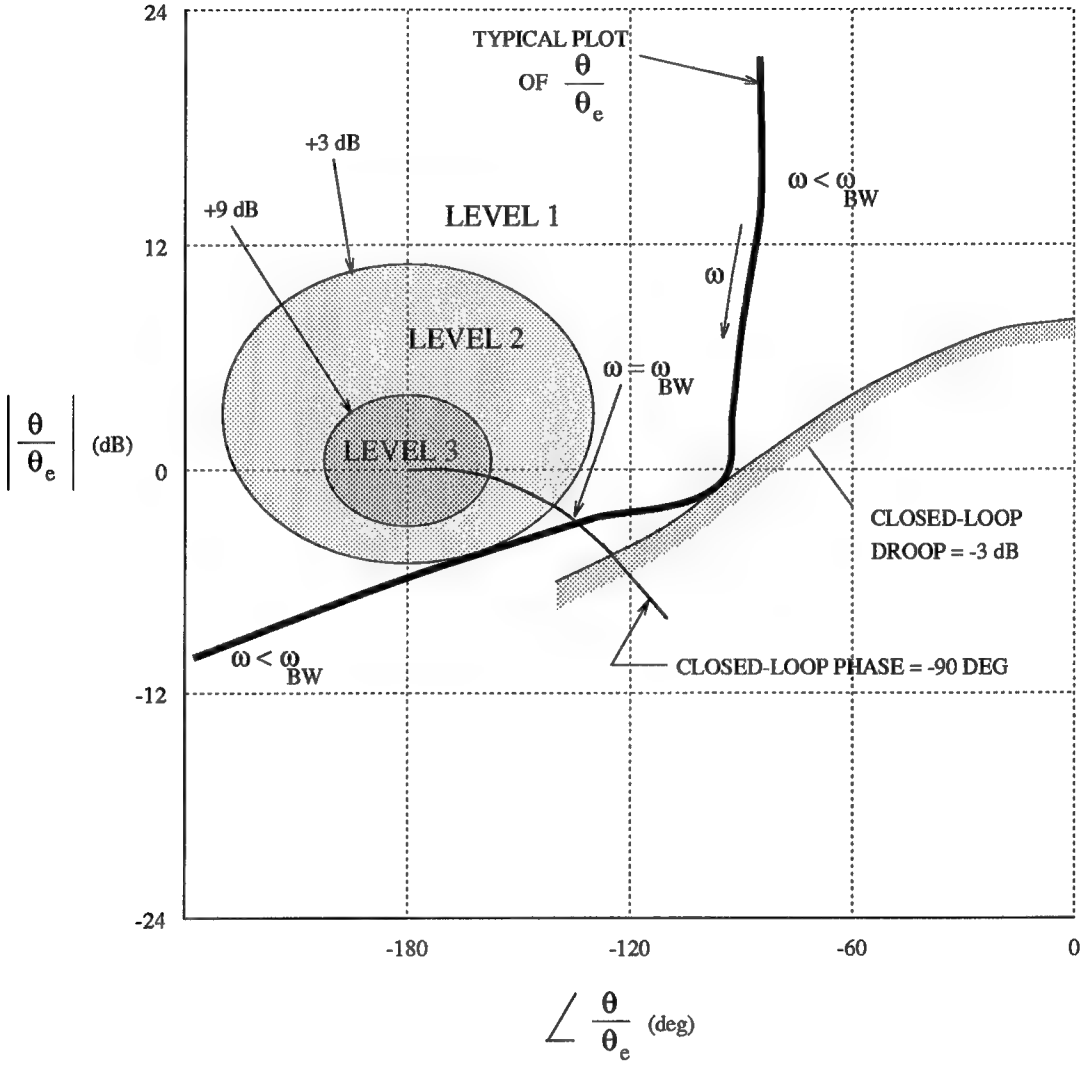

Figure 2.5 Nichol's Chart with MIL-STD-1797A Boundaries

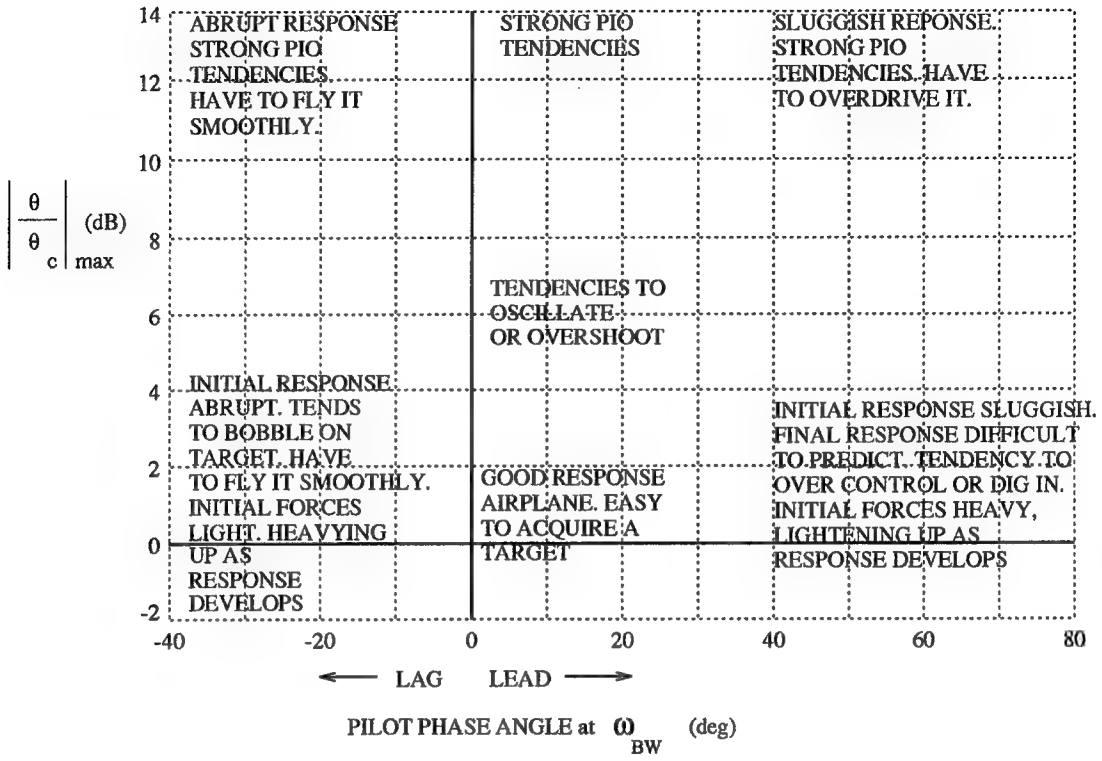

Figure 2.6 Summary of Pilot Comments

resonance is plotted against the pilot phase angle, which is defined as

$$\text{Pilot Phase Angle} = \angle\left(\frac{j\omega \cdot T_{p_1} + 1}{j\omega \cdot T_{p_2} + 1}\right)_{\omega=\omega_{BW}} . \tag{2.7}$$

From Fig. 2.6, Neal and Smith proposed the boundaries shown in Fig. 2.7. These boundaries, along with closed-loop droop and bandwidth, will serve as the design criteria when solving for K_p, T_{p_1}, and T_{p_2}. A unique solution is desired for mapping. The remainder of Chapter II and the beginning of Chapter III will show how to reduce this three-degree-of-freedom problem into a one-dimensional search.

2.2.5 Lead Compensation. The reader is referred to (7) for additional information on various forms of compensation. The following transfer function can be used to explain

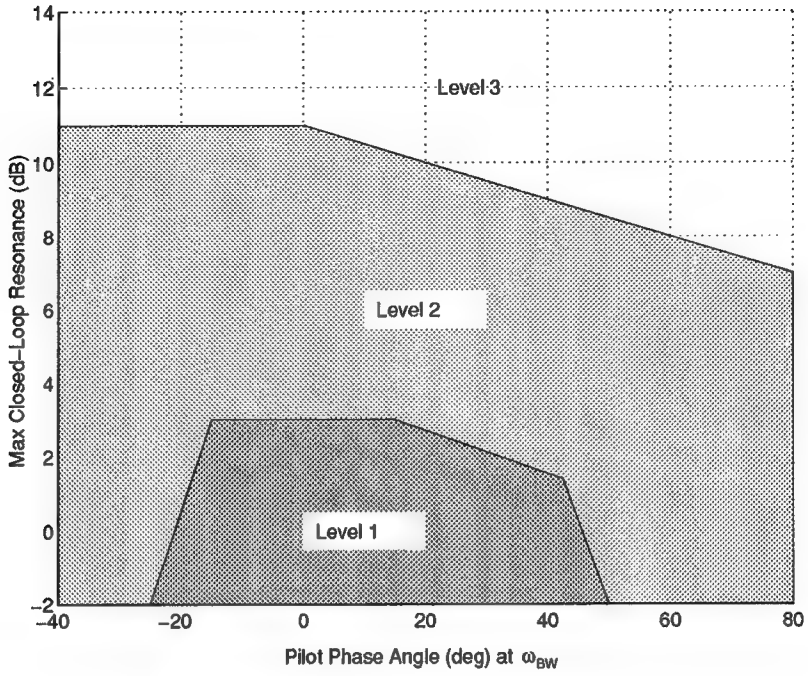

Figure 2.7 Neal-Smith Boundaries

both lead and lag compensation.

$$D(s) = \frac{K_\alpha(T_d \cdot s + 1)}{(\alpha T_d \cdot s + 1)} \tag{2.8}$$

For lead compensation, $\alpha < 1$. Equation (2.8) is similar to the variable first order compensation network used for the pilot model in Eq. (2.5). Lead compensation adds phase to the system at frequencies above the breakpoint $1/T_d$. At the same time, the magnitude of the compensation continues to grow with frequency. For nonzero α, the magnitude of the compensation levels off at frequencies above $1/\alpha T_d$. In relation to the pilot model, $\alpha < 1$ implies $T_{p_1} > T_{p_2}$.

The effects of lead compensation can also be seen on a Nichol's chart. Curve A in Fig. 2.8 meets the closed loop bandwidth requirement, but the resonance is greater than 9 dB. Lead compensation causes the lower part of curve A to shift upward and to the right (shaped

more like curve C) (12:47). The pilot gain can then be adjusted to shift curve A downward to again meet the closed-loop bandwidth requirement, while at the same time reducing resonance.

A 'target zone' can be formed from the closed-loop bandwidth and droop requirements. The $-90°$ closed-loop phase line on Fig. 2.8 terminates at the point where open-loop phase=$-180°$. The $-90°$ closed-loop phase line and the -3 dB droop line intersect at a point where the open-loop phase=$-125.3°$. As long as the point where $\omega = \omega_{BW}$ satisfies $-180° \leq$ open-loop phase $\leq -125.3°$, the closed-loop bandwidth requirement can be met by adjusting the gain. If the point where $\omega = \omega_{BW}$ corresponds to a point where the non-compensated open-loop phase $< -180°$, lead compensation is needed to shift that point to the right. The point would also shift up. The gain would need to be adjusted to bring the point back down to the original magnitude. The idea is to tune the parameters to give more movement to the right than up. The net result would be an overall shift to the right. Another time when lead compensation is needed occurs when the closed-loop bandwidth requirement is met but the droop is above the -3 dB droop line. This was already shown for curve A in Fig. 2.8. If the point where $\omega = \omega_{BW}$ is to the right of the target zone, lag compensation will be needed.

Before discussing lag compensation, the calculation of non-compensated open-loop phase needs to be addressed. $\angle Y_c$ is the open-loop phase of the aircraft with the aircraft time delay (τ_θ) included. The pilot also has a time delay. Since the two time delays are multiplied when forming G, they can be replaced by a combined time delay, τ, as in Eq. (2.9).

$$e^{-\tau_\theta \cdot s} \cdot e^{-\tau_p \cdot s} = e^{-(\tau_\theta + \tau_p)\cdot s} = e^{-\tau \cdot s} \tag{2.9}$$

$$\text{where } \tau = \tau_\theta + \tau_p$$

When calculating the non-compensated open-loop phase, the combined time delay will be used. Rather than introduce a new symbol, $\angle Y_c$ will *always* include the phase contributed by $e^{-\tau_p \cdot s}$.

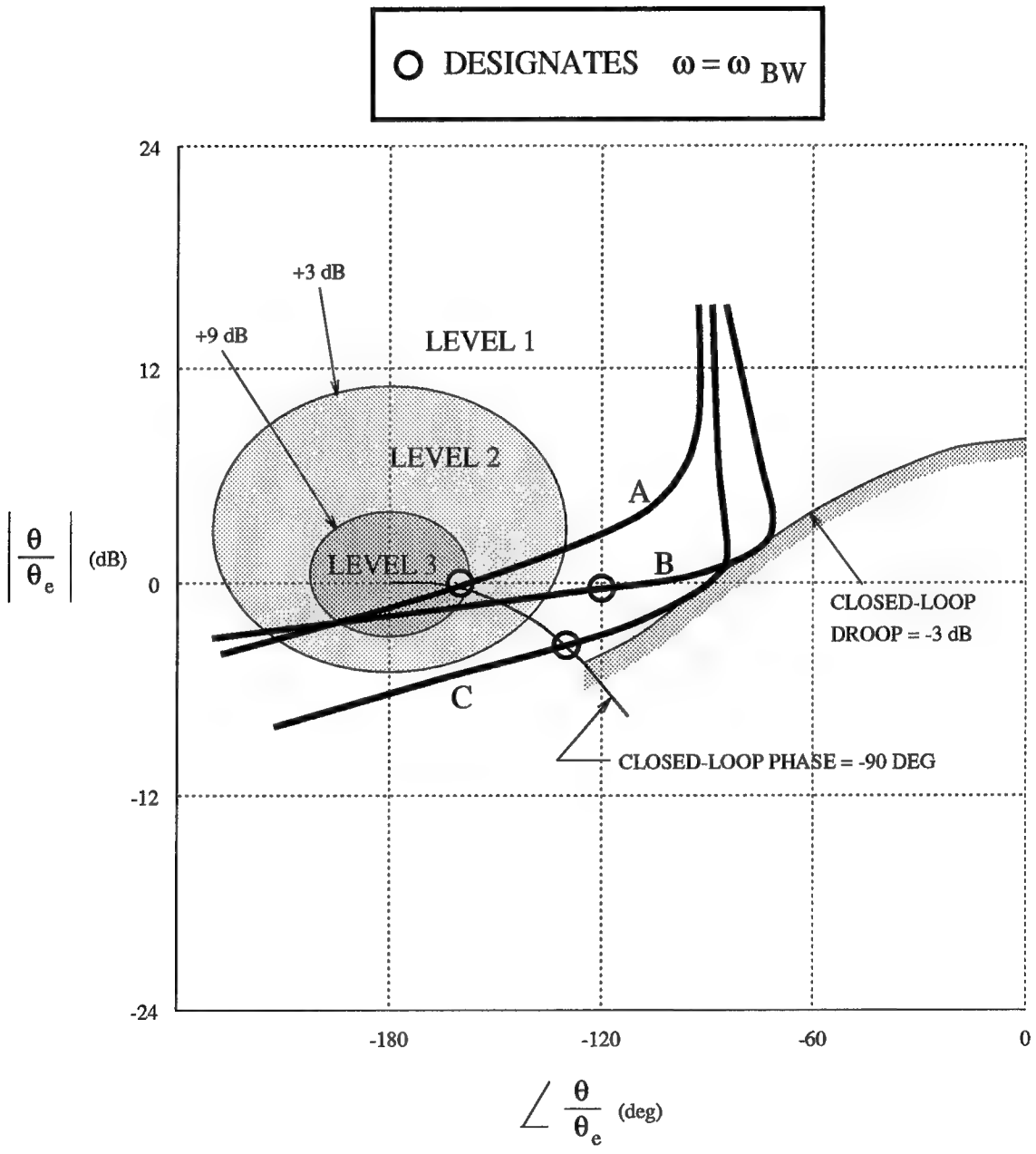

Figure 2.8 Typical Plots of Y_c

2.2.6 Lag Compensation. For lag compensation, $\alpha > 1$ or $T_{p_1} < T_{p_2}$. Lag compensation does the opposite of what lead compensation does. Phase is subtracted and magnitude decreases. This can also be seen on a Nichol's chart. Curve B in Fig. 2.8 meets the closed-loop droop requirement, but it does not meet the closed-loop bandwidth requirement. Lag compensation causes the lower part of curve B to shift downward and to the left (shaped more like curve C) (12:49). The pilot gain can be adjusted to shift curve B downward to meet the closed-loop bandwidth requirement, reduce resonance, and still meet the closed-loop droop requirement. In addition to being to the right of the target zone when $\omega = \omega_{BW}$, lag compensation is also needed when closed-loop bandwidth is met but the droop is below the -3 dB droop line. Deciding whether to use lead or lag compensation is an important part of the approach in Chapter III.

Neal and Smith state that the lowest resonance occurs when the closed-loop droop *equals* -3 dB while meeting the closed-loop bandwidth requirement simultaneously (12:47-49). Curve C in Fig. 2.8 illustrates their statement. Adding lead compensation to curve C would cause the resonance to increase if the closed-loop droop is held at -3 dB. Adding lag compensation to curve C would cause the resonance to increase if the closed-loop bandwidth is held at ω_{BW}. Changing Eq. (2.4) to an equality constraint provides a unique solution for the pilot model. A unique solution is needed to perform a mapping. Searching over a three-dimensional design space for a unique solution is not practical. Reducing the order of the problem is the next step.

2.2.7 'Optimum' Pilot Compensation. Neal and Smith define 'optimum' lead compensation as providing the most positive increase in $\angle \frac{\delta}{\theta_e}$ for the least flattening of the amplitude-phase curve, in the general vicinity of ω_{BW} (12:50). The following analysis further explains the meaning of the last statement. Equation (2.10) represents the amplitude (in dB) of the pilot model with $K_p = 1$. Equation (2.11) represents the phase (in radians) of the pilot

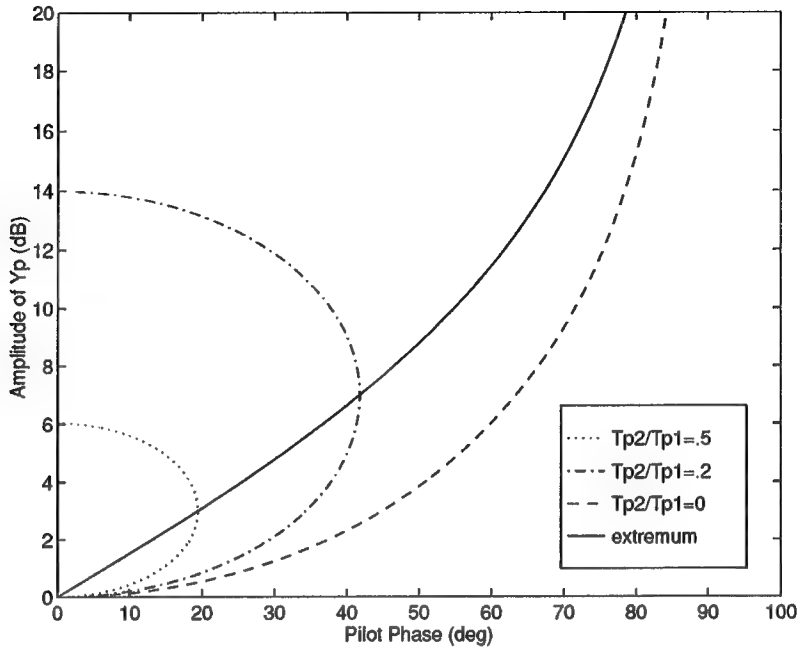

Figure 2.9 Amplitude-Phase Curve for Lead Compensation

model.

$$20\log\left|\frac{j\omega\cdot T_{p_1}+1}{j\omega\cdot T_{p_2}+1}\right| = 10\cdot\log\left(\omega^2T_{p_1}^2+1\right) - 10\cdot\log\left(\omega^2T_{p_2}^2+1\right) \quad \text{(dB)} \qquad (2.10)$$

$$\angle\left(\frac{j\omega\cdot T_{p_1}+1}{j\omega\cdot T_{p_2}+1}\right) = \tan^{-1}\left(\omega T_{p_1}\right) - \tan^{-1}\left[\frac{T_{p_2}}{T_{p_1}}\left(\omega T_{p_1}\right)\right] \qquad (2.11)$$

The flattening tendency is related to the fact that the increment in open-loop amplitude contributed by lead compensation is positive and increases with ω. Figure 2.10 illustrates this for various values of T_{p_2}/T_{p_1}. Least flattening can be thought of as providing the most amount of phase for a given amplitude. Figure 2.9 shows that for any amplitude, the maximum amount of phase occurs when $T_{p_2}/T_{p_1} = 0$. Another way to explain flattening is by examining the slopes in Fig. 2.10. Equation 2.12 is the derivative of Eq. (2.10) with respect to $\log\omega$.

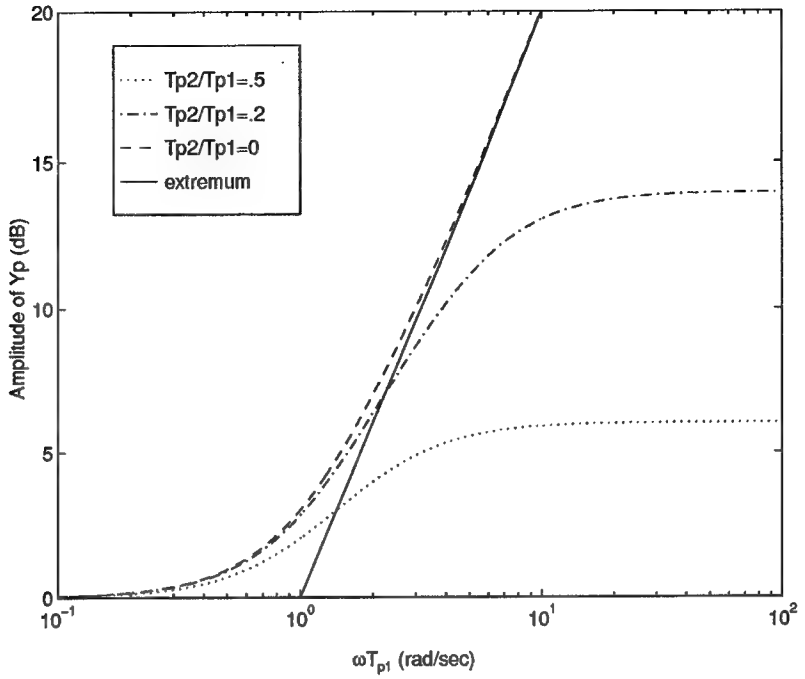

Figure 2.10 Magnitude Contribution of Lead Compensation

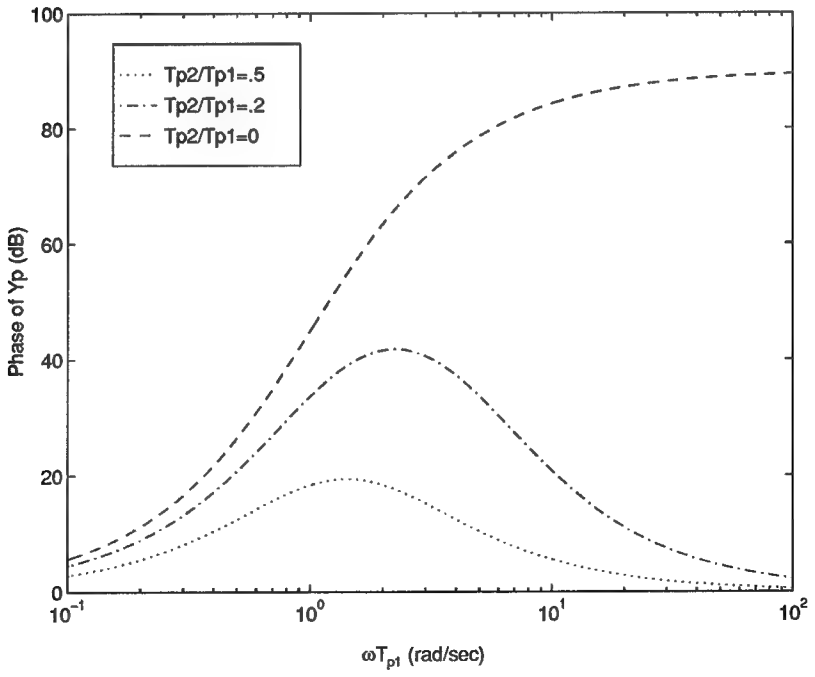

Figure 2.11 Phase Contribution of Lead Compensation

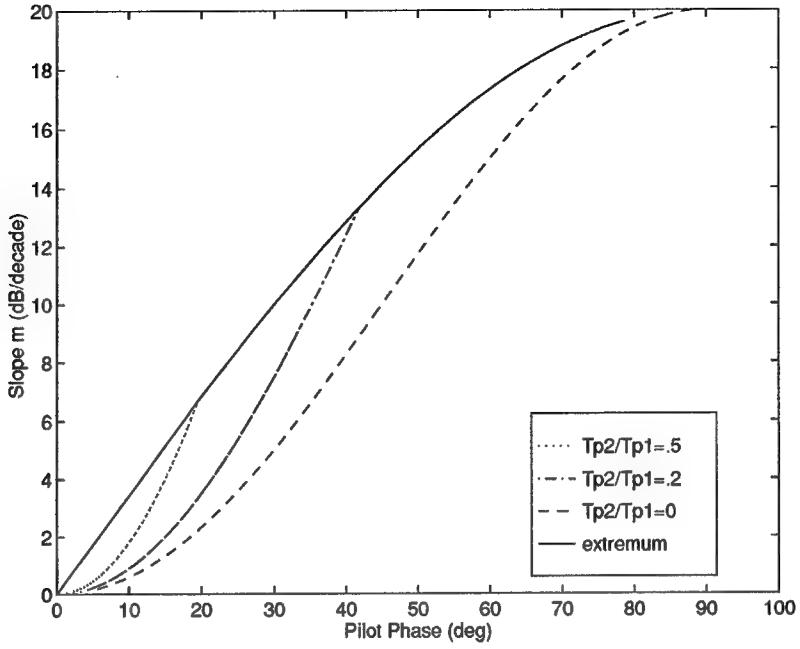

Figure 2.12 Magnitude Slope and Phase Contributed by Lead Compensation

Slope is given the symbol m.

$$m = \frac{d}{d(\log\omega)}\left\{20\log\left|\frac{j\omega\cdot T_{p_1}+1}{j\omega\cdot T_{p_2}+1}\right|\right\}$$
$$= \frac{20}{\left(1+\omega^{-2}T_{p_1}^{-2}\right)}\left[1-\frac{T_{p_2}^2T_{p_1}^{-2}\left(1+\omega^{-2}T_{p_1}^{-2}\right)}{\left(T_{p_2}^2T_{p_1}^{-2}+\omega^{-2}T_{p_1}^{-2}\right)}\right] \quad \text{(dB/decade)} \qquad (2.12)$$

Figure 2.12 plots this slope against phase. Least flattening for a given amount of phase corresponds to the least positive value in slope. Referring again to Fig. 2.10, the slopes increase to maximum values at some intermediate frequency, then decrease. To determine this extremum, the partial derivative of Eq. (2.11) with respect to ω is set equal to zero.

$$\frac{\partial}{\partial\omega}\left[\angle\left(\frac{j\omega\cdot T_{p_1}+1}{j\omega\cdot T_{p_2}+1}\right)\right] = \frac{T_{p_1}-T_{p_2}+\omega^2\left(T_{p_1}T_{p_2}^2-T_{p_1}^2T_{p_2}\right)}{\left(1+\omega^2T_{p_1}^2\right)\left(1+\omega^2T_{p_2}^2\right)} \qquad (2.13)$$

This corresponds to setting the numerator in Eq. (2.13) to zero.

$$T_{p_1} - T_{p_2} + \omega^2 \left(T_{p_1} T_{p_2}^2 - T_{p_1}^2 T_{p_2} \right) = 0 \tag{2.14}$$

The extremum, ω_{ext}, becomes

$$\omega_{ext} = \pm \frac{1}{\sqrt{T_{p_1} \cdot T_{p_2}}}. \tag{2.15}$$

To determine whether ω_{ext} is a maximum or minimum, the second partial derivative of Eq. (2.11) is taken.

$$\frac{\partial^2}{\partial \omega^2} \left[\angle \left(\frac{j\omega \cdot T_{p_1} + 1}{j\omega \cdot T_{p_2} + 1} \right) \right] = \frac{2\omega T_{p_2}^3}{\left(1 + \omega^2 T_{p_2}^2 \right)^2} - \frac{2\omega T_{p_1}^3}{\left(1 + \omega^2 T_{p_1}^2 \right)^2} \tag{2.16}$$

Setting $\omega = \omega_{ext}$ gives

$$\frac{\partial^2}{\partial \omega^2} \left[\angle \left(\frac{j\omega \cdot T_{p_1} + 1}{j\omega \cdot T_{p_2} + 1} \right) \right] = \frac{2T_{p_2}^3 \left(1 + T_{p_1} T_{p_2}^{-1} \right)^2 - 2T_{p_1}^3 \left(1 + T_{p_1}^{-1} T_{p_2} \right)^2}{\sqrt{T_{p_1} T_{p_2}} \left(1 + T_{p_1} T_{p_2}^{-1} \right)^2 \left(1 + T_{p_1}^{-1} T_{p_2} \right)^2}. \tag{2.17}$$

Since the denominator in Eq. (2.17) is positive, the numerator determines the sign. If Eq. (2.17) is positive, ω_{ext} is a minimum. If Eq. (2.17) is negative, ω_{ext} is a maximum. For lead compensation, $0 \leq T_{p_2}/T_{p_1} < 1$. Figure 2.13 illustrates the sign of the numerator as a function of T_{p_2}/T_{p_1}. The graph shows that Eq. (2.17) is negative in the region for lead compensation. Thus, ω_{ext} is the maximum for lead compensation. This can be seen on Fig. 2.12. Slope and phase increase until reaching the center frequency, then decrease along the same path back to zero. While ω_{ext} forms an upper bound to Fig. 2.12, it is not the solution for 'optimum' lead compensation as defined by Neal and Smith. Instead, the most positive phase for a given positive slope is always when $T_{p_2}/T_{p_1} = 0$. Thus, the 'optimum' lead compensation is pure lead, or

$$T_{p_2} = 0. \tag{2.18}$$

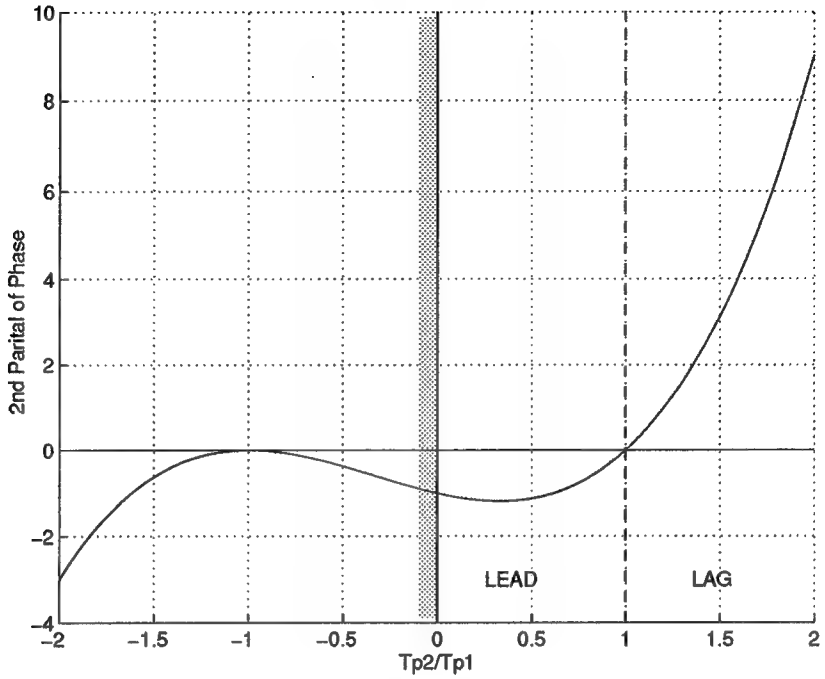

Figure 2.13 2nd partial of phase as a function of T_{p_2}/T_{p_1}

Neal and Smith define 'optimum' lag compensation as providing the most steepening of the amplitude phase curve for the least negative increase in $\angle \frac{\theta_e}{\delta}$, in the vicinity of ω_{BW} (12:50). For lag compensation, $T_{p_2}/T_{p_1} > 1$. An analysis similar to the one for lead compensation helps to explain the meaning of Neal and Smith's definition. The steepening tendency is related to the fact that the increment in open-loop magnitude contributed by lag compensation is negative and decreases with ω. Figure 2.15 illustrates this for various values of T_{p_2}/T_{p_1}. The steepest point on each curve occurs at ω_{ext}. In terms of slope, 'optimum' lag compensation provides the most negative value of m for the least negative value of phase as seen in Fig. 2.17. Slope and phase decrease to minimum values at ω_{ext}, then increase along the same path back to zero. Referring gain to Fig. 2.13, Eq. (2.17) is positive when $T_{p_2}/T_{p_1} > 1$. Therefore, ω_{ext} is the minimum for lag compensation. Unlike lead compensation, ω_{ext} *is* the solution for 'optimum' lag compensation. The most negative slope for a given negative phase is always at the center frequency. Since the primary area of interest is in the vicinity of ω_{BW}, Neal and

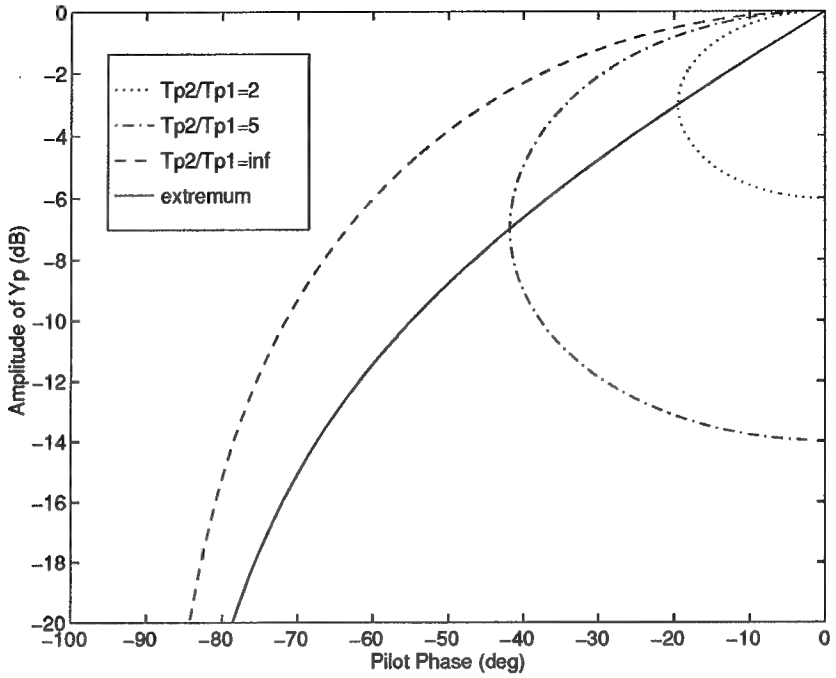

Figure 2.14 Amplitude-Phase Curve for Lag Compensation

Smith set $\omega_{ext} = \omega_{BW}$. Thus, 'optimum' lag compensation occurs when

$$\omega_{BW} = \pm \frac{1}{\sqrt{T_{p_1} \cdot T_{p_2}}}. \tag{2.19}$$

Solving Eq. (2.19) for T_{p_2} yields

$$T_{p_2} = \frac{1}{T_{p_1} \cdot \omega_{BW}^2}. \tag{2.20}$$

If either 'optimum' lead compensation or 'optimum' lag compensation is used, Eq. (2.18) or Eq. (2.20) reduce the order of the three-dimensional problem down to two.

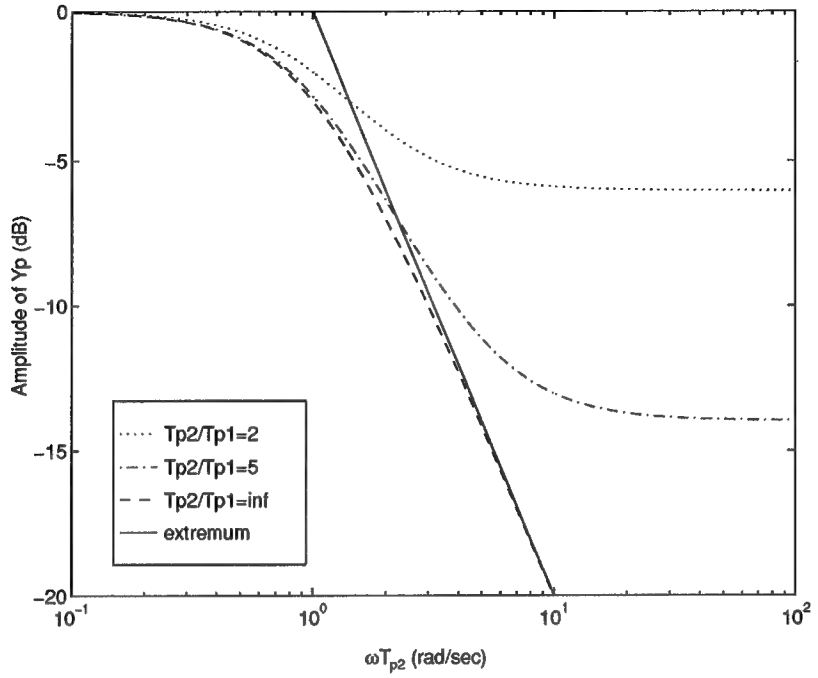

Figure 2.15 Magnitude Contribution of Lag Compensation

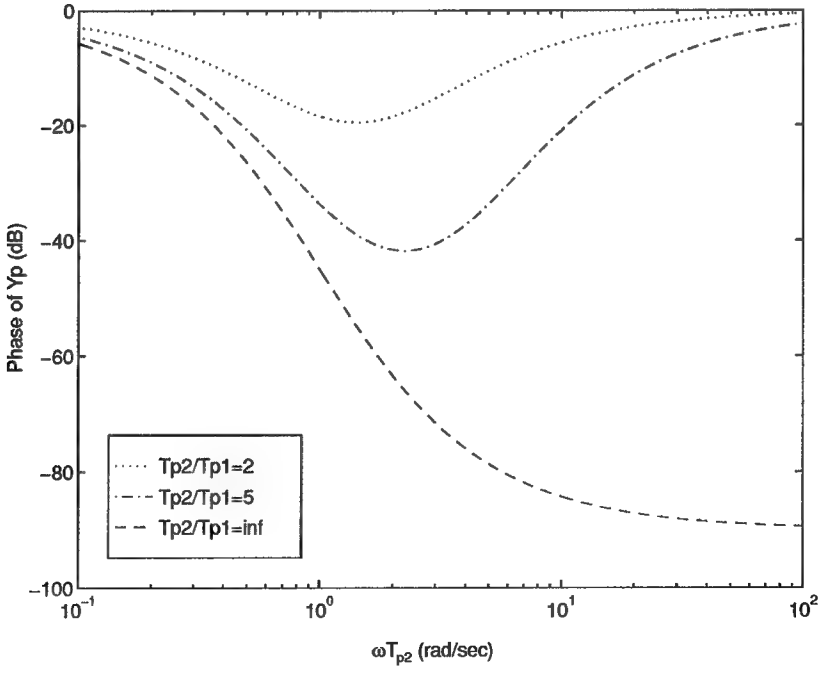

Figure 2.16 Phase Contribution of Lag Compensation

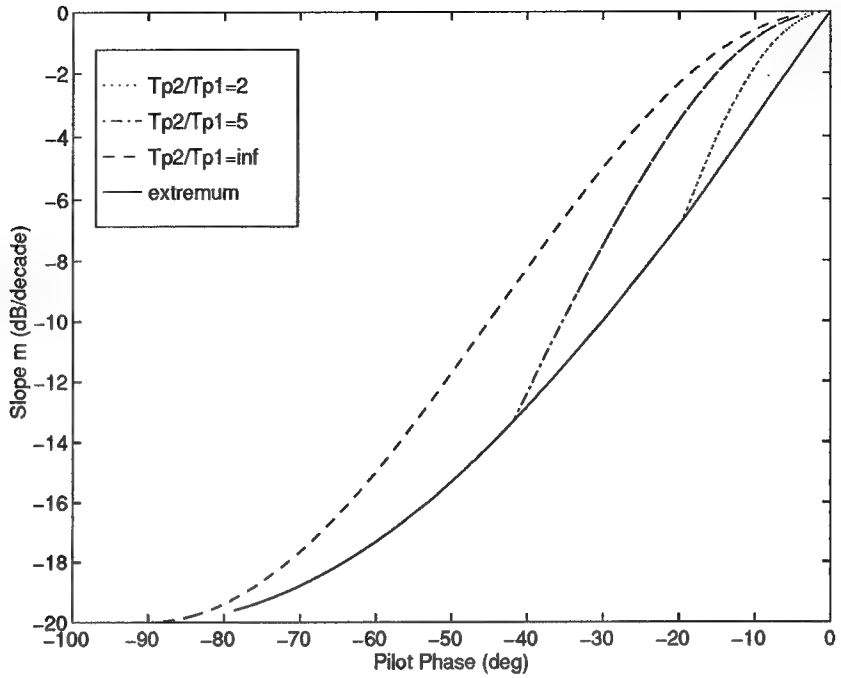

Figure 2.17 Magnitude Slope and Phase Contributed by Lag Compensation

2.3 The Pilot-in-the-Loop Criteria

The Pilot-in-the-Loop criteria is a modified version of the Neal-Smith criteria. The differences are outlined in this section. While Neal and Smith require only one form of pilot model, MIL-STD-1797A offers two pilot models for use with the Pilot-in-the-Loop criteria. The first pilot model is the same one Neal and Smith use in Eq. (2.5). The second pilot model is used when there is no free s in the denominator of the aircraft transfer function (4:237). A free s is desired in G to make the system a type I system. Type I systems have zero steady-state error to step inputs (7:108). Equation (2.21) can be used with the Pilot-in-the-Loop criteria when Y_c has no free s.

$$Y_p = \frac{K_p(5s+1)(T_{p_1} \cdot s + 1)e^{-\tau_p \cdot s}}{s \cdot (T_{p_2} \cdot s + 1)} \tag{2.21}$$

Since the short period approximation will be used for Y_c, Eq. (2.5) will be used for Y_p.

The second difference is in the value of the pilot time delay, τ_p. Neal and Smith used $\tau_p = 0.3$ seconds. MIL-STD-1797A fixes τ_p at 0.25 seconds (4:237). This difference can be

ignored if the pilot and aircraft time delays are combined. Data generated for one value of τ can be used to analyze both the Neal-Smith criteria and the Pilot-in-the-Loop criteria. The aircraft time delay, however, would be different for each criteria. For example if $\tau = 0.5$ seconds, τ_θ would be 0.25 seconds for Pilot-in-the-Loop analysis and 0.20 seconds for Neal-Smith analysis.

The final difference between the Neal-Smith and Pilot-in-the-Loop criteria is limits on closed-loop resonance. MIL-STD-1797A puts the following limits on the resonant peak values.

> A bandwidth, defined by a closed-loop phase of -90 degrees, of 2.5 rad/sec [Category C] shall be attainable with closed-loop droop no more than -3 dB for Levels 1 and 2 and closed-loop resonance no greater than 3 dB for Level 1, 9 dB for Level 2 over the frequency range from 0 to 10 rad/sec.
>
> (4:237)

These limits are displayed in Table 2.3 and are less restrictive than the Neal-Smith criteria. In addition, there is no consideration given to pilot phase angle.

Table 2.3 Limits on Closed-Loop Droop and Resonance

LEVEL	*MAX DROOP* (dB)	*MAX RES* (dB)	*C-L PHASE* @ω_{BW}
1	-3	3	$-90°$
2	-3	9	$-90°$

2.4 Summary

The $\omega_{sp}T_{\theta_2}, \zeta_{sp}, \tau_\theta$, Neal-Smith, and Pilot-in-the-Loop criteria were explained in detail. The $\omega_{sp}T_{\theta_2}, \zeta_{sp}, \tau_\theta$ criteria depends only on the aircraft. Limits on ω_{sp}, T_{θ_2}, and τ_θ were given. If τ_θ and T_{θ_2} are fixed, the parameters ω_{sp} and ζ_{sp} can be varied to form a two dimensional region for mapping. Every point in the region defines an aircraft transfer function, Y_c. Once Y_c is known, a search for a pilot transfer function can begin. The form of the pilot model has three unknown parameters (K_p, T_{p_1}, and T_{p_1}). The Neal-Smith criteria and the

Pilot-in-the-Loop criteria are identical with respect to the unknown pilot model parameters. They differ in the value of pilot time delay (τ_p). The Neal-Smith criteria fixes τ_p at 0.3 seconds, while the Pilot-in-the-Loop criteria fixes τ_p at 0.25 seconds. Neal and Smith also use different boundaries to distinguish between handling qualities levels. Pilot phase angle is taken into account, whereas the Pilot-in-the-Loop criteria only evaluates the maximum closed-loop resonance. Despite these differences, the same approach will be used to determine the pilot model parameters. Depending on whether lead or lag compensation is needed determines if Eq. (2.18) or Eq. (2.20) is used. Either equation reduces the problem to a two-dimensional problem in terms of K_p and T_{p_1}. In Chapter III, an equation will be derived for the closed-loop bandwidth requirement. This equation will serve to reduce the remaining two-dimensional problem down to a one-dimensional search.

III. Approach

This chapter outlines the approach used to map the $\omega_{sp}T_{\theta_2}, \zeta_{sp}, \tau_\theta$ criteria into the Neal-Smith and Pilot-in-the-Loop criteria. Neal and Smith developed a graphical method for determining the pilot model parameters. This method is discussed followed by an alternate method that makes use of numerical optimization. Finally, a step-by-step procedure is given.

3.1 Neal-Smith Graphical Method

Computer power and numerical optimization techniques have increased since Neal and Smith developed their criteria in 1970 (12). Nonetheless, they developed a method for determining the pilot model parameters. The method involved iteration based on graphical interpretations. The first step was plotting the Nichol's chart of Y_c as in Fig. 2.8. By visual inspection, they decided whether lead or lag compensation was needed. An initial guess at the unknown parameters for either 'optimal' lead compensation or 'optimal' lag compensation was made. Another Nichol's chart was generated, this time of the pilot-aircraft system (G) as in Fig. 2.5. The pilot gain, K_p, was adjusted to meet the closed-loop bandwidth requirement. If the closed-loop droop was *greater* than -3 dB, additional *lead* was needed to meet the closed-loop droop exactly. If the closed-loop droop was *less* than -3 dB, additional *lag* was needed. They would then iterate on this process until both the closed-loop bandwidth and the closed-loop droop requirements were met simultaneously. Each iteration required looking at plots in order to make decisions about the next guess. Although they derived a way to make the initial guess close to the solution, the process still involved iterations based on visual examination of plots. Performing this process for a grid of 1000 different aircraft transfer functions would be a formidable task. Developing a method that does not require human interaction at each step became a primary goal of this research. The remainder of this chapter outlines an alternate method where the problem is posed as a constrained optimization problem.

Table 3.1 General Problem Statement

Minimize:	$f(\boldsymbol{x})$	$\boldsymbol{x} \in \Re$	objective function
Subject to:	$g_i(\boldsymbol{x}) \leq 0$	$i = 1, l$	inequality constraints
	$h_j(\boldsymbol{x}) = 0$	$j = 1, m$	equality constraints
	$x_k^l \leq x_k \leq x_k^u$	$k = 1, n$	side constraints

3.2 Sequential Quadratic Programming

Since there are criteria (i.e. constraints) on this problem, a constrained optimization routine can be used to solve for the unknown pilot model parameters. The reader is referred to Vanderplaats (16) for various methods of numerical optimization. The author chose to use Sequential Quadratic Programming (SQP). "SQP methods represent state-of-the-art in nonlinear programming methods" (8:2-23). Schittowski (15) has implemented and tested a version of SQP that out performs every other method tested in terms of efficiency, accuracy, and percentage of successful solutions (over a large number of test problems). The remainder of this section provides a brief overview of SQP.

The general problem statement is shown in Table 3.1 where $\boldsymbol{x}$ is the design vector, f is the objective function, $\boldsymbol{h}$ is a vector of equality constraints, and $\boldsymbol{g}$ is a vector of inequality constraints. Elements in the design vector, x_k, also have side constraints. The principal idea behind SQP is the formulation of the quadratic programming (QP) sub-problem based on a quadratic approximation of the Lagrangian function, L, given by Eq. (3.1).

$$L(\boldsymbol{x}, \lambda) = f(\boldsymbol{x}) + \sum_{i=1}^{l} \lambda_i g_i(\boldsymbol{x}) + \sum_{j=1}^{m} \lambda_{(l+j)} h_j(\boldsymbol{x}) \tag{3.1}$$

The symbol λ represents the Lagrange multiplier of each constraint. If a constraint is not active (e.g. $g_1 < 0$), the corresponding Lagrange multiplier must be zero. The QP sub-problem is obtained by linearizing the nonlinear constraints. The QP problem statement is shown in Table 3.2. The subscript b represents iteration number. This sub-problem can be solved using

Table 3.2 QP Problem Statement

Minimize:	$\frac{1}{2}\boldsymbol{d}_b^T \boldsymbol{H}_b \boldsymbol{d}_b + \nabla f(\boldsymbol{x}_b)^T \boldsymbol{d}_b$	$\boldsymbol{x} \in \Re$
Subject to:	$\nabla g_i(\boldsymbol{x})^T \boldsymbol{d}_b + g_i(\boldsymbol{x}) \leq 0$	$i = 1, l$
	$\nabla h_j(\boldsymbol{x})^T \boldsymbol{d}_b + h_j(\boldsymbol{x}) = 0$	$j = 1, m$

any QP algorithm. The solution, $\boldsymbol{d}_b$, is used to form a new iterate $\boldsymbol{x}_{b+1}$ as in Eq. (3.2).

$$\boldsymbol{x}_{b+1} = \boldsymbol{x}_b + \alpha_b \boldsymbol{d}_b \tag{3.2}$$

The step length, α_b, is determined by an appropriate line search procedure such that a sufficient decrease in a merit function is obtained. The merit function $\Psi(\boldsymbol{x})$ in Eq.(3.3) will be used.

$$\Psi(\boldsymbol{x}) = f(\boldsymbol{x}) + \sum_{i=1}^{l} r_i \max(0, g_i(\boldsymbol{x})) + \sum_{j=1}^{m} r_{(l+j)} h_j(\boldsymbol{x}) \tag{3.3}$$

The variable, r, is a penalty parameter. The matrix $\boldsymbol{H}_b$ from the QP sub-problem is a positive definite approximation of the Hessian matrix of the Lagrangian function in Eq. (3.1). $\boldsymbol{H}_b$ will be updated using the Broyden, Fletcher, Goldfarb, and Shanno (BFGS) method shown in Eq. (3.4).

$$\boldsymbol{H}_{b+1} = \boldsymbol{H}_b + \frac{q_b q_b^T}{q_b^T s_b} - \frac{H_b^T H_b}{s_b^T H_b s_b} \tag{3.4}$$

where $\boldsymbol{s}_b = \boldsymbol{x}_{b+1} - \boldsymbol{x}_b$

$$\boldsymbol{q}_b = \nabla f(\boldsymbol{x}_{b+1}) - \nabla f(\boldsymbol{x}_b)$$

3.3 'Optimizing' the Pilot Model

SQP will be used to solve for the pilot model parameters. Strictly speaking, SQP is not 'optimizing' the pilot model. Instead, SQP is used to solve the complicated equations used to determine T_{p_1} and T_{p_2} according to the Neal-Smith definitions of 'optimum'. Neal

and Smith state that the lowest resonance occurs when the closed-loop droop *equals* -3 dB while meeting the closed-loop bandwidth requirement simultaneously (12:47-49). In other words, they assume the lowest resonance always occurs when the droop inequality constraint is active.

Edkins developed a computer program that automated the original Neal-Smith method (6:14). Given a range on T_{p_1} and T_{p_2}, the program calculates handling qualities levels for various combinations in the search interval. Based on the these results, the ranges on T_{p_1} and T_{p_2} are modified until a satisfactory result is obtained. The program still involves human interaction at each iteration step. Edkins even stated that "the iteration process is fairly lengthy" (6:14).

Since the pilot wants to minimize closed-loop resonance while keeping droop above the -3 dB line, the problem can be posed in the general format of Table 3.1. In other words, minimize closed-loop resonance subject to droop$\geq$-3 dB. This is the same as minimizing the ∞-norm of the complimentary sensitivity, T. If the goal is to 'optimize' the pilot model, why restrict the form of compensation to either 'optimal' lead or 'optimal' lag defined by Eq. (2.18) and Eq. (2.20)? There could be a combination of T_{p_1} and T_{p_2} that leads to an overall better solution. The problem then becomes a two-dimensional search for the best combination of T_{p_1} and T_{p_2} that minimizes closed-loop resonance subject to the droop inequality constraint. This approach has the disadvantage of requiring two initial guesses. Since SQP looks for the minimum solution in vicinity of the initial guesses, there is also a greater chance of SQP returning a local minimum. SQP had to be frequently restarted with different initial guesses to obtain smaller values of the objective function. Edkins' program was run a few times to determine acceptable initial guesses. This, however, greatly increased computational time. Hence, an alternate formulation was sought.

Using the Neal-Smith assumption that the lowest resonance occurs when both constraints are met with equality provides a unique solution. The issue of whether a solution is a local or global minimum goes away. The objective is to drive the droop to -3 dB exactly while meeting the closed-loop bandwidth requirement. The remainder of this chapter outlines this

type of approach. K_p and T_{p_1} are still unknown. The next section derives an equation for K_p which depends only on T_{p_1}.

3.4 Closed-Loop Bandwidth

Figure 2.2 can be manipulated to look like Fig. 3.1 if the pilot gain (K_p) and the aircraft gain (K_θ) are separated from both transfer functions and given their own block K.

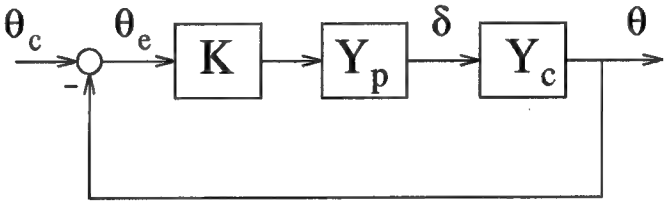

Figure 3.1 Block Diagram of Pilot-Aircraft System with Separate Combined Gain

This does not change the problem. Equation (3.5) defines the new combined gain. Equation (3.6) becomes the pilot transfer function, and Eq. (3.7) becomes the aircraft transfer function.

$$K \equiv K_p \cdot K_\theta \tag{3.5}$$

$$Y_p = \frac{(T_{p_1} \cdot s + 1)}{(T_{p_2} \cdot s + 1)} \tag{3.6}$$

$$Y_c = \frac{(T_{\theta_2} \cdot s + 1)e^{-\tau \cdot s}}{s\left(s^2 + 2\zeta_{sp}\omega_{sp} \cdot s + \omega_{sp}^2\right)} \tag{3.7}$$

The pilot-aircraft system still is given the symbol G, but Eq. (3.8) is used.

$$G = K \cdot Y_p Y_c \tag{3.8}$$

In the frequency domain, G can be represented by its magnitude multiplied by its phase.

$$G = |G| \cdot \cos\phi_G + j\,|G| \cdot \sin\phi_G \tag{3.9}$$

where $|G|$ = Magnitude of G and ϕ_G = Phase of G

The closed-loop transfer function becomes

$$T = \frac{G}{1+G} = \frac{|G| \cdot \cos\phi_G + j\,|G| \cdot \sin\phi_G}{1 + |G| \cdot \cos\phi_G + j\,|G| \cdot \sin\phi_G}. \tag{3.10}$$

Multiplying the numerator and denominator of Eq. (3.10) by the complex conjugate of its denominator yields

$$T = \frac{|G| \cdot \cos\phi_G + |G|^2 + j\,|G| \cdot \sin\phi_G}{1 + 2\,|G| \cdot \cos\phi_G + |G|^2}. \tag{3.11}$$

The phase, or argument, of T becomes

$$\phi_{CL} = \arg[T] = \arctan\left[\frac{Imag(T)}{Real(T)}\right] = \arctan\left[\frac{\sin\phi_G}{\cos\phi_G + |G|}\right]. \tag{3.12}$$

For ϕ_{CL}=−90° (defines closed-loop bandwidth), the following two equations must be met.

$$\sin\phi_G < 0 \tag{3.13}$$

$$\cos\phi_G + |G| = 0 \tag{3.14}$$

Equation (3.14) can be used to solve for K from Eq. (3.8).

$$|G| = |K| \cdot |Y_p Y_c| = -\cos\phi_G \tag{3.15}$$

$$|K| = \frac{-\cos\phi_G}{|Y_p Y_c|} \tag{3.16}$$

In order for $|G| > 0$,

$$\cos\phi_G < 0. \tag{3.17}$$

The only place where both Eq. (3.13) and Eq. (3.17) are satisfied is when

$$-180° < \phi_G < -90°. \tag{3.18}$$

If all the parameters that make up Y_pY_c are known except for T_{p_1} and T_{p_2}, $|Y_pY_c|$ and ϕ_G become functions of T_{p_1} and T_{p_2}.

$$|Y_pY_c| = f_1(T_{p_1}, T_{p_2}) \quad \text{and} \quad \phi_G = f_2(T_{p_1}, T_{p_2}). \tag{3.19}$$

Therefore, K is a function of T_{p_1} and T_{p_2}. Equation (3.16) is the equation that reduces the two-dimensional problem from Chapter 2 down to a one-dimensional search over T_{p_1}. If 'optimum' lead compensation is used, T_{p_2} is known ($T_{p_2} = 0$). If 'optimum' lag compensation is known, T_{p_2} is a function of only T_{p_1} (assuming ω_{BW} is fixed). This makes K a function of only T_{p_1}. The original three-dimensional problem is finally reduced to a one-dimensional search over T_{p_1}. Now the approach can be outlined.

3.5 Step-by-Step Procedure

This section only applies to mapping the $\omega_{sp}T_{\theta_2}, \zeta_{sp}, \tau_\theta$ criteria into the Neal-Smith and Pilot-in-the-Loop criteria. Figure 3.2 provides a flow chart of a major part of the process. The steps before the flow chart begins involve fixing some of the parameters of Y_c in Eq. (3.7).

Step 1: Select a flight phase. This determines ω_{BW}. MIL-STD-1797A lists two different values of ω_{BW} for Category C (4:237). For landing, $\omega_{BW} = 2.5$ (rad/sec). For any other Category C maneuver, $\omega_{BW} = 1.5$ (rad/sec).

Step 2: Fix τ_θ. Depending on whether a level 1 region or a level 2 region is to be mapped determines the maximum allowable τ_θ. Table 2.1 lists these limits. The most conservative mapping would fix τ_θ at one of the maximum values (e.g. $\tau_\theta = 0.10$ seconds for level 1).

Step 3: Fix T_{θ_2}. Choosing an aircraft fixes T_{θ_2}. For example, the F-16 VISTA has $T_{\theta_2} = 1.96$.

Step 4: Check if T_{θ_2} is within correct limits. Table 2.2 outlines these limits.

Step 5: Determine the minimum value of $\omega_{sp}T_{\theta_2}$. Table 2.2 also lists minimum values for ω_{sp}. Multiplying one of these values by T_{θ_2} determines the minimum value of $\omega_{sp}T_{\theta_2}$. For

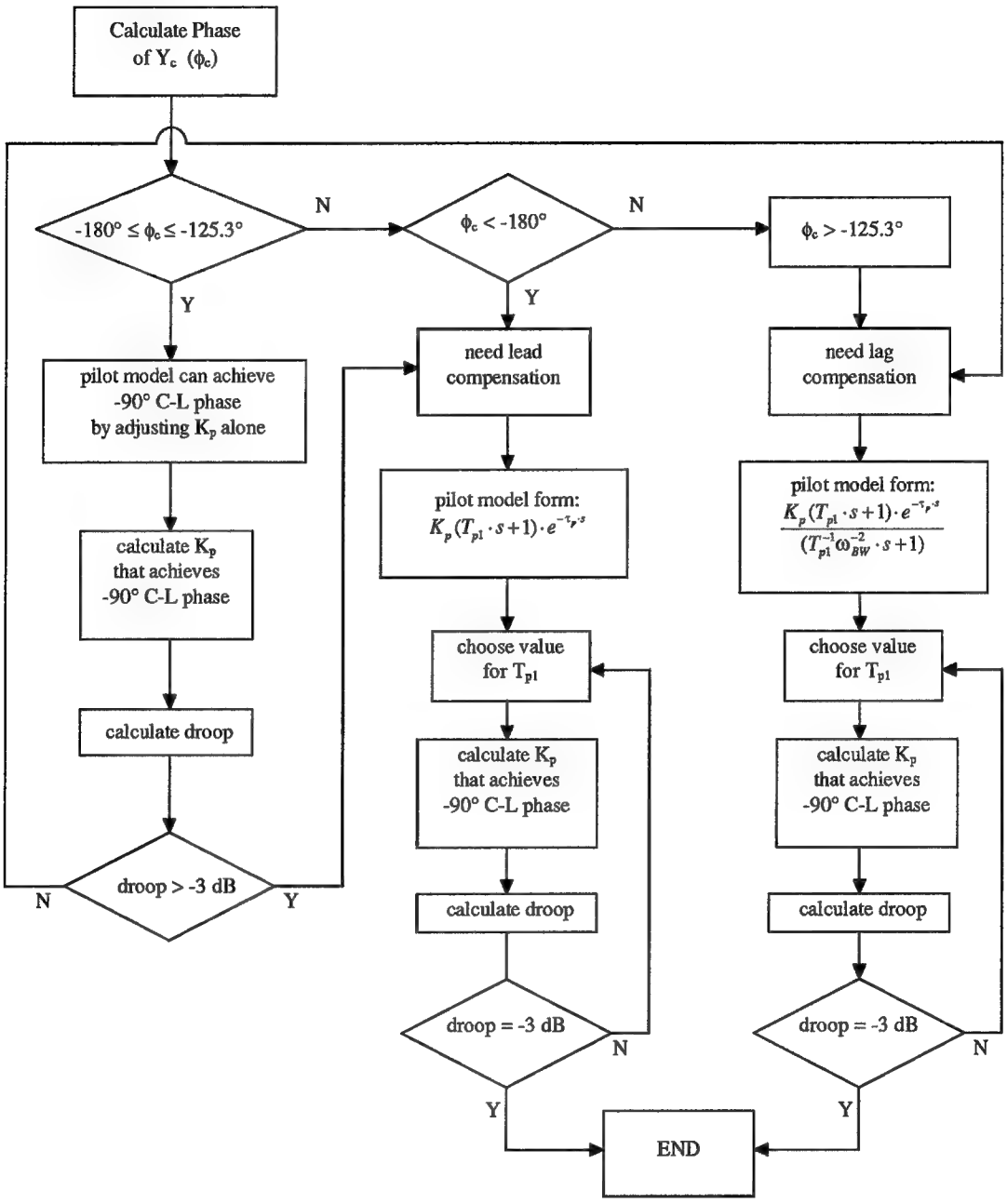

Figure 3.2 Process Flow Chart

example, the minimum value of $\omega_{sp}T_{\theta_2}$ for a level 1 region for the F-16 VISTA would be 1.7. Note that this is above the 1.3 boundary shown in Fig. 2.1.

Step 6: Determine range for ω_{sp} and ζ_{sp} that defines a region to be mapped. If the level 1 region is to be mapped, Eq. (3.20) and Eq. (3.21) would be the range.

$$0.87 \leq \omega_{sp} \leq \frac{10}{T_{\theta_2}} \tag{3.20}$$

$$0.35 \leq \zeta_{sp} \leq 1.30 \tag{3.21}$$

It should be noted there is no upper bound on $\omega_{sp}T_{\theta_2}$. Since MIL-STD-1797A only plots the criteria up to $\omega_{sp}T_{\theta_2} = 10$ (4:191), the upper bound in Eq. (3.20) will be used.

Step 7: Choose one point that satisfies Eq. (3.20) and Eq. (3.21). At this point, all the parameters of Y_c are known.

Step 8: Calculate the phase of Y_c and determine whether lead or lag compensation is required. This is where the flow chart in Fig. 3.2 begins. If $\angle Y_c < -180°$ or $\angle Y_c$ is in the target zone but droop < -3 dB, lead compensation is needed. 'Optimal' lead compensation will be used, so Eq. (2.18) applies. If $\angle Y_c > -125.3°$ or $\angle Y_c$ is in the target zone but droop > -3 dB, lag compensation is needed. 'Optimal' lag compensation will be used, so Eq. (2.20) applies.

There are limits on the amount of phase the pilot model can add or subtract. Figures 2.11 and 2.16 asymptotically approach $\pm 90°$ respectively. Therefore, the maximum amount of phase the pilot model can add or subtract is $90°$. If closed-loop bandwidth and droop are to be met simultaneously, Eq. (3.22) must be satisfied. The computer code is designed to check for this and flag those points that do not satisfy Eq. (3.22).

$$-270° < \angle Y_c < -35.3° \tag{3.22}$$

Step 9: Find 'optimal' values for K, T_{p_1}, and T_{p_2} by doing a one-dimensional search over T_{p_1}. Here, 'optimal' means a combination of K, T_{p_1}, and T_{p_2} that makes the pilot-aircraft system meet the closed-loop bandwidth and droop requirements simultaneously. The

command 'constr' in MATLAB^{TM} solves constrained optimization problems using SQP. Tolerances are needed to determine if convergence is achieved. The default tolerances in the *Optimization Toolbox* (8) are used and shown in Table 3.3.

Table 3.3 Tolerances for Convergence

Parameter	*Tolerance*
Objective function (f)	10^{-4}
Constraint violation ($\boldsymbol{g}$)	10^{-6}
Design vector ($\boldsymbol{x}$)	10^{-4}

Droop is determined by doing a frequency search for the minimum value of $|T|$ over $\omega \leq \omega_{BW}$. The 'min' command in MATLAB^{TM} accomplishes this. The design vector becomes a scalar (T_{p_1}). The cost function becomes the square of the difference between the closed-loop droop and -3 dB. The specific problem statement for optimizing with lead compensation is given by Table 3.4. The specific problem statement for optimizing with lag compensation is given by Table 3.5.

Side constraints are placed on the pilot parameters ($T_{p_1} \geq 0$ and $K \geq 0$). Negative values would lead to non-minimum phase systems. The next section outlines the approach for identifying regions of agreement and regions of conflict after the mapping of $\omega_{sp} T_{\theta_2}, \zeta_{sp}, \tau_\theta$ is complete.

Table 3.4 Lead Problem Statement

Minimize:	$(DROOP + 3)^2$ (dB)^2
Subject to:	$DROOP \geq -3$ dB
	$-180° \leq \phi_G \leq -125.3°$
	$K \geq 0$
	$T_{p_1} \geq 0$

Table 3.5 Lag Problem Statement

Minimize:	$(DROOP + 3)^2$ (dB)^2
Subject to:	$DROOP \geq -3$ dB
	$-180° \leq \phi_G \leq -125.3°$
	$K \geq 0$
	$T_{p_1} \geq 0$
	$T_{p_2} > T_{p_1}$

3.6 Region Identification

Both the Pilot-in-the-Loop and Neal-Smith criteria involve finding values for the pilot model with respect to a given aircraft model. A point from either criteria represents the pilot-aircraft system in the form of *one* transfer function. The individual pilot and aircraft parameters are not easily distinguished. Rather than trying to accomplish this for a grid of points, bookkeeping of the original mapping from the last section will be used. Entire regions from either criteria will never be mapped. Only those parts corresponding to the region from $\omega_{sp}T_{\theta_2}, \zeta_{sp}, \tau_\theta$ will be evaluated. The identification of conflict and agreement regions involves pass-fail logic. For example, when a level 1 point from $\omega_{sp}T_{\theta_2}, \zeta_{sp}, \tau_\theta$ is mapped into Neal-Smith, does it fall within the Neal-Smith level 1 boundaries? If the answer is yes, a certain flag is attached to that point. If the answer is no, a different flag is used. All the points with the 'yes' flag can be mapped back to the $\omega_{sp}T_{\theta_2}, \zeta_{sp}, \tau_\theta$ criteria showing the region of agreement. The region of conflict is identified in the same fashion. Before beginning Chapter IV, a summary of Chapter III is given.

3.7 Summary

The original three-dimensional problem of determining K, T_{p_1}, and T_{p_2} was reduced to a one-dimensional search over T_{p_1}. With all of the parameters fixed except T_{p_1} and T_{p_2}, the open-loop transfer function G is a function of only T_{p_1} and T_{p_2}. If T_{p_1} is known, $T_{p_2} = 1/(\omega_{BW}^2 \cdot T_{p_1})$ when 'optimum' lag compensation is used and $T_{p_2} = 0$ when 'optimum'

lead compensation is used. Therefore $G = f_1(T_{p_1})$. A formula for $|K|$ as a function of the magnitude and phase of G results in $K = f_2(G) \Rightarrow K = f_2(T_{p_1})$. Hence, if T_{p_1} is known, so is K and T_{p_2}. The closed-loop bandwidth and droop requirements are turned into constraints. If $\angle Y_c$ is to left of the target zone, lead compensation is needed. If $\angle Y_c$ is to right of the target zone, lag compensation is needed. If $\angle Y_c$ is in the target zone, lead compensation is needed if the droop>-3 dB and lag compensation is needed if the droop<-3 dB. Both the lead and lag problem fit the general form for SQP to solve. Once a solution for the pilot model is found, the mapping of a region from $\omega_{sp} T_{\theta_2}, \zeta_{sp}, \tau_\theta$ into either Neal-Smith or Pilot-in-the-Loop can be accomplished. From there, bookkeeping of the original mapping produces the 'inverse' mapping.

IV. Results

In order to perform a mapping, the parameters ω_{BW}, τ_θ, and T_{θ_2} need to be fixed. There is an infinite number of combinations. Twelve combinations are given in this thesis. The intent is to provide a sample that will illustrate trends and highlight problems.

Since ω_{BW}, τ_θ, and T_{θ_2} are fixed, trends can be examined when different values are used. For example, $\omega_{BW} = 2.5$ (rad/sec) for landing and $\omega_{BW} = 1.5$ (rad/sec) for any other Category C maneuver. Holding τ_θ and T_{θ_2} constant while ω_{BW} varies enables the trend of increasing ω_{BW} to be examined. Holding ω_{BW} and T_{θ_2} constant enables the trend of increasing τ_θ to be examined. τ_θ will be placed at its maximum value depending on which handling qualities level is being mapped (see Table 2.1). τ_θ will also be placed at the level 1 maximum value for level 2 mappings. Finally, holding ω_{BW} and τ_θ constant for the two different aircraft enables the trend of increasing T_{θ_2} to be examined.

In total, six cases will be examined for each aircraft. Table 4.1 defines each case. The 'Level' column refers to the region from the $\omega_{sp}T_{\theta_2}, \zeta_{sp}, \tau_\theta$ criteria that is mapped. The region is formed by fixing ω_{BW}, τ_θ, and T_{θ_2} to their respective values while varying ω_{sp} and ζ_{sp}. The boundaries defined in Fig. 2.1 are used. However, the minimum boundary for $\omega_{sp}T_{\theta_2}$ is different for the F-16 VISTA. The minimum values of ω_{sp} in Table 2.2 come into effect. The minimum boundary for level 1 becomes 1.7 instead of 1.3 as in Fig. 2.1. For level 2, the minimum boundary becomes 1.18 instead of 0.75. The results of a sample point will be presented followed by the results of a sample case. The results of all 12 cases are in Appendices (A-L).

4.1 Sample Point

This section will show the information required to map one point in case 2 from the $\omega_{sp}T_{\theta_2}, \zeta_{sp}, \tau_\theta$ criteria into both the Neal-Smith and Pilot-in-the-Loop criteria. The point will have level 1 handling qualities for the $\omega_{sp}T_{\theta_2}, \zeta_{sp}, \tau_\theta$ and the Pilot-in-the-Loop criteria, but

Table 4.1 Test Cases

Case	*Level*	ω_{BW}	τ_θ	T_{θ_2}
1	1	1.50	0.10	1.67
2	1	2.50	0.10	1.67
3	2	1.50	0.10	1.67
4	2	2.50	0.10	1.67
5	2	1.50	0.20	1.67
6	2	2.50	0.20	1.67
7	1	1.50	0.10	1.96
8	1	2.50	0.10	1.96
9	2	1.50	0.10	1.96
10	2	2.50	0.10	1.96
11	2	1.50	0.20	1.96
12	2	2.50	0.20	1.96

will have level 2 handling qualities for the Neal-Smith criteria. The required parameters that define the point are shown in Table 4.2.

Table 4.2 Sample Point

Case	*Level*	ω_{BW}	τ_θ	T_{θ_2}	ω_{sp}	ζ_{sp}
2	1	2.50	0.10	1.67	1.25	0.83

Equation 4.1 becomes the aircraft transfer function.

$$Y_c = \frac{(1.67 \cdot s + 1)\, e^{-0.10 \cdot s}}{s\,(s^2 + 2.08s + 1.56)} \tag{4.1}$$

Figure 4.1 illustrates that the sample point is contained by the level 1 boundary of the $\omega_{sp}T_{\theta_2}, \zeta_{sp}, \tau_\theta$ criteria. The next step involves determining whether lead or lag compensation is needed. On Fig. 4.2, (o) marks the open-loop magnitude and phase of Y_c where $\omega = \omega_{BW}$. Since $\angle Y_c < -180°$ at $\omega = \omega_{BW}$, lead compensation is needed. Figure 4.3 shows the result of $K \cdot Y_p Y_c$ after 'optimum' lead compensation has been applied. Both the closed-loop bandwidth requirement and closed-loop phase requirement are met simultaneously. From Fig. 4.4, the closed-loop droop satisfies the MIL-STD-1797A requirements, and

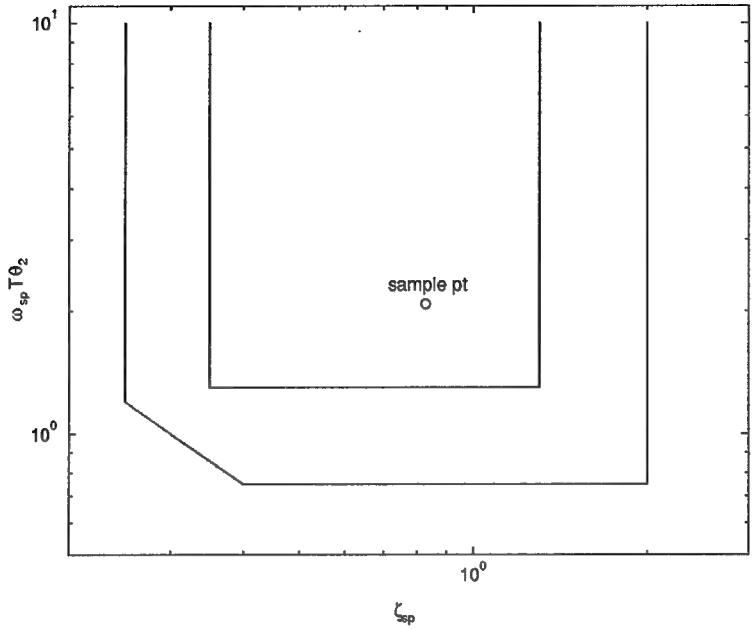

Figure 4.1 Sample Point on the $\omega_{sp}T_{\theta_2}, \zeta_{sp}, \tau_\theta$ Criteria

the closed-loop resonance is well below the 3 dB line. Figure 4.5 shows the closed-loop phase equals -90 degrees when $\omega = \omega_{BW}$. Hence, the point maps to level 1 for the Pilot-in-the-Loop criteria. Figure 4.6, however, shows the pilot's phase is high enough to map the point to the level 2 region on the Neal-Smith criteria. This sample point illustrates a conflicting result between the Neal-Smith and Pilot-in-the-Loop criteria. A sample case is mapped in the next section. Conflicts among all three criteria will be illustrated.

The computer code allows Fig. 4.1 - Fig. 4.6 to be viewed simultaneously on a computer monitor. When mapping a grid of points, the monitor displays all six plots for each point in a 'picture show' fashion. In other words, the monitor displays the results frame by frame at a user specified time increment. This tool enables the user to see trends as they occur and ensure the closed-loop bandwidth and droop requirements are being met for each point.

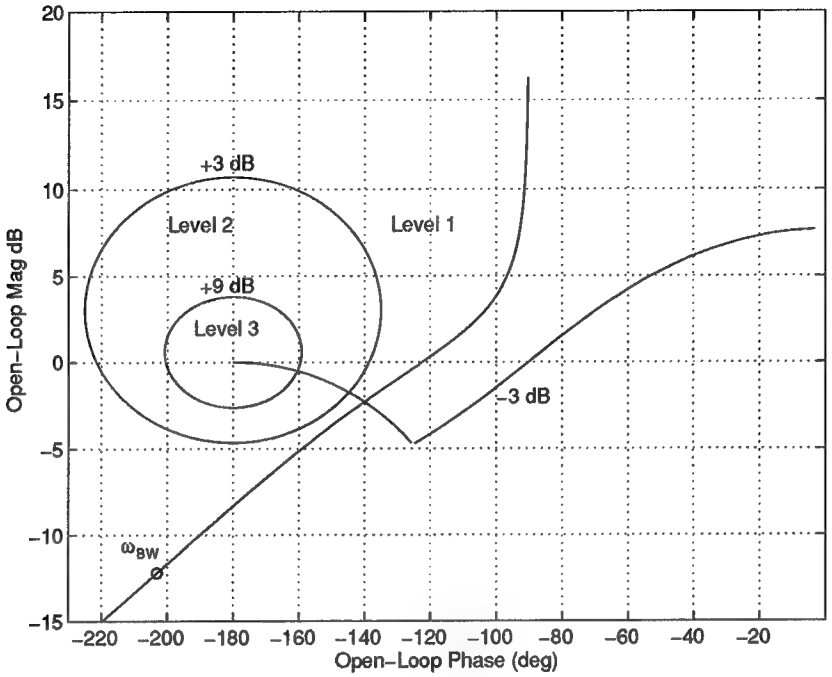

Figure 4.2 Nichols Chart of Y_c

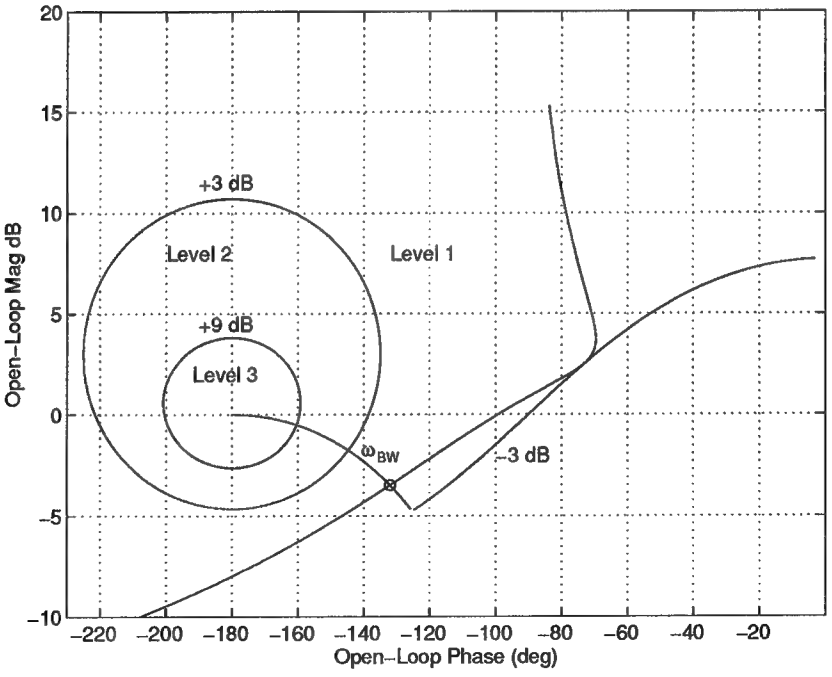

Figure 4.3 Nichols Chart of $Y_c Y_p$ after Convergence

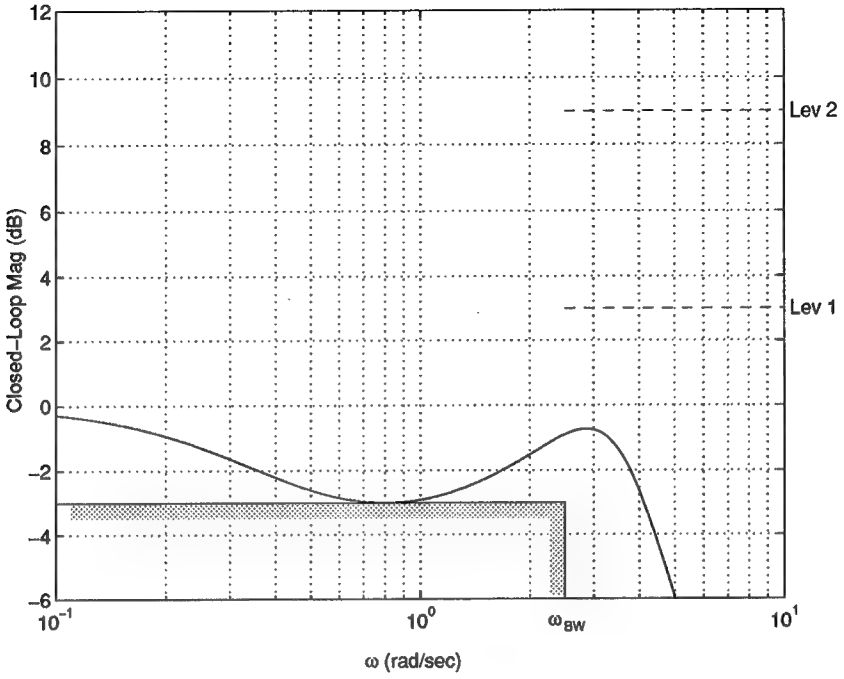

Figure 4.4 Closed-Loop Bode Mag Plot of Sample Point

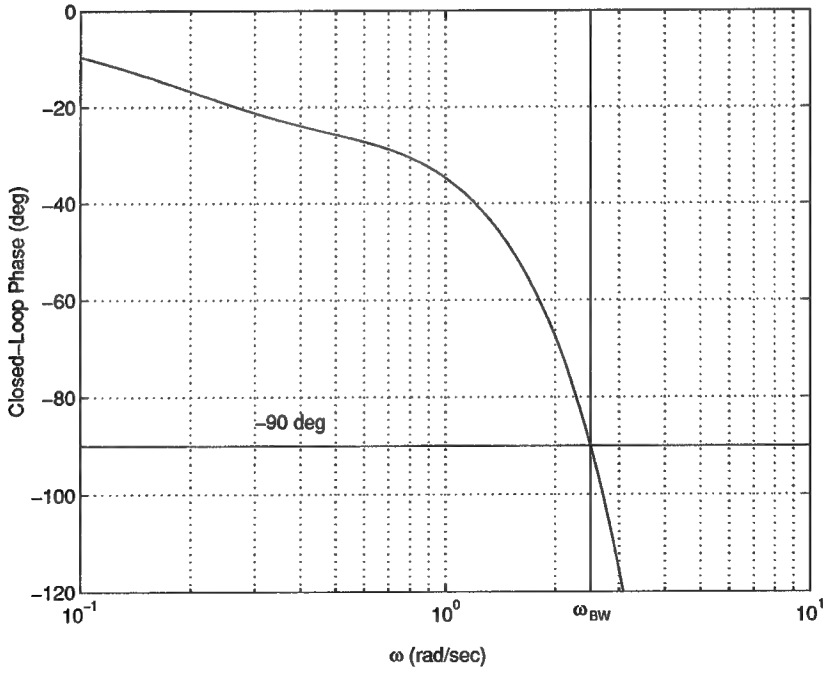

Figure 4.5 Closed-Loop Bode Phase Plot of Sample Point

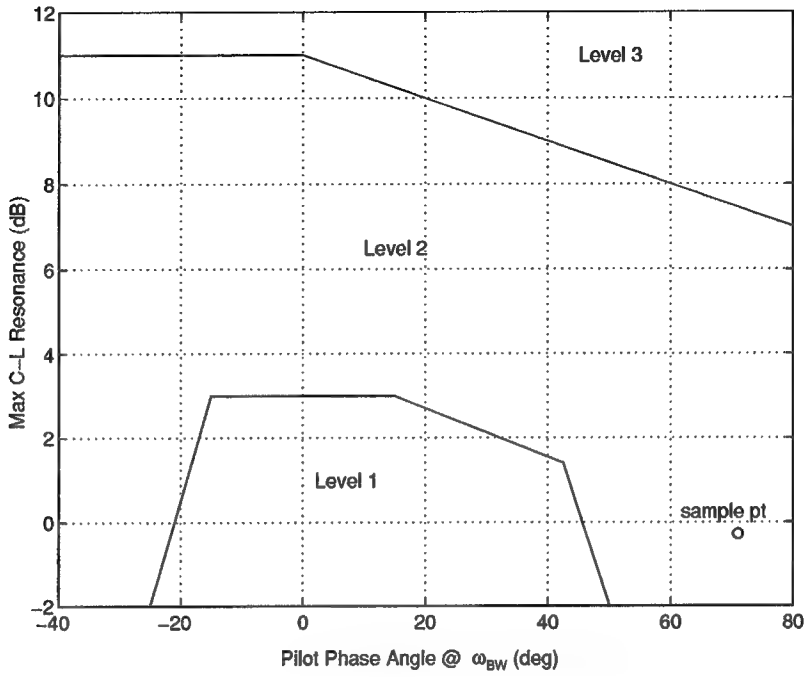

Figure 4.6 Sample Point Mapped to Neal-Smith Boundaries

4.2 Sample Case

This section will show all the plots involved in mapping 1 of the 12 cases. Case 2 from Table 4.1 will be mapped because it shows that infeasible regions are possible. Here, infeasible means the closed-loop bandwidth and droop requirements cannot be met simultaneously. When this happens, the 'constr' command in MATLAB^{TM} produces a 'Warning: No feasible solution found' message. Figure 4.7 shows the Nichol's plot of Y_c for one of the points in the infeasible region shown in Fig. 4.8. The point where $\omega = \omega_{BW}$ (o) is to the left of the target zone, and the magnitude is 0 dB. Also, the droop is below the -3 dB closed-loop droop line. The $-90°$ closed-loop phase line does not extend above the 0 dB open-loop magnitude line. Lead compensation would cause the point to move up and to the right. The open-loop magnitude of (o) would move above the 0 dB line. The gain could be adjusted to lower the curve to meet the closed-loop bandwidth constraint. This would cause the droop to fall back below the -3 dB closed-loop droop line. The result is both constraints cannot be met simultaneously. Hence, the point cannot be mapped into the Neal-Smith criteria and will

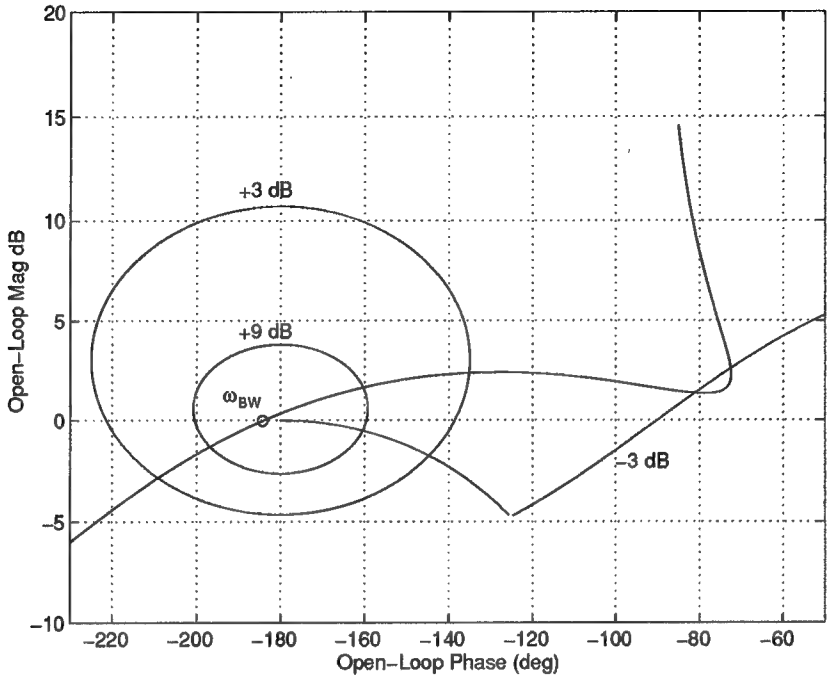

Figure 4.7 Infeasible Point from the $\omega_{sp}T_{\theta_2}, \zeta_{sp}, \tau_\theta$ Criteria

be considered infeasible. Infeasible regions occur because the assumed pilot model cannot provide the required compensation needed to meet both constraints. These regions occur for both lead and lag compensation. The results show that infeasible regions are only found in regions corresponding to Neal-Smith and Pilot-in-the-Loop level 3. The next few paragraphs describe the plots involved in mapping Case 2. Six plots will be made for each case. Again, the plots for all 12 cases are shown in Appendices (A-L).

4.2.1 Plot 1. This plot shows the region from the $\omega_{sp}T_{\theta_2}, \zeta_{sp}, \tau_\theta$ criteria that will be mapped. The region is divided into areas requiring lead compensation and areas requiring lag compensation. The infeasible area is also shown. Figure 4.8 shows that the dividing line between lead and lag compensation is fairly smooth. If the logic from Chapter III determines that lead compensation is needed, that point is flagged 'lead'. Otherwise, it is flagged 'lag'. The original grid can then be divided into a lead area and a lag area. Corners on the grid, as well as other dividing points, are marked with letters to show where those points end up

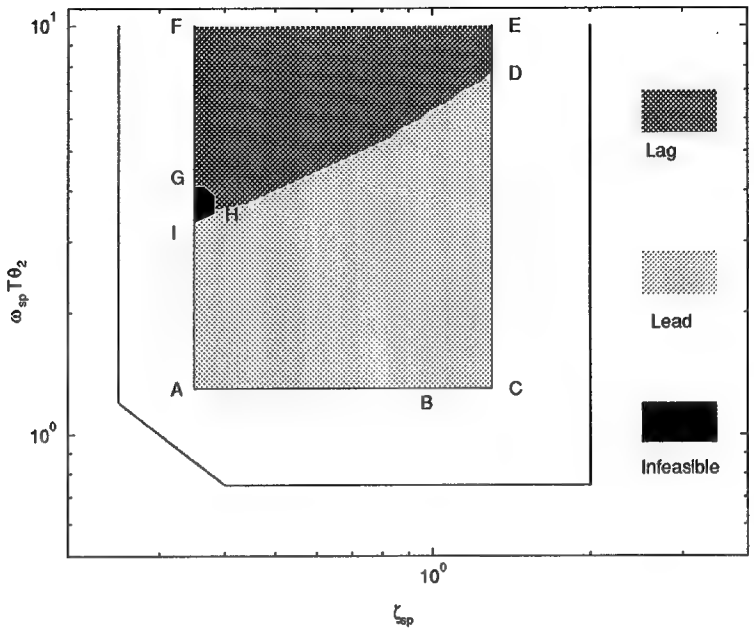

Figure 4.8 (Plot 1) Lead, Lag, and Infeasible Regions on $\omega_{sp}T_{\theta_2}, \zeta_{sp}, \tau_\theta$

after the mapping. Level 1 mappings use an evenly spaced 30x50 grid on a log-log scale. The approach in Chapter III is called 1500 times. Data required to produce the information in Fig. 4.1 - Fig. 4.6 is calculated and stored for all 1500 points. A mapping of this size takes about three hours to run on a Sun SPARCstation 20. Level 2 mappings use an evenly spaced 50x60 grid on a log-log scale. The computer time doubles by increasing the number of points to 3000.

4.2.2 Plot 2. This plot shows the region from plot 1 mapped into the Neal-Smith criteria. Figure 4.9 shows that conflicts indeed exist between the $\omega_{sp}T_{\theta_2}, \zeta_{sp}, \tau_\theta$ and Neal-Smith Criteria. The shaded regions in Fig. 4.9 were made by connecting the outer points that form the boundary for a given area. The marked points from Fig. 4.8 are also shown on Fig. 4.9. The letters G, H, and I are on the border of the infeasible region shown in Fig. 4.8. These letters map well into the Neal-Smith level 3 region on Fig. 4.9.

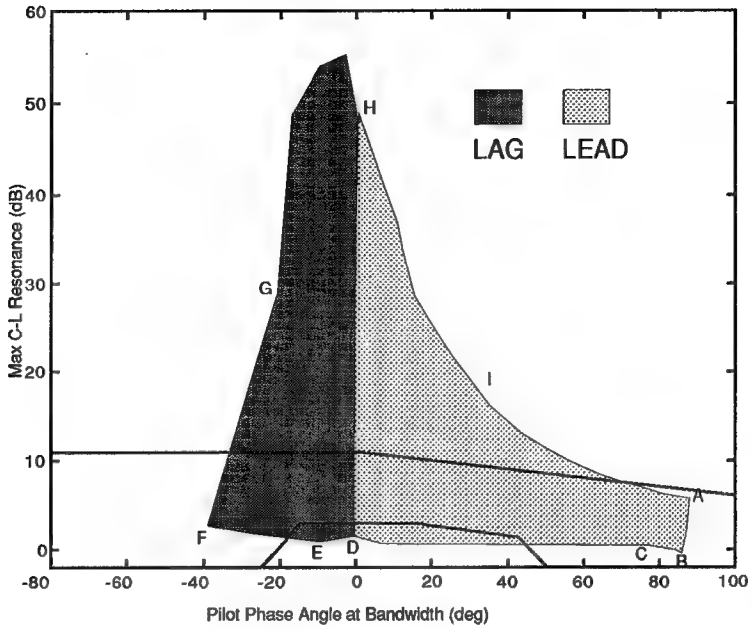

Figure 4.9 (Plot 2) $\omega_{sp}T_{\theta_2}, \zeta_{sp}, \tau_\theta$ Mapped into Neal-Smith

4.2.3 Plot 3 and Plot 4. Plot 3 is the same as plot 2 except regions corresponding to Neal-Smith levels 1-3 are highlighted. Figure 4.10 shows the three different handling qualities regions according to Neal-Smith standards. Plot 4 shows these highlighted regions mapped back into the $\omega_{sp}T_{\theta_2}, \zeta_{sp}, \tau_\theta$ criteria. Like Fig. 4.9, Fig. 4.11 shows both regions of agreement and regions of conflict. The region of agreement marked by J, K, and L is fairly small compared to original level 1 region from the $\omega_{sp}T_{\theta_2}, \zeta_{sp}, \tau_\theta$ criteria.

4.2.4 Plot 5 and Plot 6. Plot 5 is the same as plot 2 except regions corresponding to Pilot-in-the-Loop levels 1-3 are highlighted. Figure 4.12 shows the three different handling qualities regions according to Pilot-in-the-Loop standards. Plot 6 shows these highlighted regions mapped back into the $\omega_{sp}T_{\theta_2}, \zeta_{sp}, \tau_\theta$ criteria. Not surprisingly, the level 1 region of agreement between the $\omega_{sp}T_{\theta_2}, \zeta_{sp}, \tau_\theta$ and Pilot-in-the-Loop criteria is larger than the level 1 region of agreement between the $\omega_{sp}T_{\theta_2}, \zeta_{sp}, \tau_\theta$ and Neal-Smith criteria. The Pilot-in-the-Loop criteria does not take pilot phase angle into consideration. Hence, its level 1 boundary

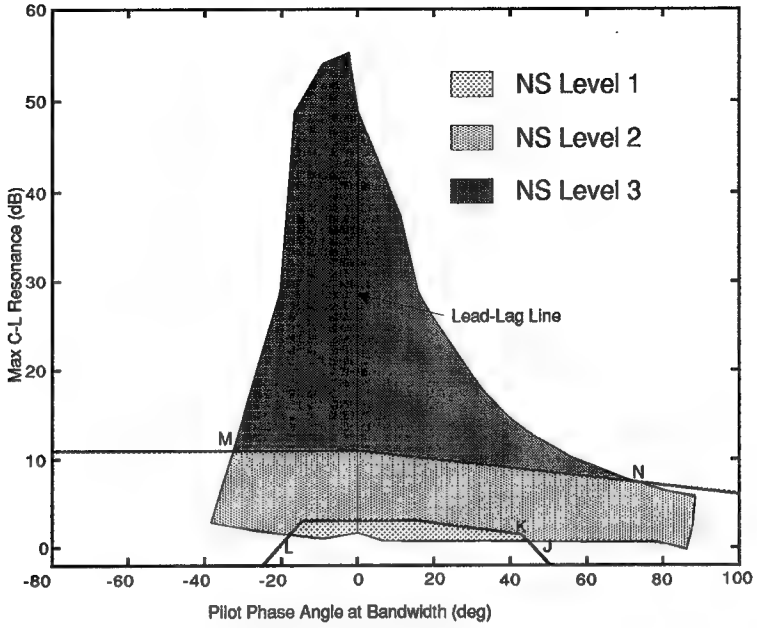

Figure 4.10 (Plot 3) Neal-Smith Regions (NS)

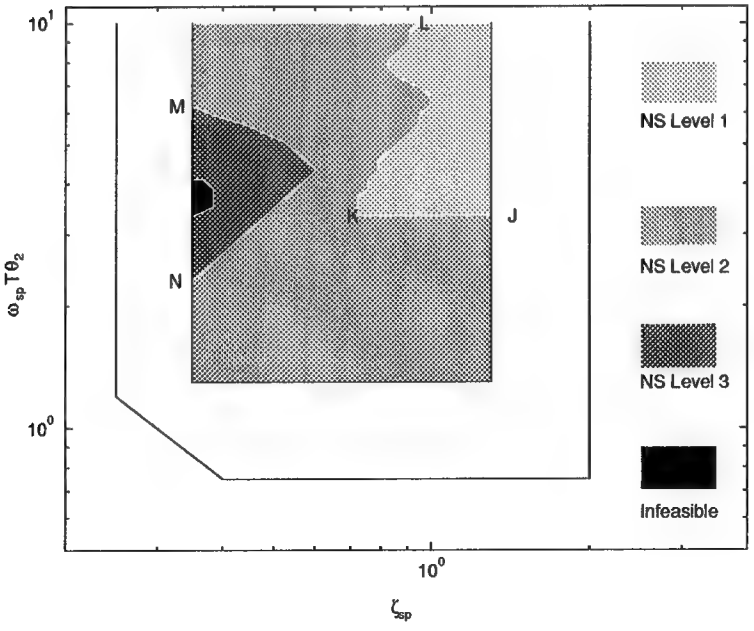

Figure 4.11 (Plot 4) Neal-Smith Regions Mapped into $\omega_{sp}T_{\theta_2}, \zeta_{sp}, \tau_\theta$

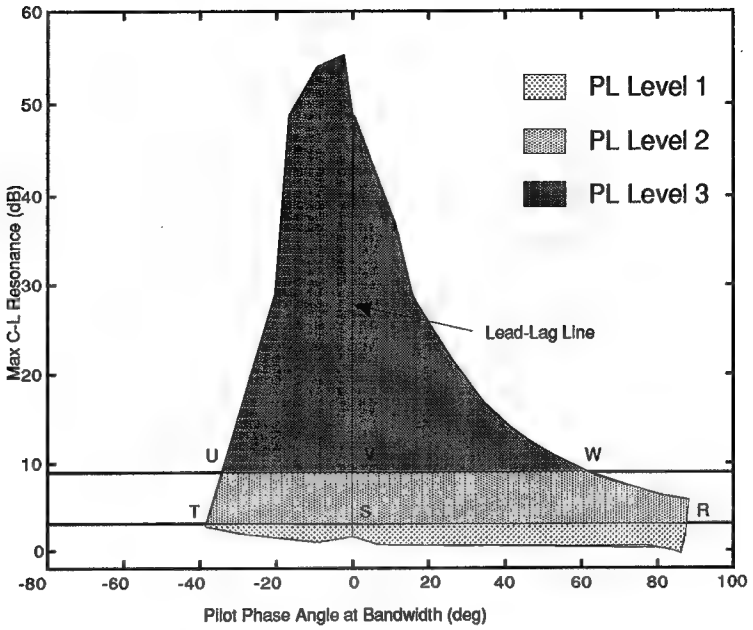

Figure 4.12 (Plot 5) Pilot-in-the-Loop Regions (PL)

shows up a straight line at 3 dB on Fig. 4.10. Compared to the Neal-Smith level 1 boundary in Fig. 4.9, the Pilot-in-the-Loop will always cover an area greater than or equal to the Neal-Smith criteria. This is evident when comparing Fig. 4.11 to Fig. 4.13.

The level 2 region is not as straightforward. The Pilot-in-the-Loop level 2 border is a straight line at 9 dB on Fig. 4.10. The Neal-Smith level 2 border is greater than 9 dB for pilot phase angles less than about 40° and less than 9 dB elsewhere. The level 1 borders for both criteria have already been shown to be different. The level 1 borders determine the lower limit of the level 2 regions. Since both the upper and lower limits are different, no general conclusions can be made. For the sample case, the region corresponding to Pilot-in-the-Loop level 3 was greater than Neal-Smith level 3. This again can be seen by comparing Fig. 4.11 to Fig. 4.13.

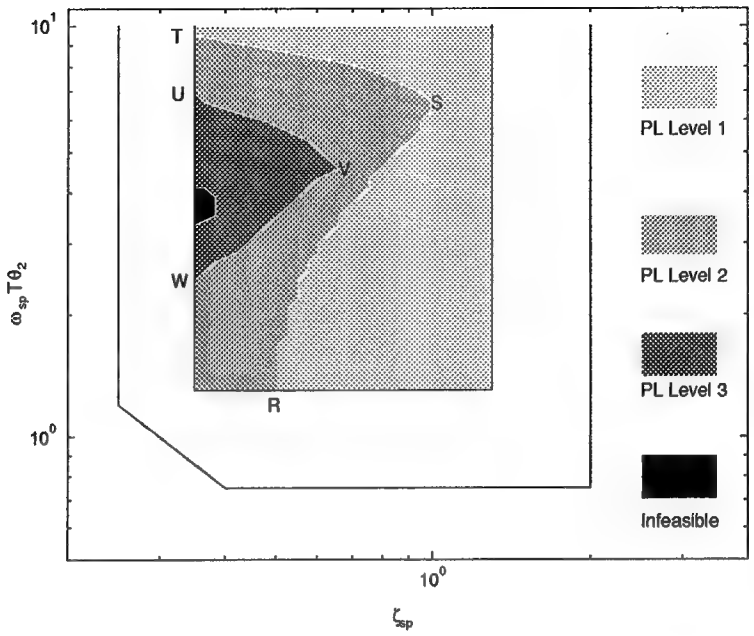

Figure 4.13 (Plot 6) Pilot-in-the-Loop Mapped into the $\omega_{sp}T_{\theta_2}, \zeta_{sp}, \tau_\theta$

4.3 Regions Excluded by $(\omega_{sp})_{min}$

As explained earlier, the minimum boundary for $\omega_{sp}T_{\theta_2}$ is moved up for the F-16 VISTA. This excludes parts of the general level 1 and level 2 regions on the $\omega_{sp}T_{\theta_2}, \zeta_{sp}, \tau_\theta$ criteria. These regions were mapped separately for Cases 7-12. Plots 4 and 6 were also generated for the excluded regions and appear in Appendices (G-L). They are designated with an 'x'. Since the excluded regions are fairly small, only one plot is generated to show the $\omega_{sp}T_{\theta_2}, \zeta_{sp}, \tau_\theta$ criteria mapping. Both Neal-Smith and Pilot-in-the-Loop boundaries are shown on the same plot. Individual points are used instead of the shaded regions. Figure 4.14 is a sample of this mapping. As seen in Appendices(G-L), the excluded regions map to areas in the lower right corner of the Neal-Smith criteria. This generates a conflict for level 1 mappings.

The Pilot-in-the-Loop criteria stayed one level above the Neal-Smith criteria. If the excluded region mapped to Neal-Smith level 2, it mapped to Pilot-in-the-Loop level 1. Again, this is not surprising since the Pilot-in-the-Loop criteria does not account for pilot phase. The only general statement that can be made is the same as above. The Neal-Smith criteria will

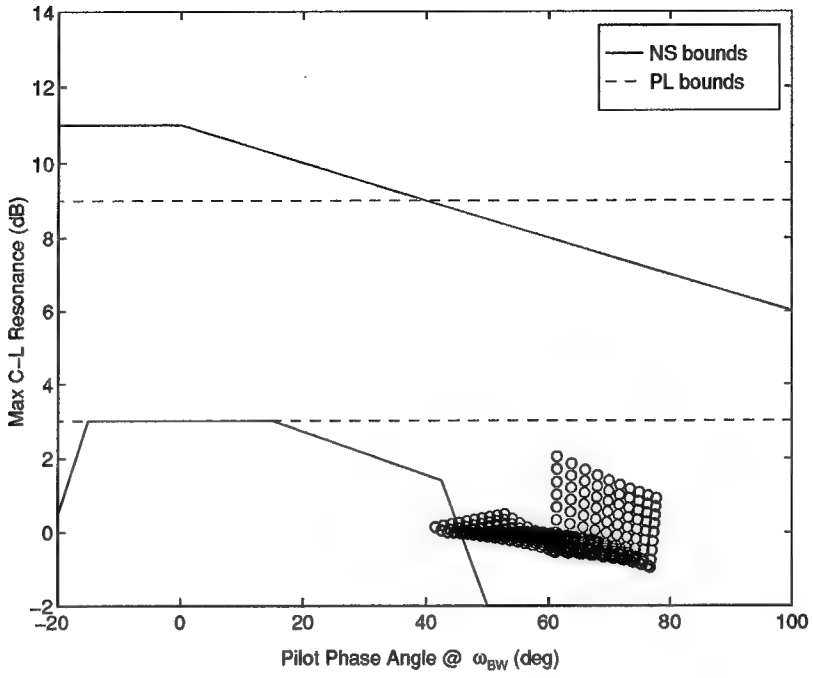

Figure 4.14 (Case 7x) Mapping of Excluded Region from $\omega_{sp}T_{\theta_2}, \zeta_{sp}, \tau_\theta$

never predict level 1 handling qualities more times than the Pilot-in-the-Loop criteria. That is, the Pilot-in-the-Loop criteria is more liberal for level 1 handling qualities.

4.4 Trends

For a better understanding of trends, all the plots in Appendices (A-L) need to be examined. This section will present a simplified analysis of trends. Rather than plotting all 12 cases on a plot, an example comparing two cases is shown for each trend. The examples represent general trends. Trends shown are for the $\omega_{sp}T_{\theta_2}, \zeta_{sp}, \tau_\theta$ and Neal-Smith mappings.

4.4.1 Effect of Changing ω_{BW}. The figures referenced in this paragraph apply to the Lear jet. Increasing ω_{BW} from 1.5 to 2.5 (rad/sec) causes the line dividing lead and lag regions on the $\omega_{sp}T_{\theta_2}, \zeta_{sp}, \tau_\theta$ criteria to move up as shown in Fig. 4.15. The region corresponding to Neal-Smith and $\omega_{sp}T_{\theta_2}, \zeta_{sp}, \tau_\theta$ level 1 moves up and to the right as shown in Fig. 4.16.

Finally, the region corresponding to Neal-Smith level 2 moves up and to the right as shown in Fig. 4.17.

4.4.2 Effect of Changing T_{θ_2}. The figures referenced in this paragraph correspond to $\omega_{BW} = 1.5$ (rad/sec). Increasing T_{θ_2} from 1.67 (Lear jet) to 1.96 (F-16 VISTA) causes the line dividing lead and lag regions on the $\omega_{sp}T_{\theta_2}, \zeta_{sp}, \tau_\theta$ criteria to move up as shown in Fig. 4.18. The region corresponding to Neal-Smith and $\omega_{sp}T_{\theta_2}, \zeta_{sp}, \tau_\theta$ level 1 moves slightly up and to the right as shown in Fig. 4.19. Finally, the region corresponding to Neal-Smith level 2 moves up and to the right as shown in Fig. 4.20.

4.4.3 Effect of Changing τ_θ. The figures referenced in this paragraph correspond to $\omega_{BW} = 1.5$ (rad/sec). Increasing τ_θ from 0.1 to 0.2 seconds causes the line dividing lead and lag regions on the $\omega_{sp}T_{\theta_2}, \zeta_{sp}, \tau_\theta$ criteria to move up as shown in Fig. 4.21. The region corresponding to Neal-Smith and $\omega_{sp}T_{\theta_2}, \zeta_{sp}, \tau_\theta$ level 1 moves up and to the right as shown in Fig. 4.22. Finally, the region corresponding to Neal-Smith level 2 moves up and to the right as shown in Fig. 4.23.

4.5 Summary

The information required to map 12 cases was outlined in Table 4.1. The results of a sample point and sample case were discussed. Parametric studies were performed and analyzed for trends. Increasing ω_{BW}, T_{θ_2}, or τ_θ resulted in smaller regions of agreement.

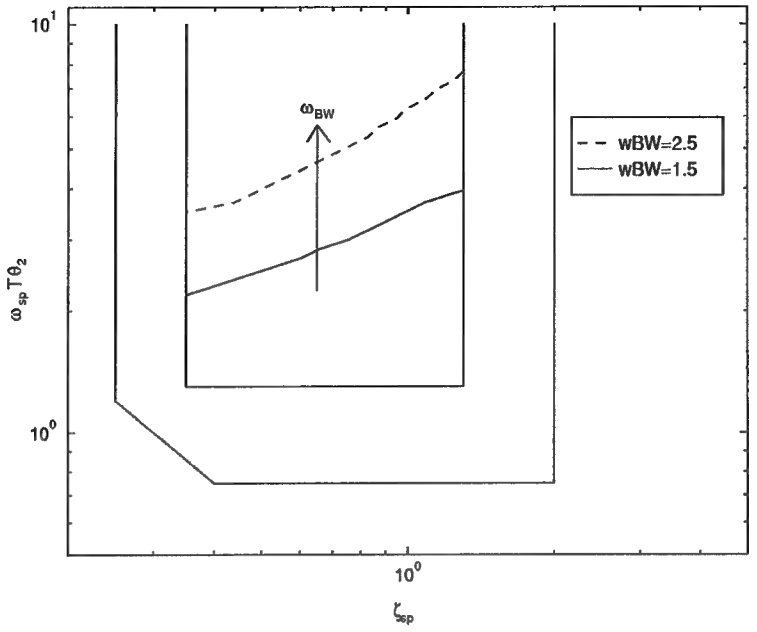

Figure 4.15 Effect of Increasing ω_{BW} on Lead and Lag

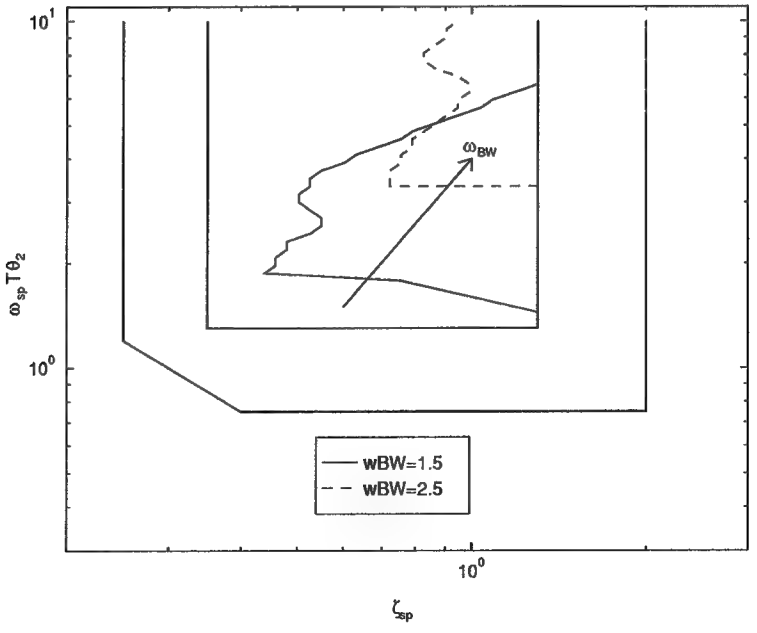

Figure 4.16 Effect of Increasing ω_{BW} on Level 1 Region of Agreement

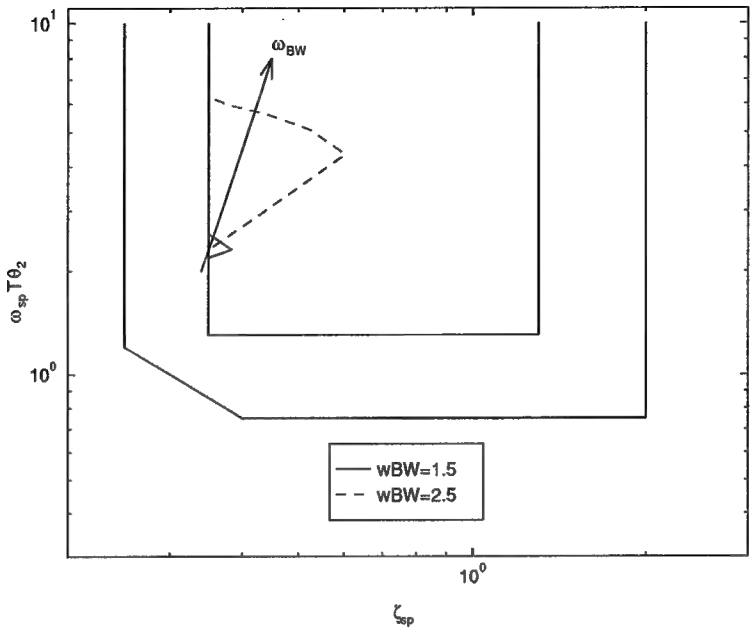

Figure 4.17 Effect of Increasing ω_{BW} on NS Level 2 Region

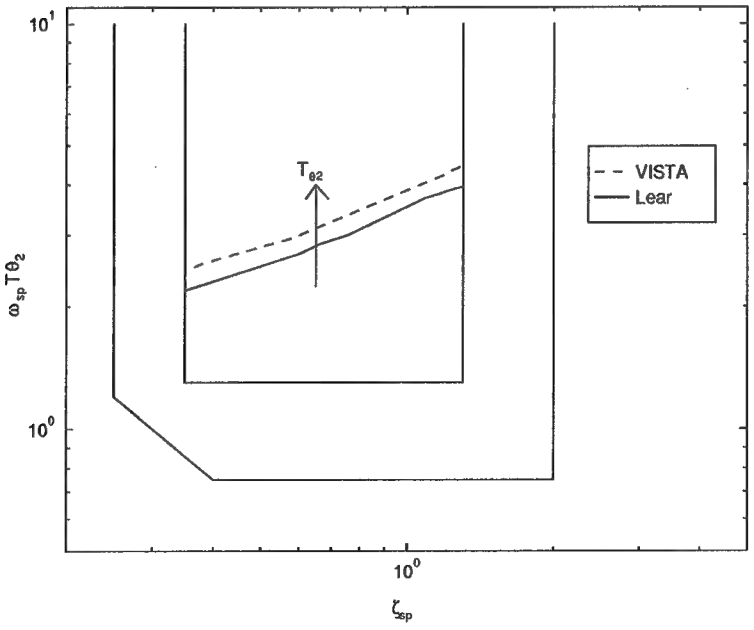

Figure 4.18 Effect of Increasing T_{θ_2} on Lead and Lag

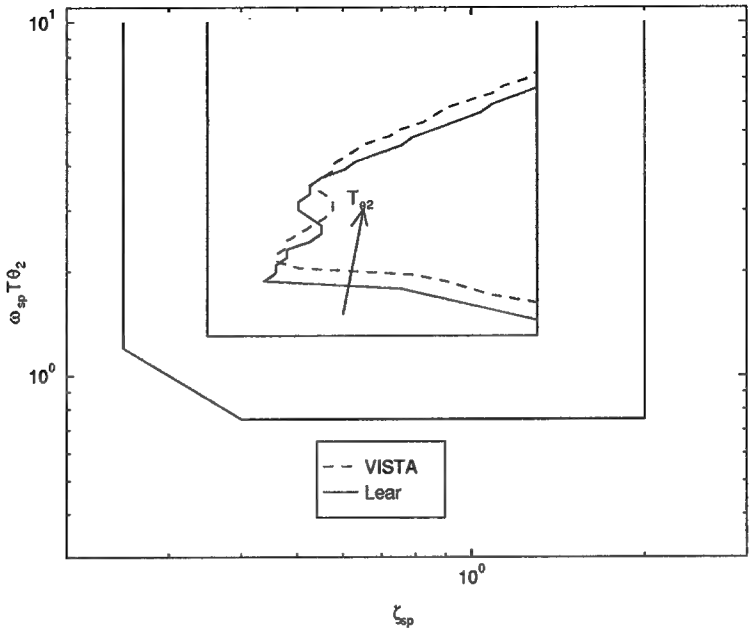

Figure 4.19 Effect of Increasing T_{θ_2} on Level 1 Region of Agreement

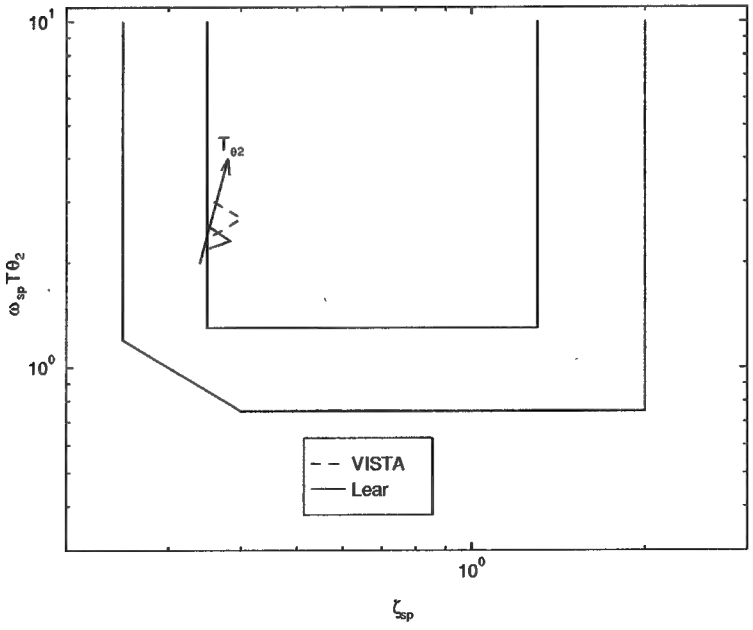

Figure 4.20 Effect of Increasing T_{θ_2} on NS Level 2 Region

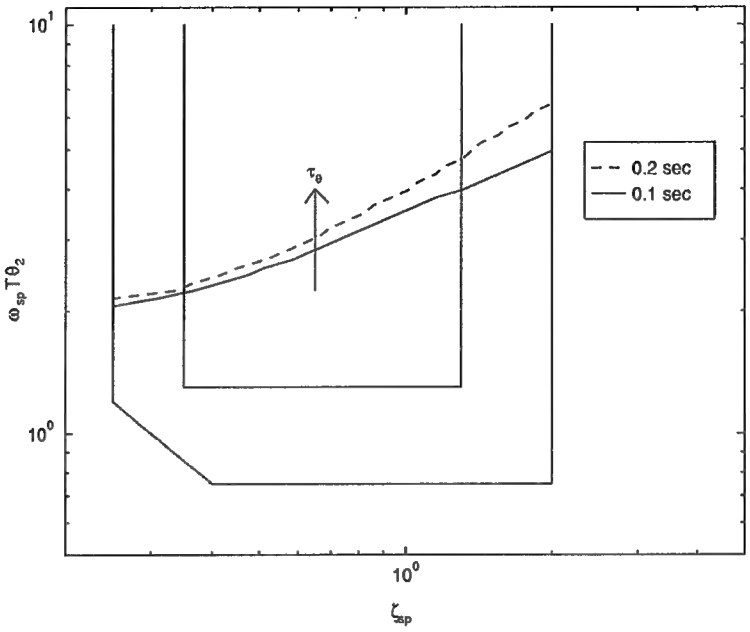

Figure 4.21 Effect of Increasing τ_θ on Lead and Lag

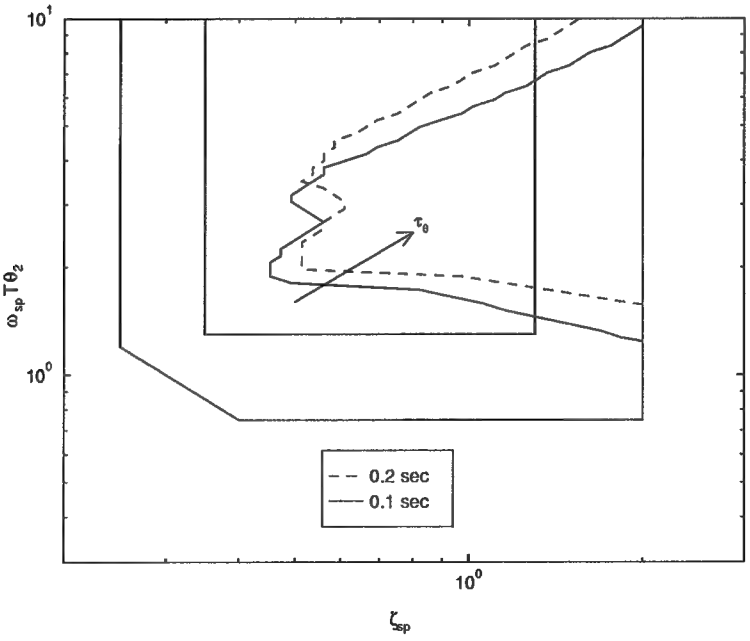

Figure 4.22 Effect of Increasing τ_θ on Level 1 Region of Agreement

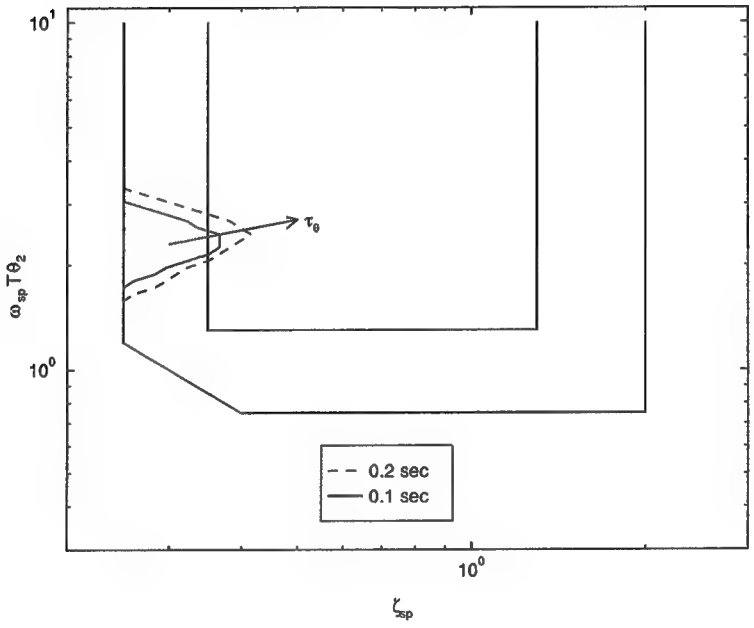

Figure 4.23 Effect of Increasing τ_θ on NS Level 2 Region

V. Conclusions and Recommendations

5.1 Conclusions

All the objectives for this thesis were accomplished. The development of a computerized tool that performs a mapping of the $\omega_{sp}T_{\theta_2}, \zeta_{sp}, \tau_\theta$ criteria into the Neal-Smith criteria has been presented. The problem of calculating the parameters of the Neal-Smith pilot model was posed as a constrained optimization problem. Initially, the problem involved the three unknowns K, T_{p_1}, and T_{p_2}. Deriving equations for 'optimal' lead and 'optimal' lag compensation left T_{p_2} in terms of T_{p_1}. Deriving an equation for the closed-loop phase and setting it equal to $-90°$ left K in terms of T_{p_1}. Finding the solution that met both the closed-loop bandwidth and droop requirements came down to a one-dimensional search over T_{p_1}. Sequential Quadratic Programming was needed to solve for T_{p_1} because no closed form solutions exist for the complicated functions of frequency. Bookkeeping of the original mapping produced the information required to do an inverse mapping.

Six cases for two T_{θ_2} values were mapped. The $\omega_{sp}T_{\theta_2}, \zeta_{sp}, \tau_\theta$ criteria was mapped into both the Neal-Smith and Pilot-in-the-Loop criteria. The regions corresponding to both Neal-Smith and Pilot-in-the-Loop levels 1-3 were mapped back into $\omega_{sp}T_{\theta_2}, \zeta_{sp}, \tau_\theta$ criteria. Regions of agreement and regions of conflict could be easily seen in the six plots that were generated for each case. The trends of varying the three fixed parameters were identified.

5.2 Recommendations for Future Research

The results produced by this thesis lay the foundation for a flight test program. Selected points from any region of conflict could be flown to determine the actual handling qualities. The results could then be analyzed to determine if either the $\omega_{sp}T_{\theta_2}, \zeta_{sp}, \tau_\theta$ or Neal-Smith criteria needs modification. The information learned from this type of analysis is the next step towards deriving one clear-cut, generally applicable set of requirements.

Appendix A. Case 1

Case	*Level*	ω_{BW}	τ_θ	T_{θ_2}
1	1	1.50	0.10	1.67

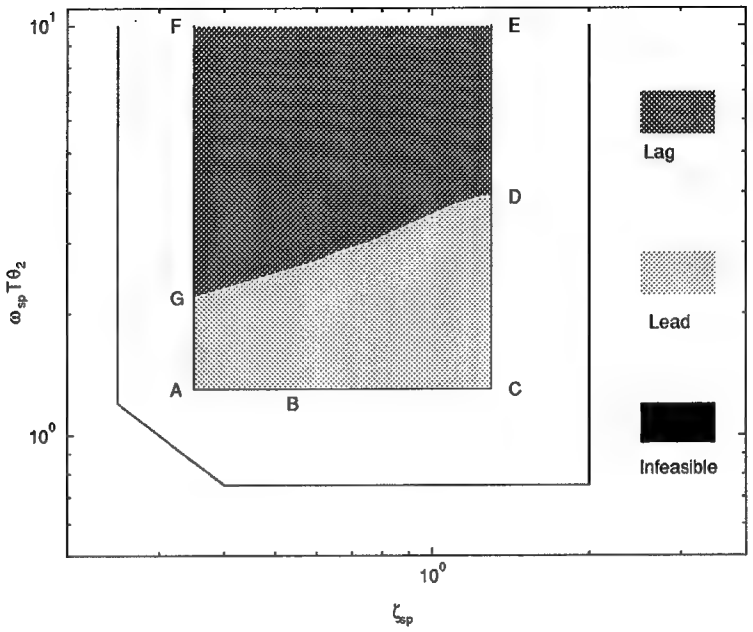

Figure A.1 (Case 1) Lead, Lag, and Infeasable Regions on $\omega_{sp}T_{\theta_2}, \zeta_{sp}, \tau_\theta$

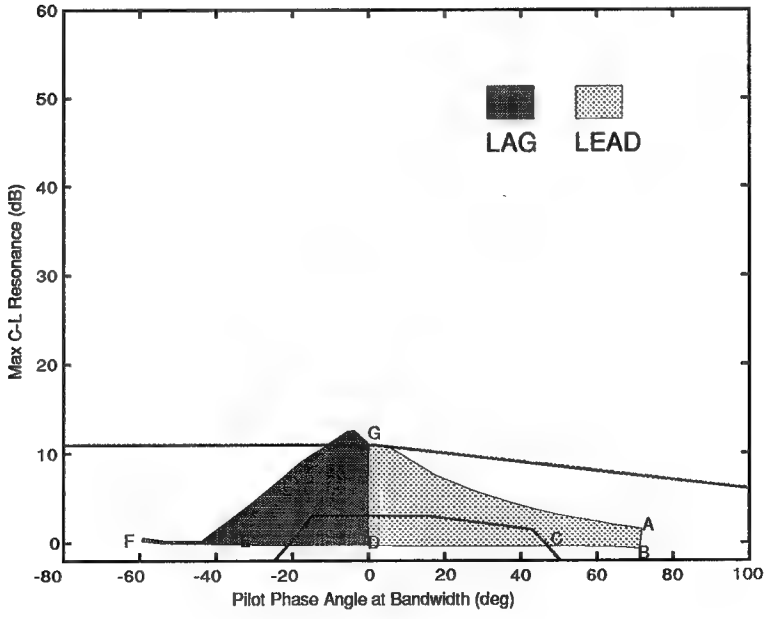

Figure A.2 (Case 1) $\omega_{sp}T_{\theta_2}, \zeta_{sp}, \tau_\theta$ Mapped into Neal-Smith

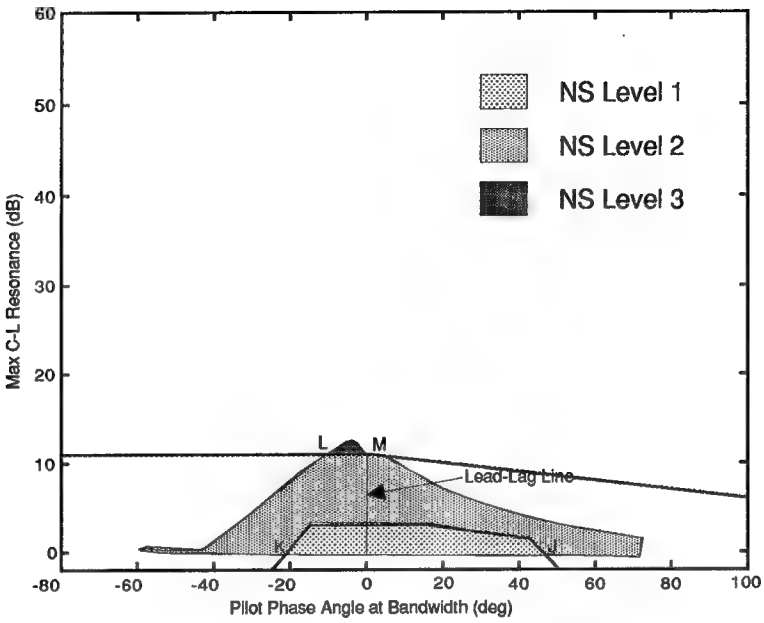

Figure A.3 (Case 1) Neal-Smith Regions (NS)

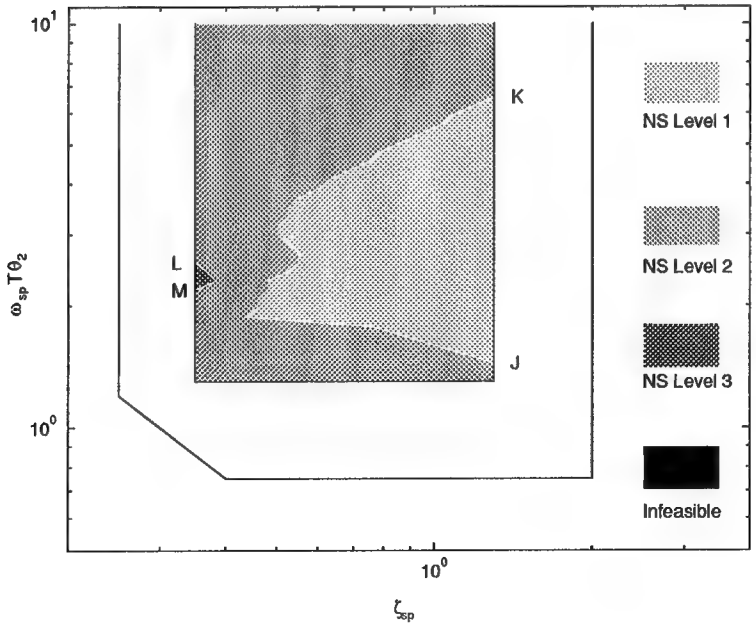

Figure A.4 (Case 1) Neal-Smith Regions Mapped into $\omega_{sp}T_{\theta_2}, \zeta_{sp}, \tau_\theta$

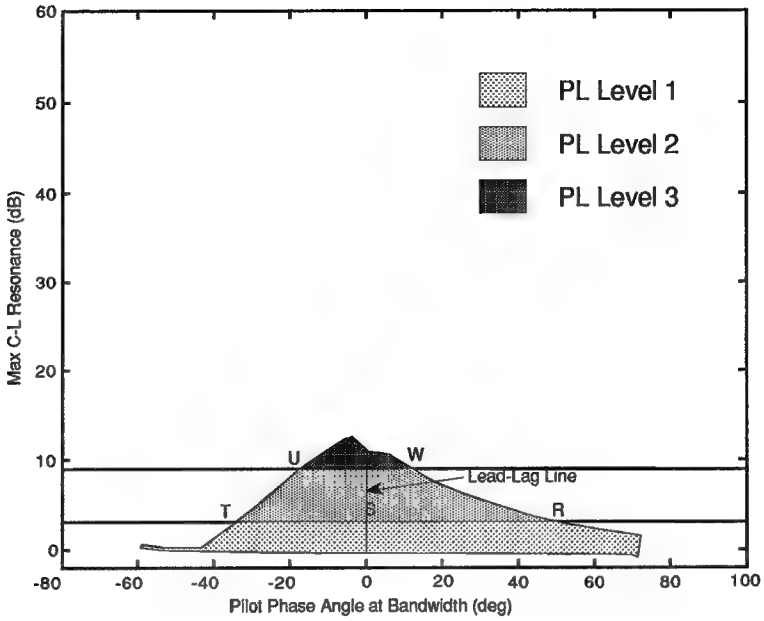

Figure A.5 (Case 1) Pilot-in-the-Loop Regions (PL)

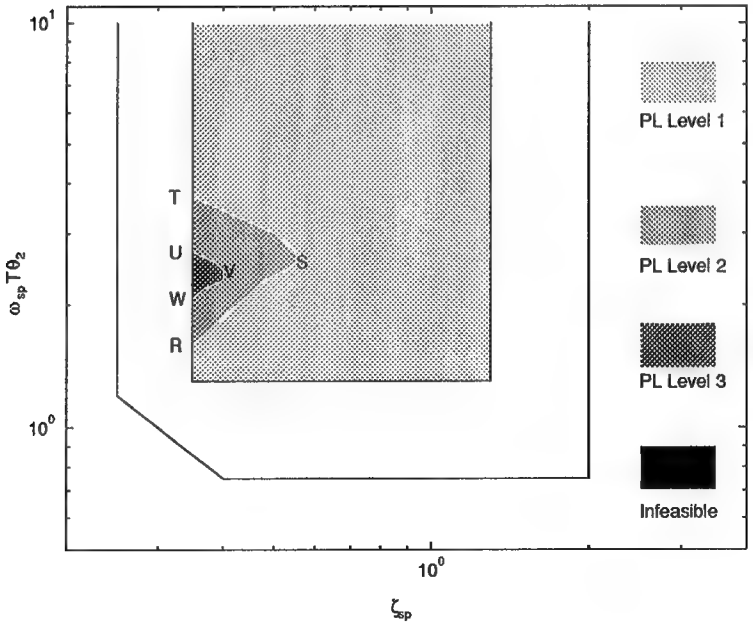

Figure A.6 (Case 1) Pilot-in-the-Loop Mapped into the $\omega_{sp}T_{\theta_2}, \zeta_{sp}, \tau_\theta$

Appendix B. Case 2

Case	*Level*	ω_{BW}	τ_θ	T_{θ_2}
2	1	2.50	0.10	1.67

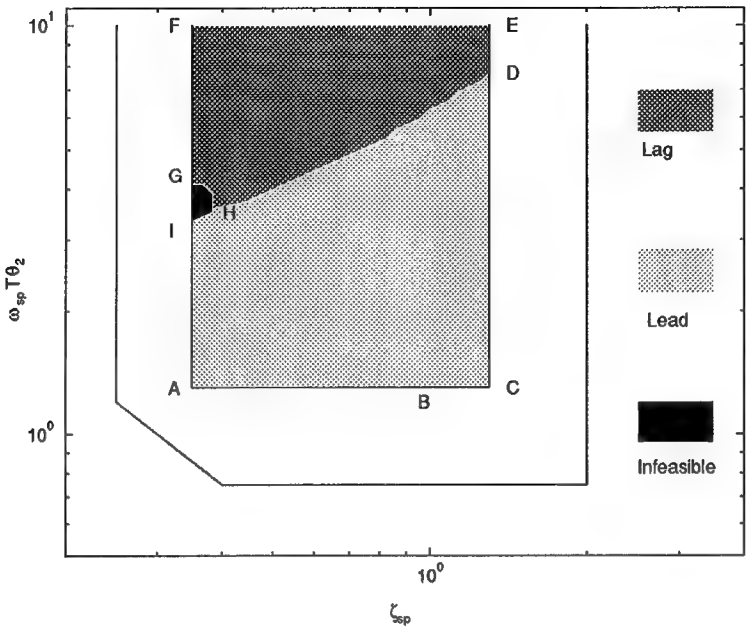

Figure B.1 (Case 2) Lead, Lag, and Infeasible Regions on $\omega_{sp}T_{\theta_2}, \zeta_{sp}, \tau_\theta$

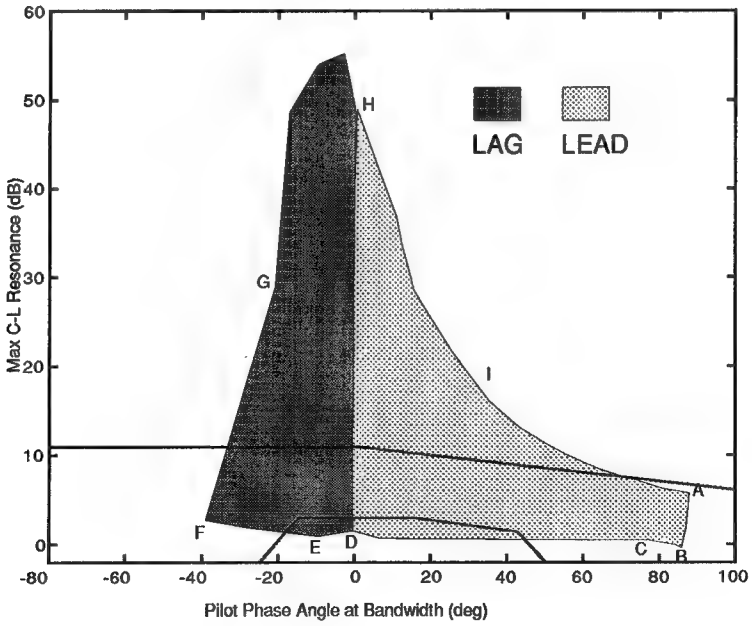

Figure B.2 (Case 2) $\omega_{sp}T_{\theta_2}, \zeta_{sp}, \tau_\theta$ Mapped into Neal-Smith

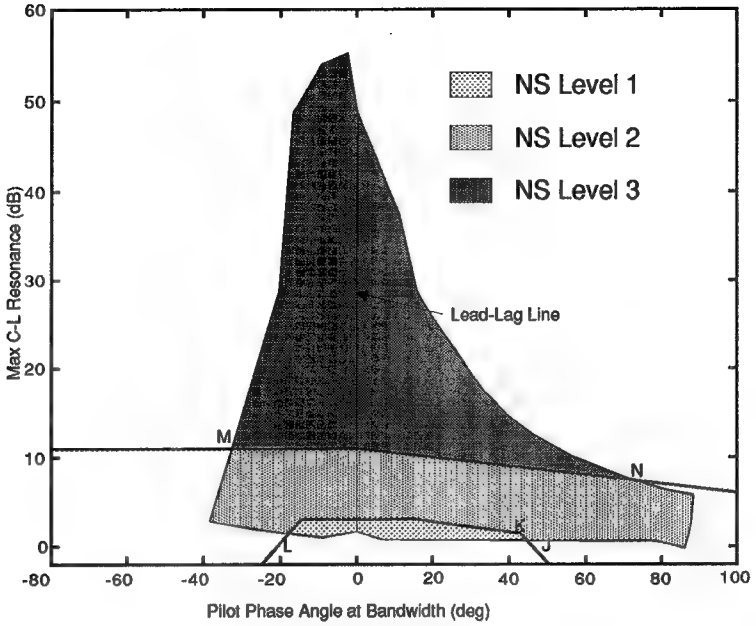

Figure B.3 (Case 2) Neal-Smith Regions (NS)

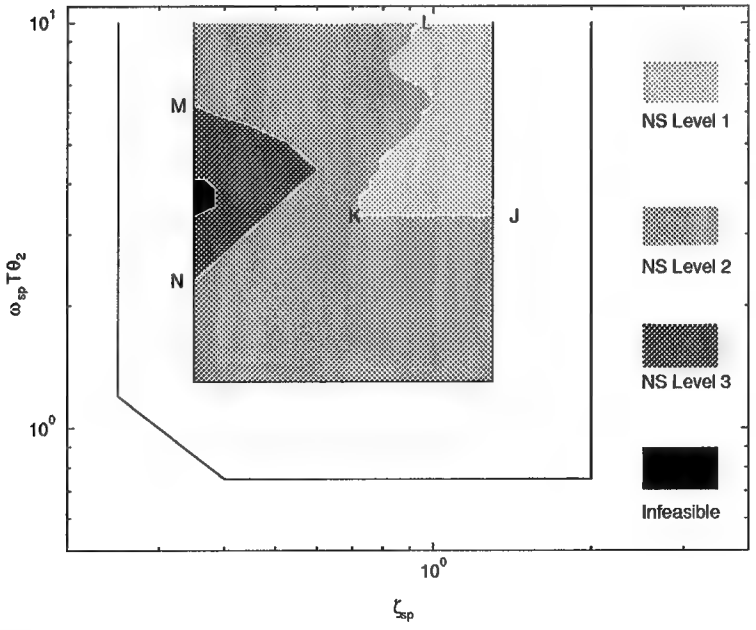

Figure B.4 (Case 2) Neal-Smith Regions Mapped into $\omega_{sp}T_{\theta_2}, \zeta_{sp}, \tau_\theta$

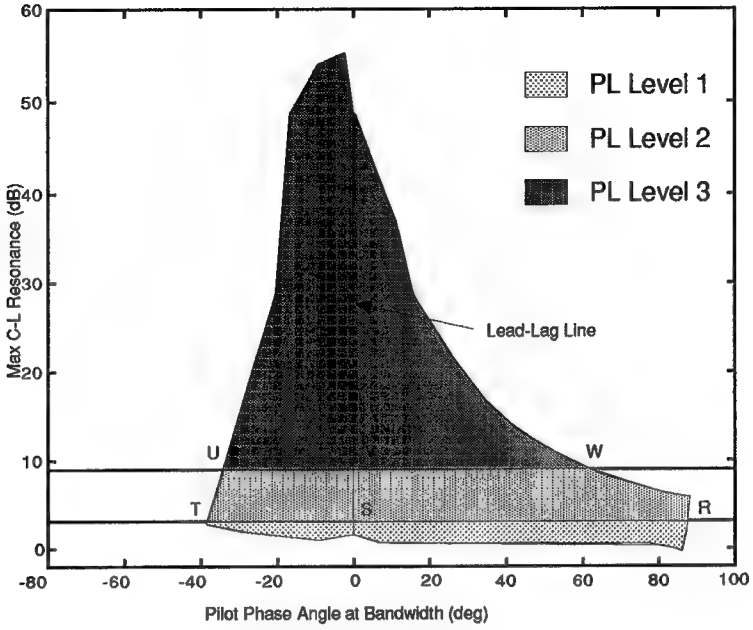

Figure B.5 (Case 2) Pilot-in-the-Loop Regions (PL)

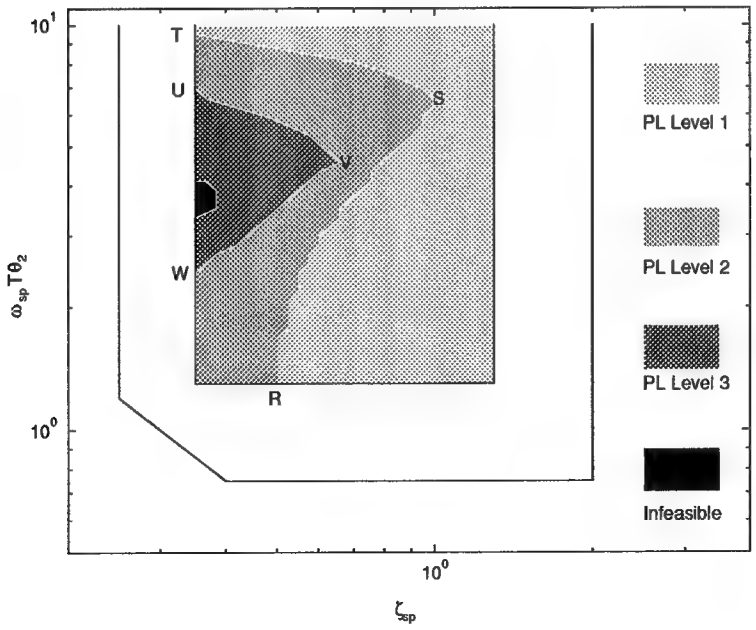

Figure B.6 (Case 2) Pilot-in-the-Loop Mapped into the $\omega_{sp}T_{\theta_2}, \zeta_{sp}, \tau_\theta$

Appendix C. Case 3

Case	*Level*	ω_{BW}	τ_θ	T_{θ_2}
3	2	1.50	0.10	1.67

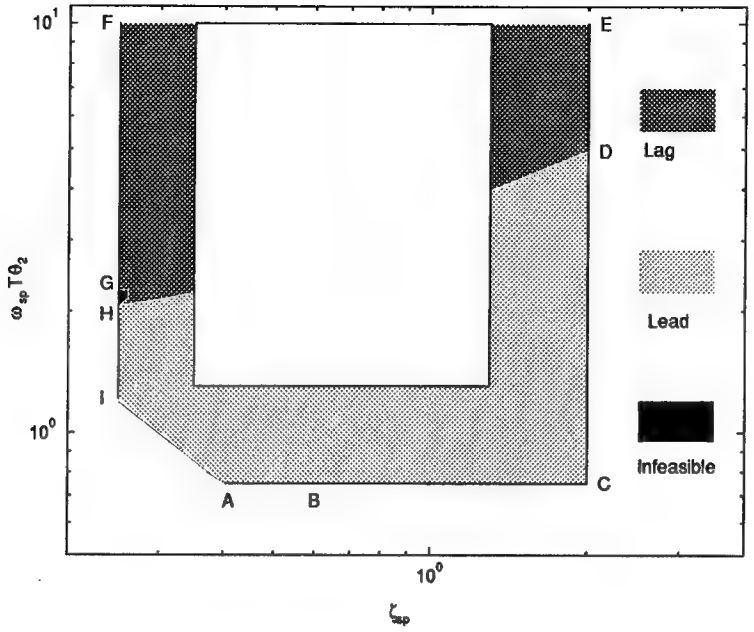

Figure C.1 (Case 3) Lead, Lag, and Infeasible Regions on $\omega_{sp}T_{\theta_2}, \zeta_{sp}, \tau_\theta$

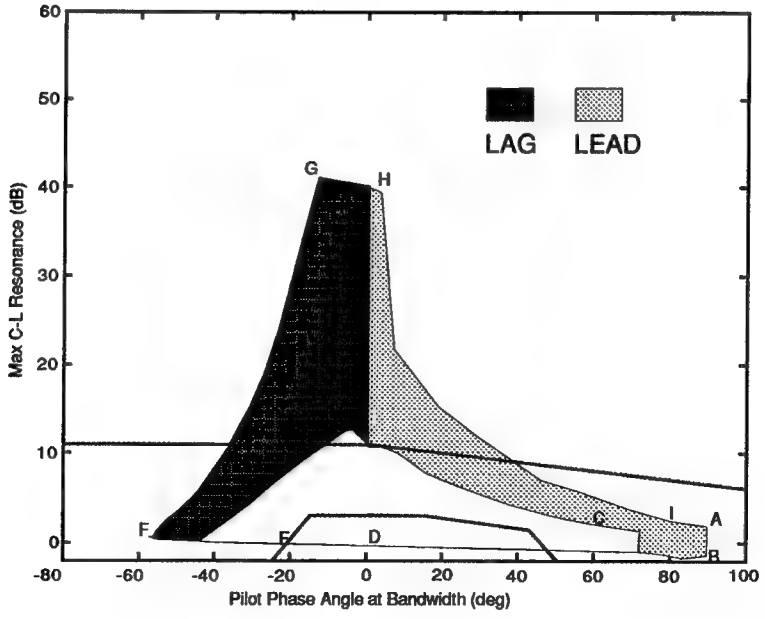

Figure C.2 (Case 3) $\omega_{sp}T_{\theta_2}, \zeta_{sp}, \tau_\theta$ Mapped into Neal-Smith

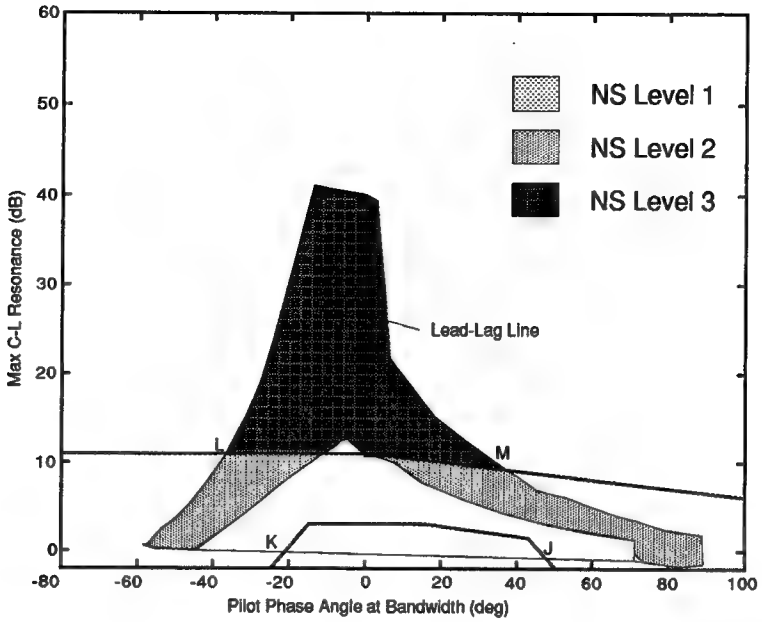

Figure C.3 (Case 3) Neal-Smith Regions (NS)

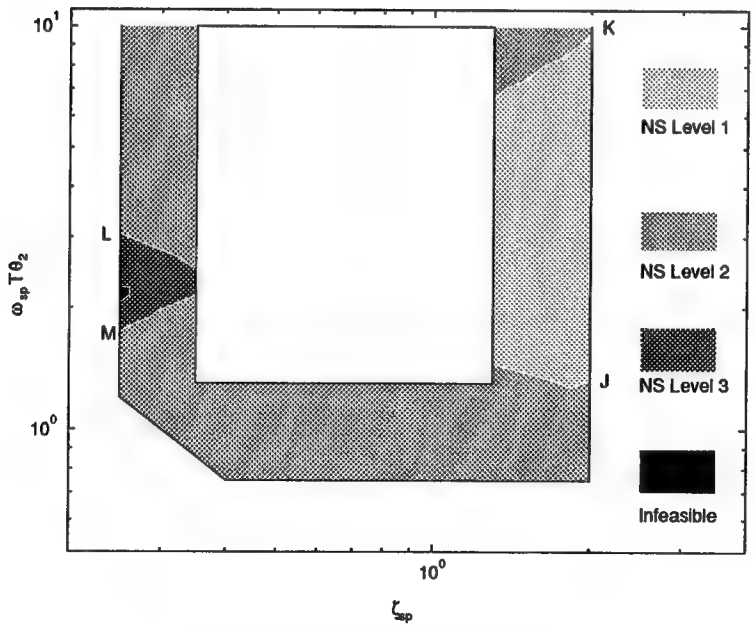

Figure C.4 (Case 3) Neal-Smith Regions Mapped into $\omega_{sp}T_{\theta_2}, \zeta_{sp}, \tau_\theta$

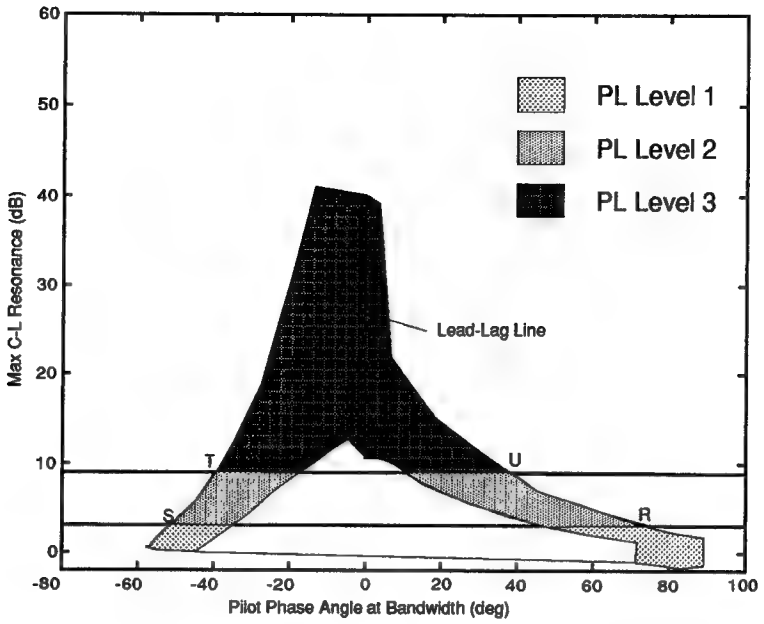

Figure C.5 (Case 3) Pilot-in-the-Loop Regions (PL)

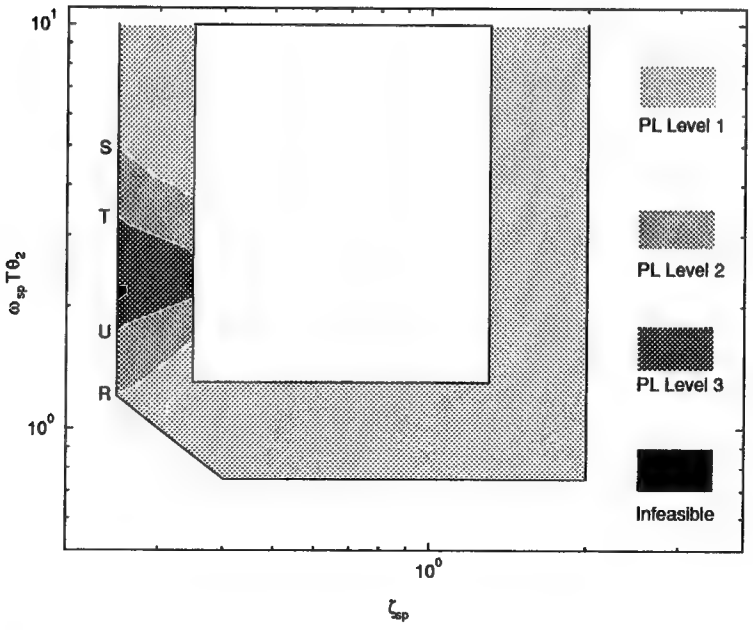

Figure C.6 (Case 3) Pilot-in-the-Loop Mapped into the $\omega_{sp}T_{\theta_2}, \zeta_{sp}, \tau_\theta$

Appendix D. Case 4

Case	*Level*	ω_{BW}	τ_θ	T_{θ_2}
4	2	2.50	0.10	1.67

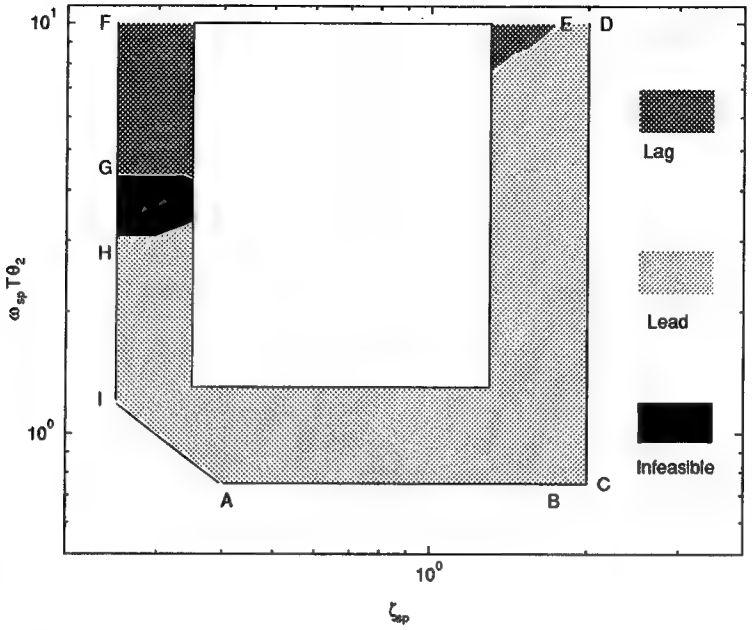

Figure D.1 (Case 4) Lead, Lag, and Infeasible Regions on $\omega_{sp}T_{\theta_2}, \zeta_{sp}, \tau_\theta$

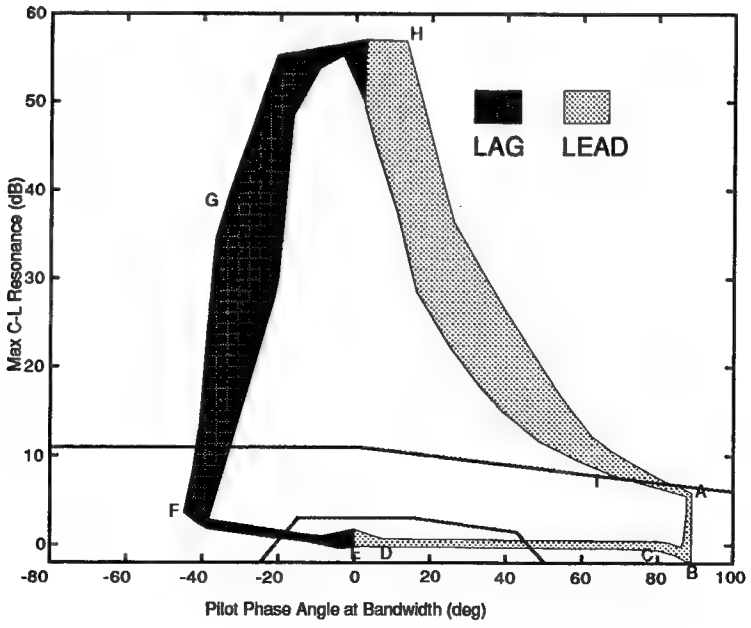

Figure D.2 (Case 4) $\omega_{sp}T_{\theta_2}, \zeta_{sp}, \tau_\theta$ Mapped into Neal-Smith

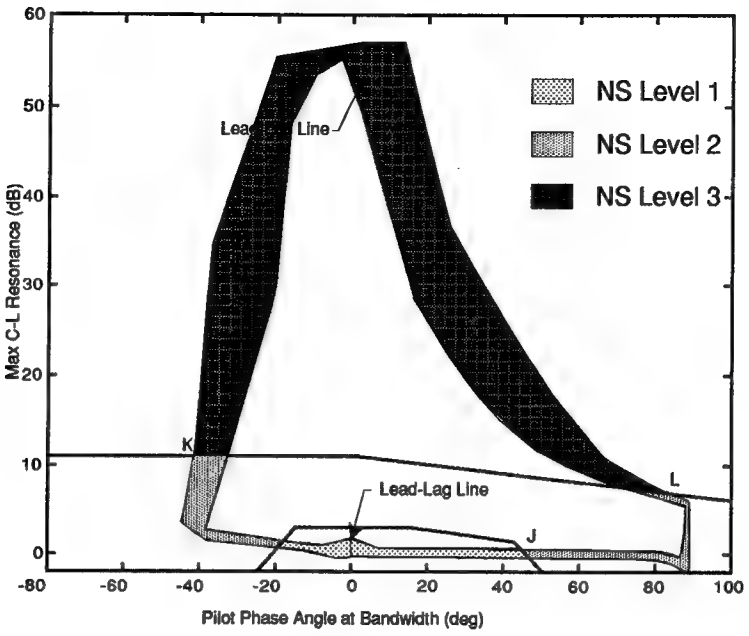

Figure D.3 (Case 4) Neal-Smith Regions (NS)

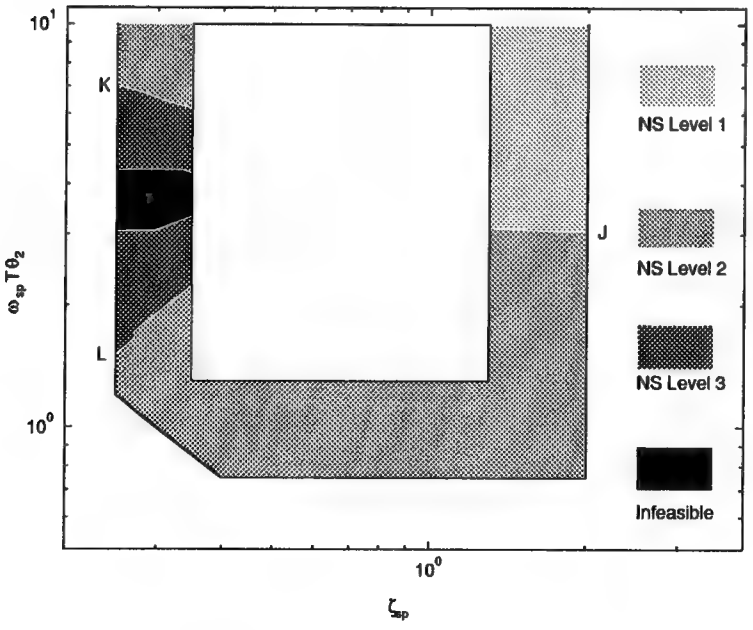

Figure D.4 (Case 4) Neal-Smith Regions Mapped into $\omega_{sp}T_{\theta_2}, \zeta_{sp}, \tau_\theta$

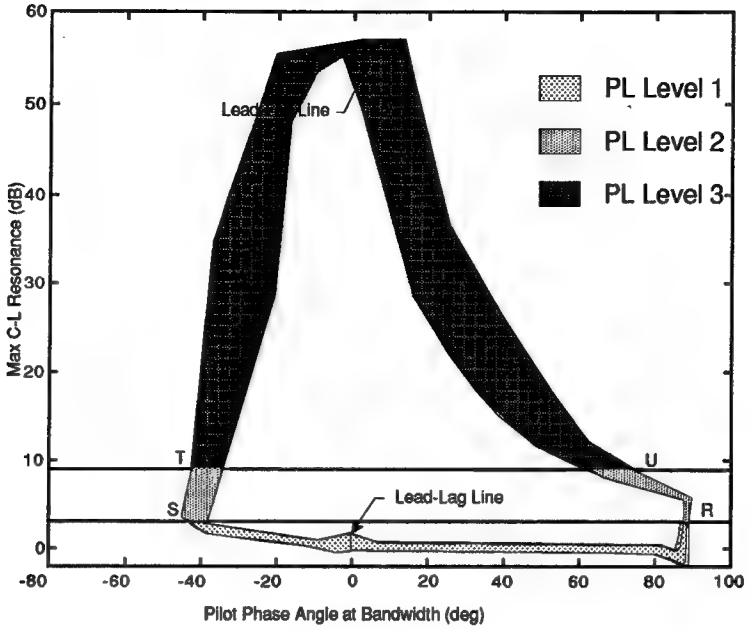

Figure D.5 (Case 4) Pilot-in-the-Loop Regions (PL)

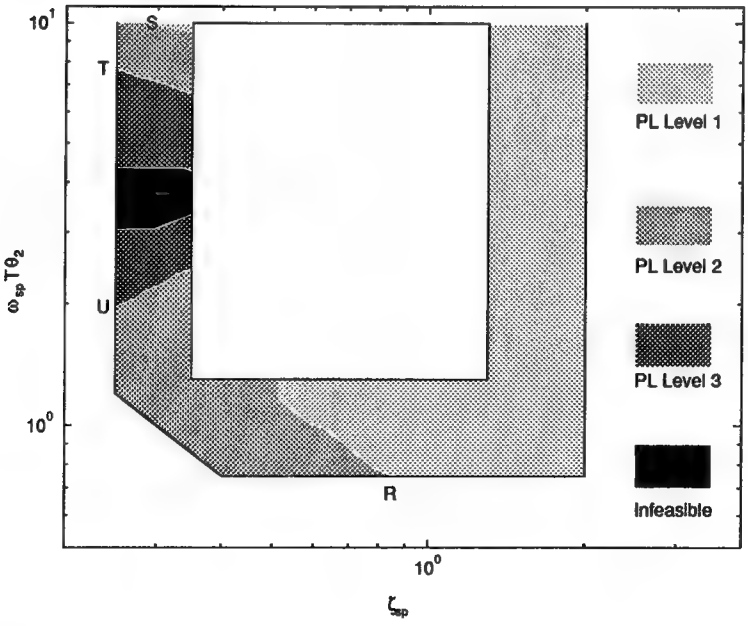

Figure D.6 (Case 4) Pilot-in-the-Loop Mapped into the $\omega_{sp}T_{\theta_2}, \zeta_{sp}, \tau_\theta$

Appendix E. Case 5

Case	*Level*	ω_{BW}	τ_θ	T_{θ_2}
5	2	1.50	0.20	1.67

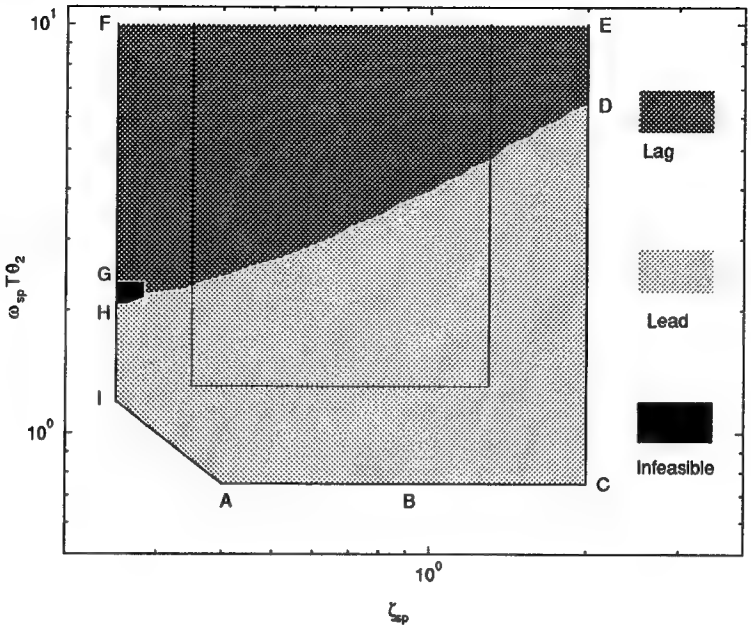

Figure E.1 (Case 5) Lead, Lag, and Infeasible Regions on $\omega_{sp}T_{\theta_2}, \zeta_{sp}, \tau_\theta$

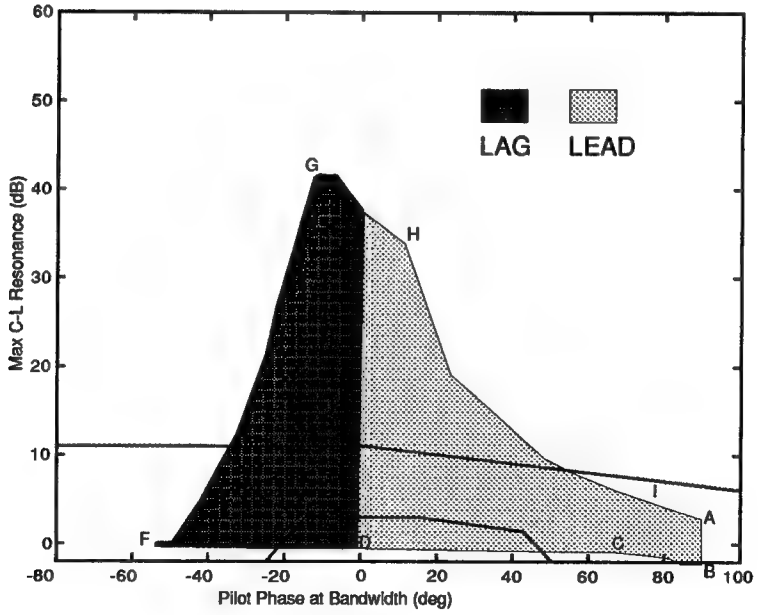

Figure E.2 (Case 5) $\omega_{sp}T_{\theta_2}, \zeta_{sp}, \tau_\theta$ Mapped into Neal-Smith

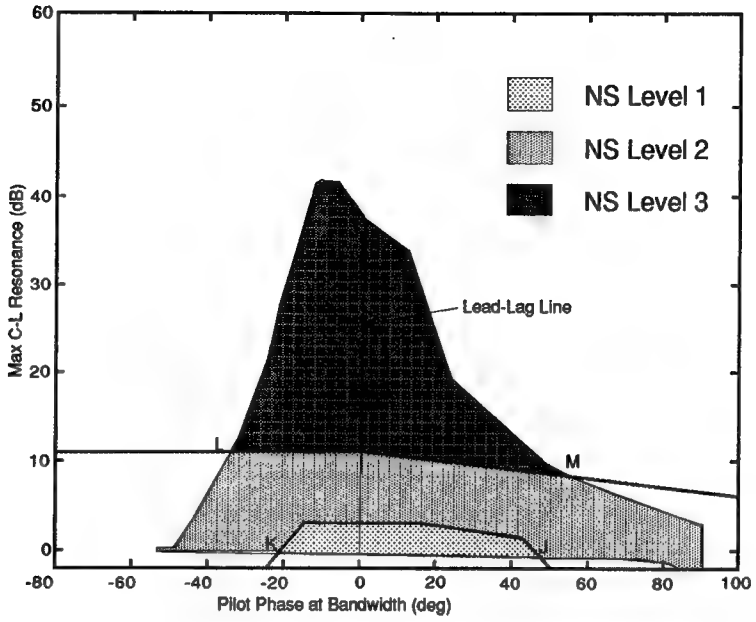

Figure E.3 (Case 5) Neal-Smith Regions (NS)

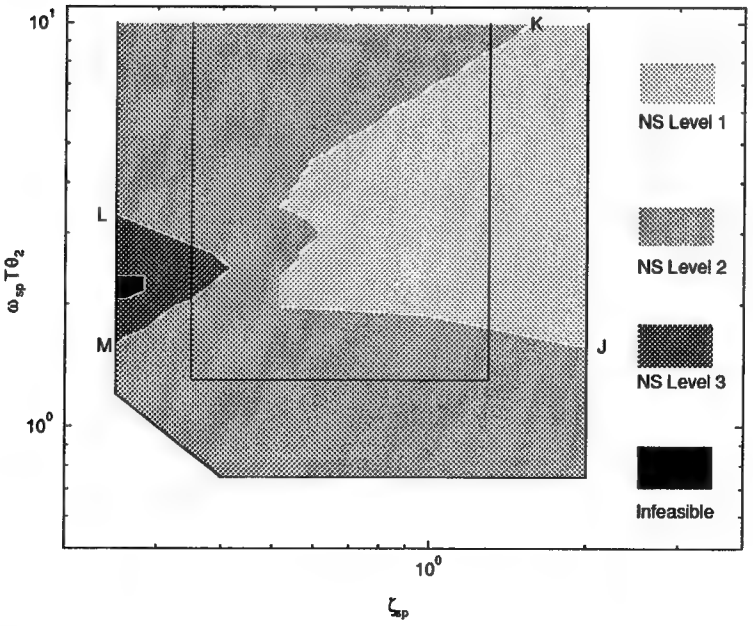

Figure E.4 (Case 5) Neal-Smith Regions Mapped into $\omega_{sp}T_{\theta_2}, \zeta_{sp}, \tau_\theta$

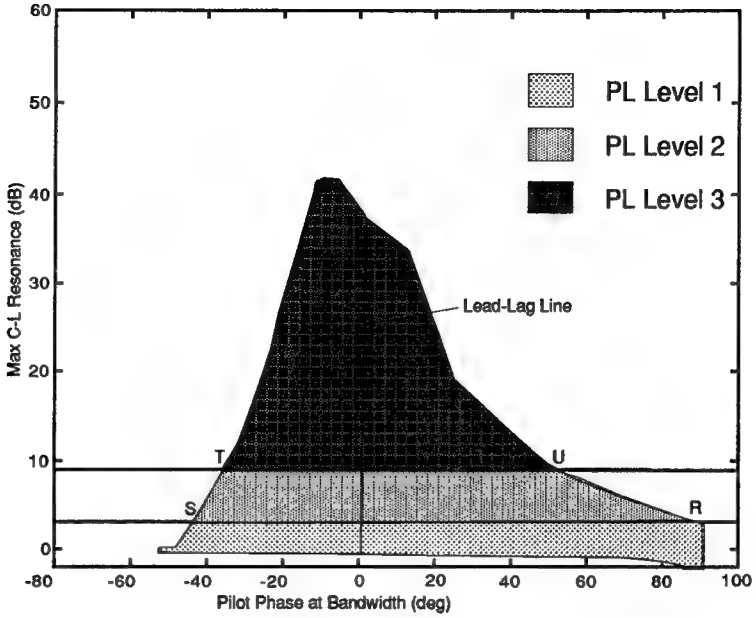

Figure E.5 (Case 5) Pilot-in-the-Loop Regions (PL)

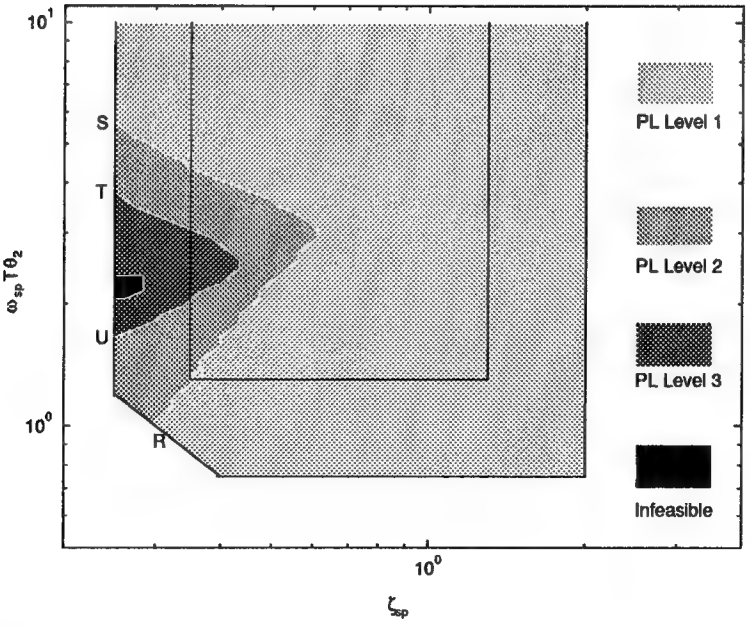

Figure E.6 (Case 5) Pilot-in-the-Loop Mapped into the $\omega_{sp}T_{\theta_2}, \zeta_{sp}, \tau_\theta$

Appendix F. Case 6

Case	*Level*	ω_{BW}	τ_θ	T_{θ_2}
6	2	2.50	0.20	1.67

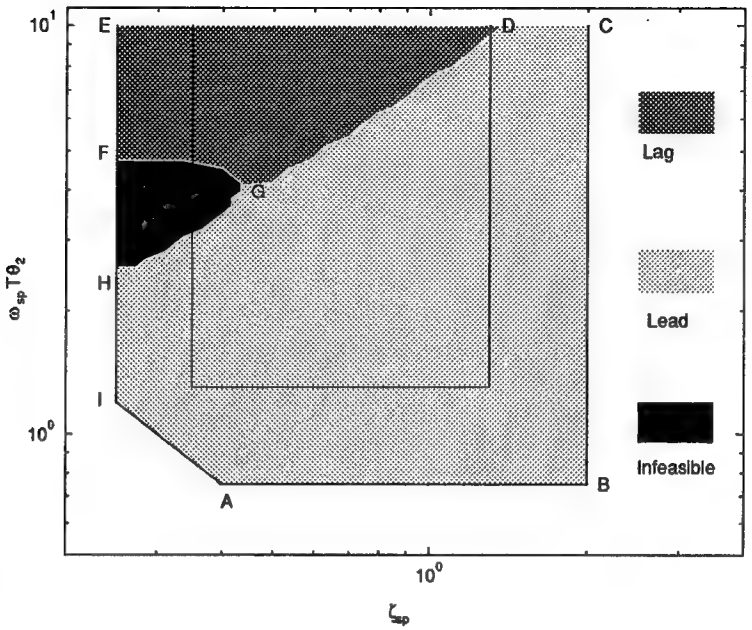

Figure F.1 (Case 6) Lead, Lag, and Infeasible Regions on $\omega_{sp}T_{\theta_2}, \zeta_{sp}, \tau_\theta$

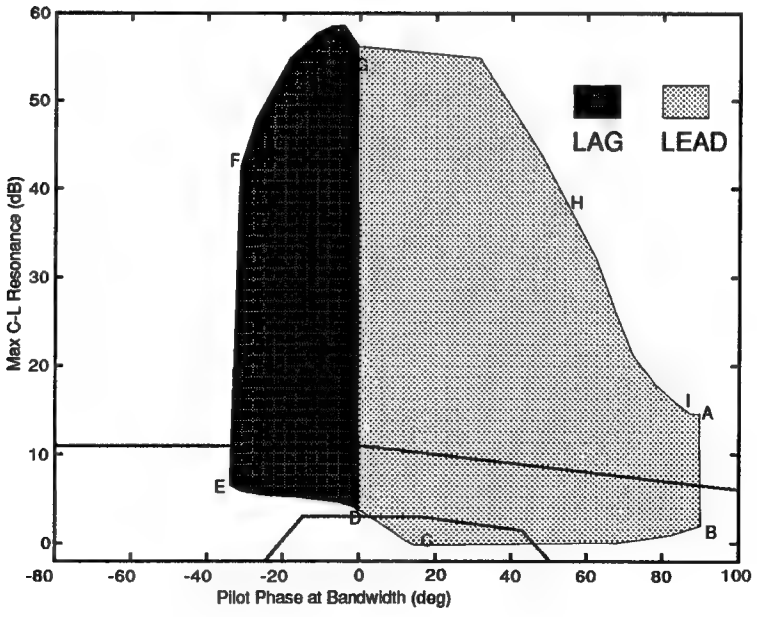

Figure F.2 (Case 6) $\omega_{sp}T_{\theta_2}, \zeta_{sp}, \tau_\theta$ Mapped into Neal-Smith

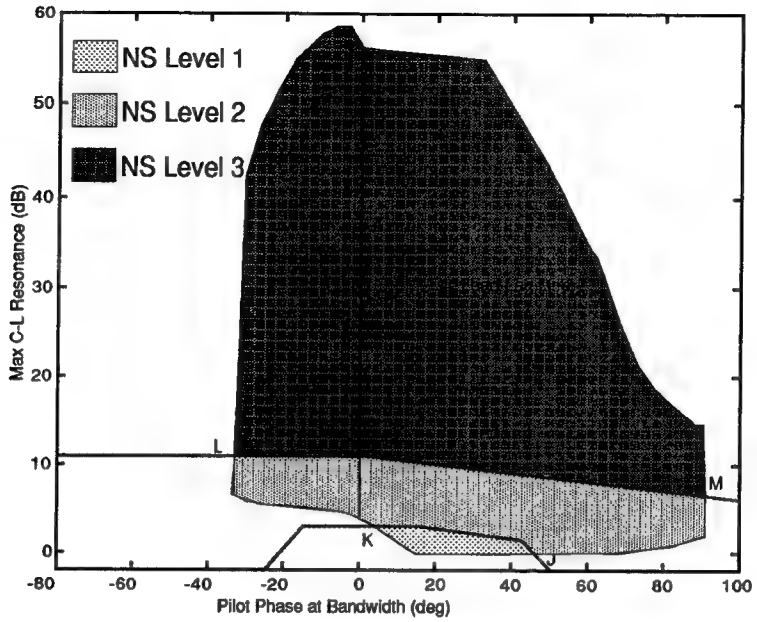

Figure F.3 (Case 6) Neal-Smith Regions (NS)

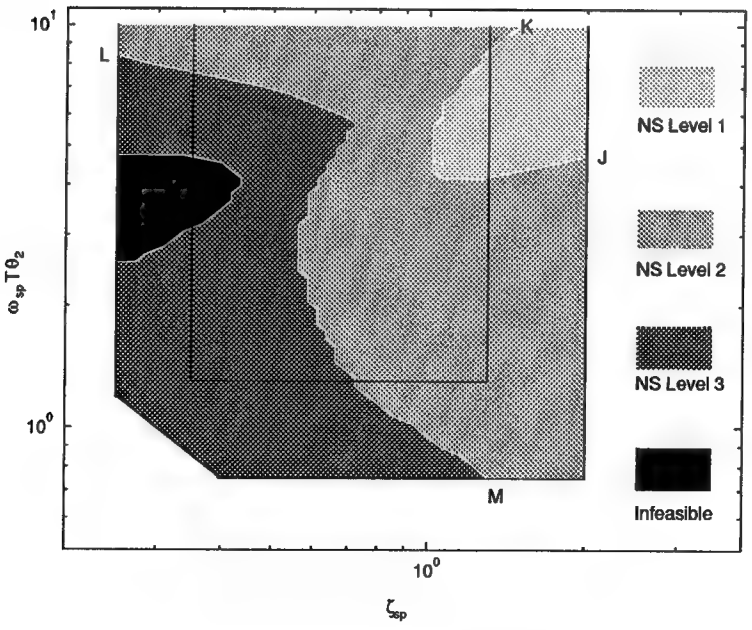

Figure F.4 (Case 6) Neal-Smith Regions Mapped into $\omega_{sp}T_{\theta_2}, \zeta_{sp}, \tau_\theta$

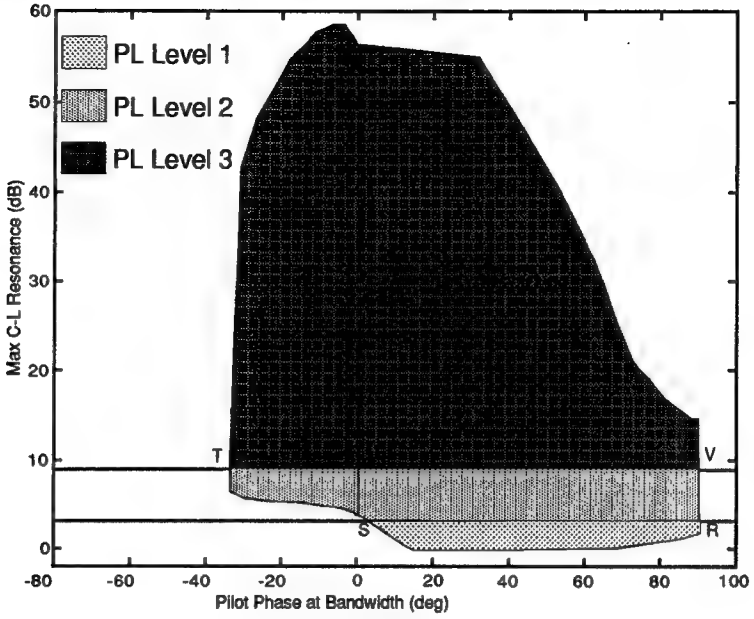

Figure F.5 (Case 6) Pilot-in-the-Loop Regions (PL)

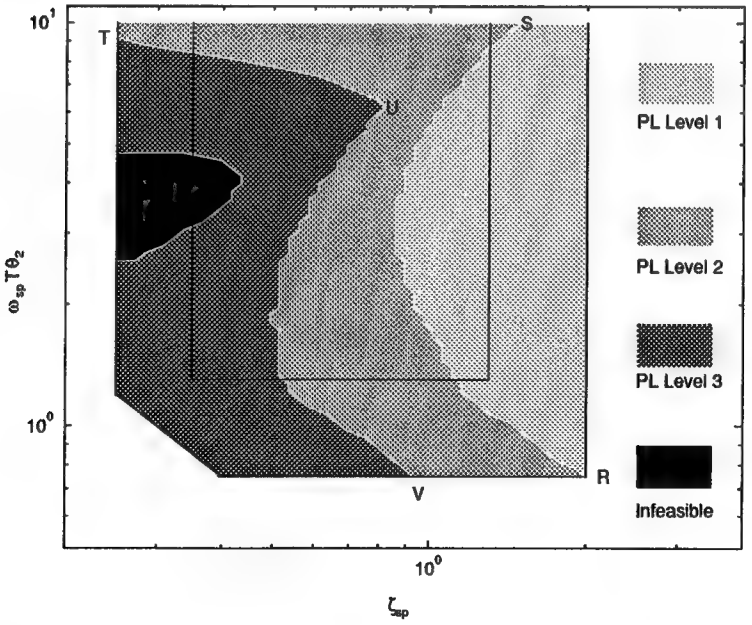

Figure F.6 (Case 6) Pilot-in-the-Loop Mapped into the $\omega_{sp}T_{\theta_2}, \zeta_{sp}, \tau_\theta$

Appendix G. Case 7

Case	*Level*	ω_{BW}	τ_θ	T_{θ_2}
7	1	1.50	0.10	1.96

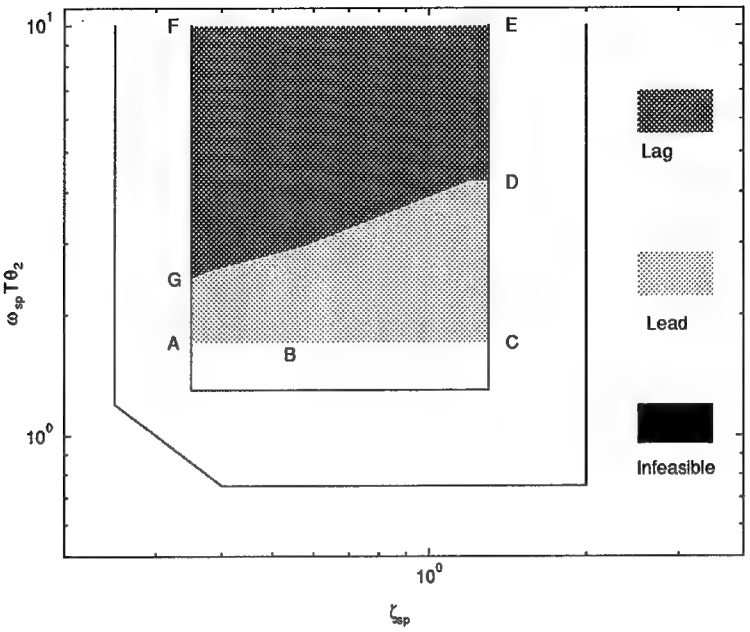

Figure G.1 (Case 7) Lead, Lag, and Infeasible Regions on $\omega_{sp}T_{\theta_2}, \zeta_{sp}, \tau_\theta$

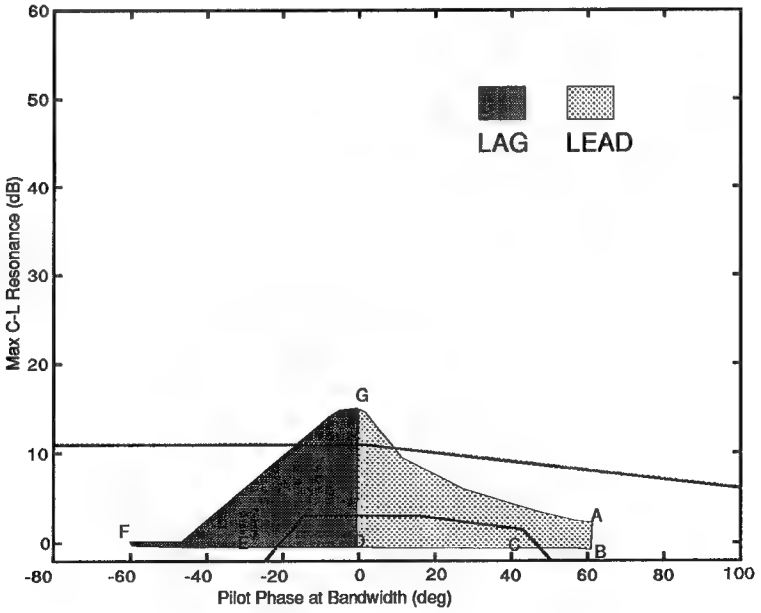

Figure G.2 (Case 7) $\omega_{sp}T_{\theta_2}, \zeta_{sp}, \tau_\theta$ Mapped into Neal-Smith

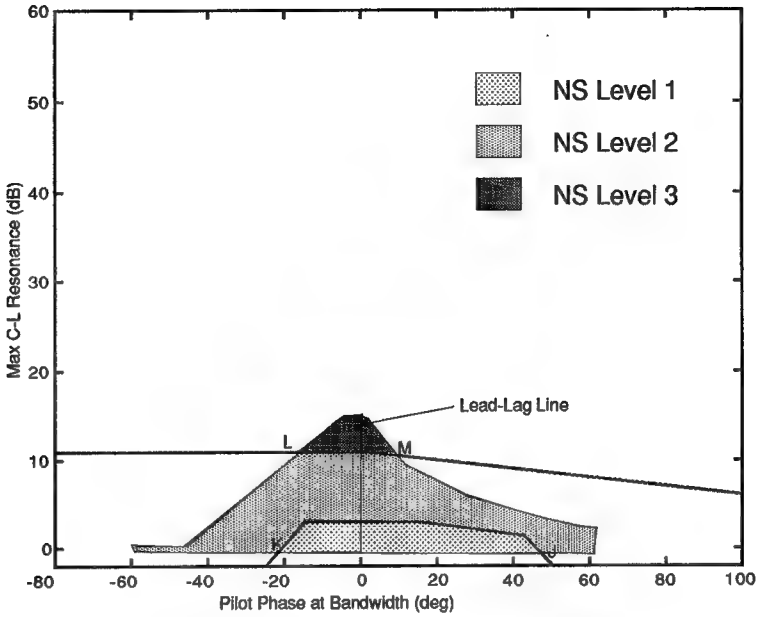

Figure G.3 (Case 7) Neal-Smith Regions (NS)

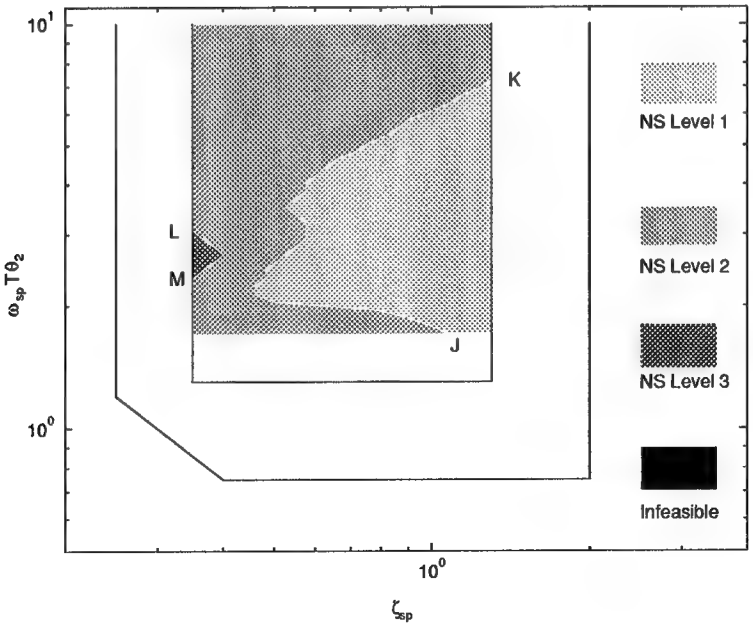

Figure G.4 (Case 7) Neal-Smith Regions Mapped into $\omega_{sp}T_{\theta_2}, \zeta_{sp}, \tau_\theta$

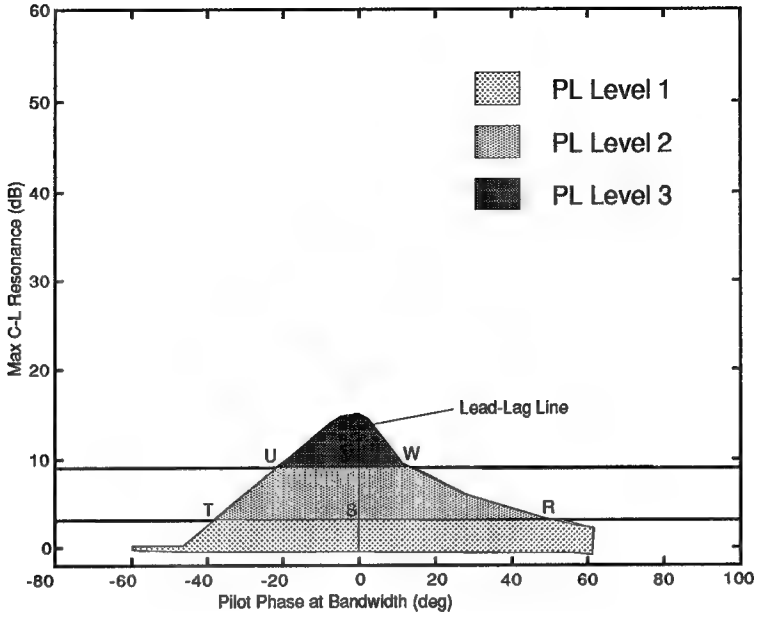

Figure G.5 (Case 7) Pilot-in-the-Loop Regions (PL)

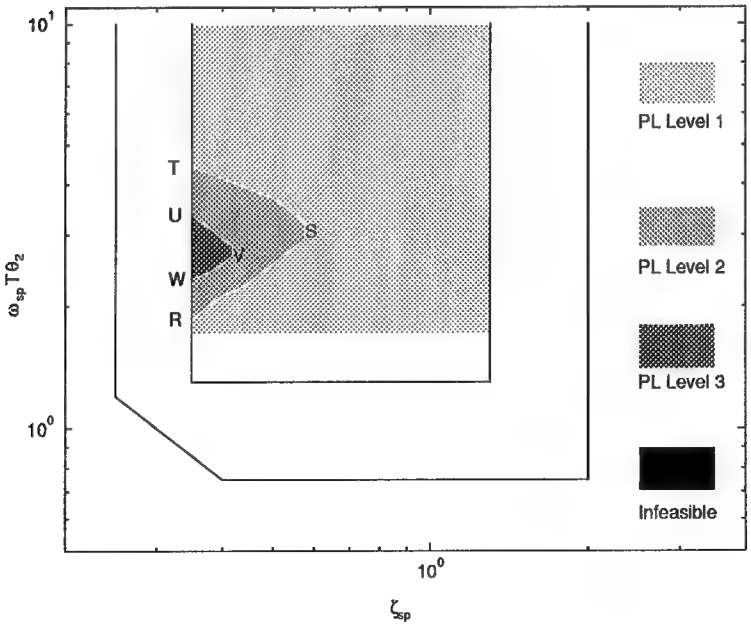

Figure G.6 (Case 7) Pilot-in-the-Loop Mapped into the $\omega_{sp}T_{\theta_2}, \zeta_{sp}, \tau_\theta$

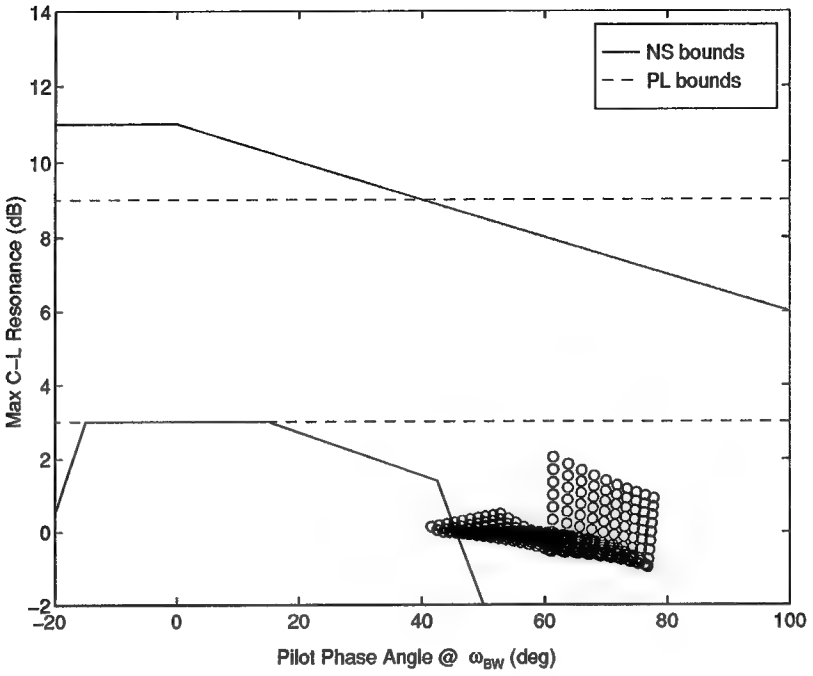

Figure G.7 (Case 7x) Mapping of Excluded Region from $\omega_{sp}T_{\theta_2}, \zeta_{sp}, \tau_\theta$

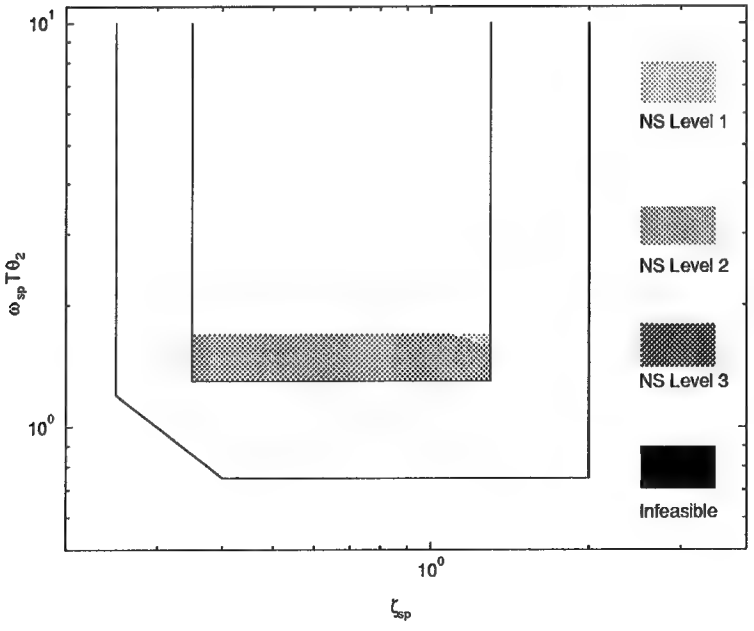

Figure G.8 (Case 7x) Neal-Smith Regions Mapped into $\omega_{sp}T_{\theta_2}, \zeta_{sp}, \tau_\theta$

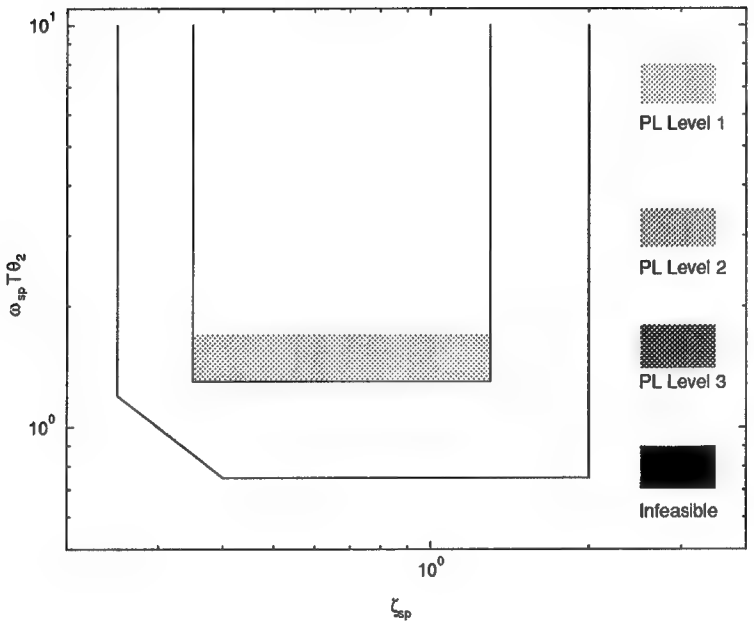

Figure G.9 (Case 7x) Pilot-in-the-Loop Regions Mapped into $\omega_{sp}T_{\theta_2}, \zeta_{sp}, \tau_\theta$

Appendix H. Case 8

Case	*Level*	ω_{BW}	τ_θ	T_{θ_2}
8	1	2.50	0.10	1.96

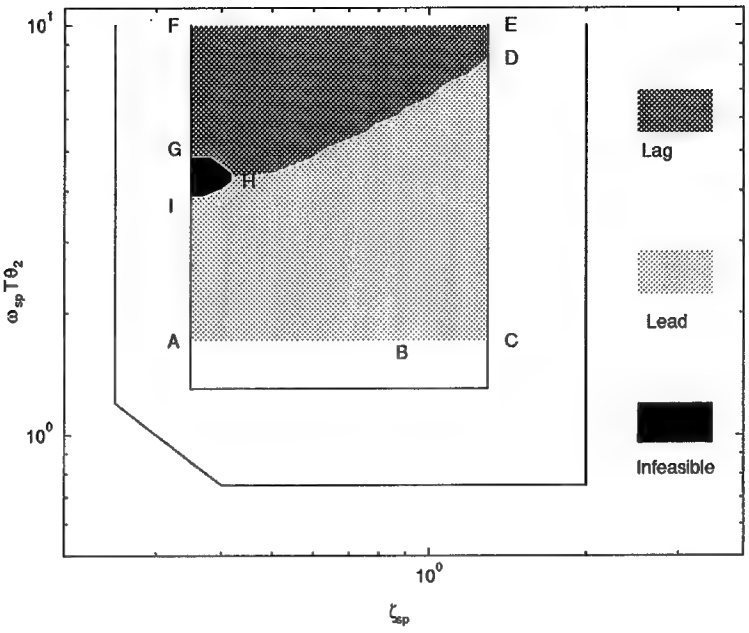

Figure H.1 (Case 8) Lead, Lag, and Infeasible Regions on $\omega_{sp}T_{\theta_2}, \zeta_{sp}, \tau_\theta$

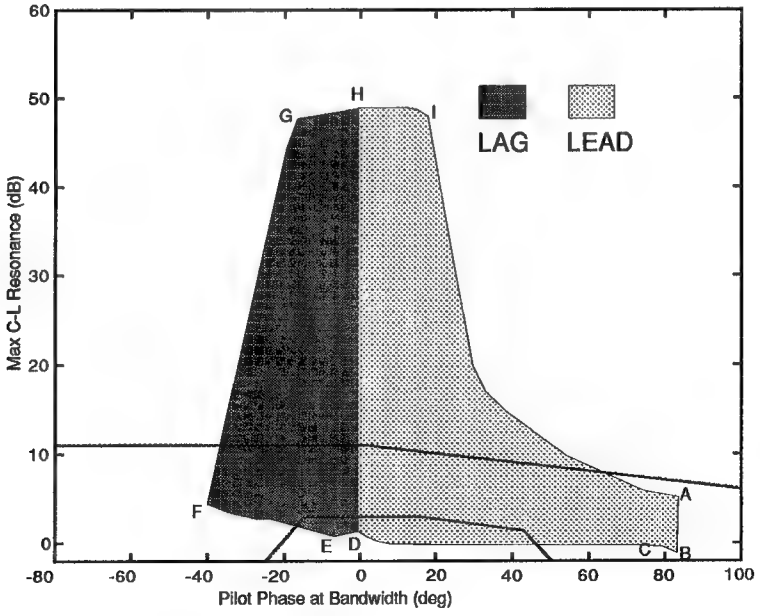

Figure H.2 (Case 8) $\omega_{sp}T_{\theta_2}, \zeta_{sp}, \tau_\theta$ Mapped into Neal-Smith

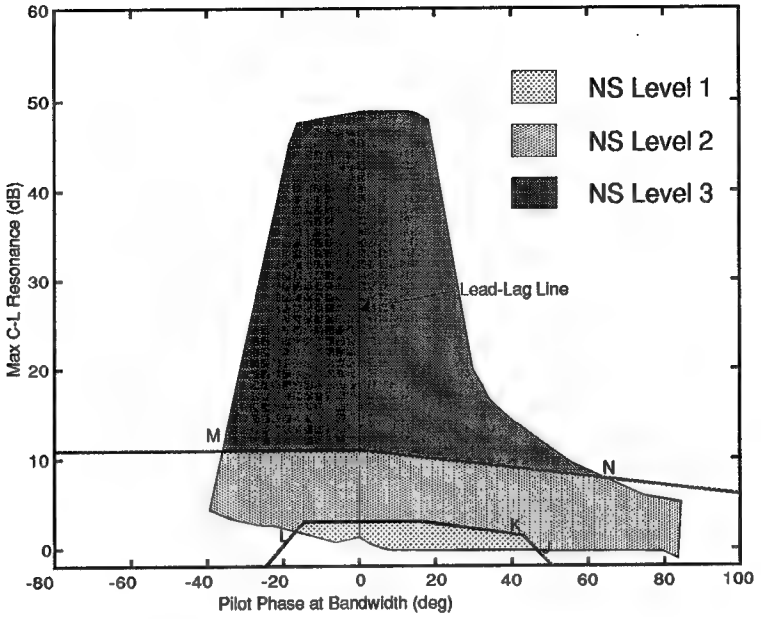

Figure H.3 (Case 8) Neal-Smith Regions (NS)

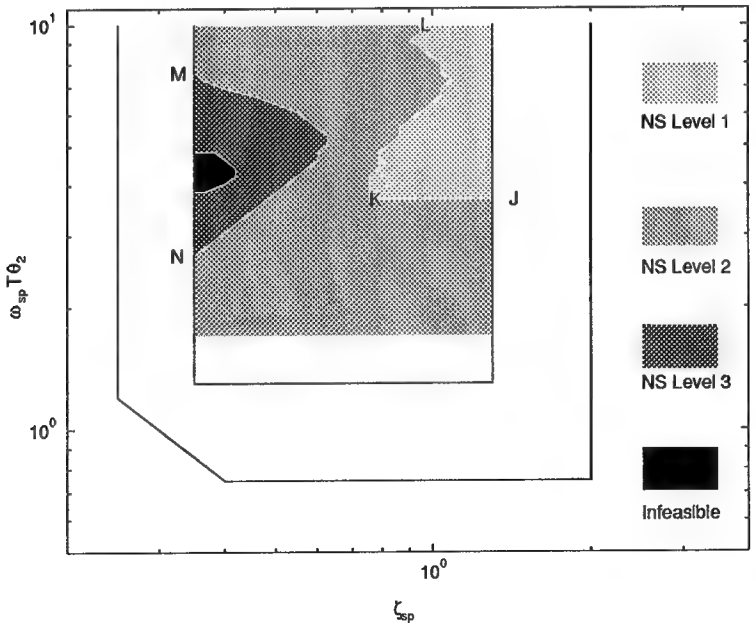

Figure H.4 (Case 8) Neal-Smith Regions Mapped into $\omega_{sp}T_{\theta_2}, \zeta_{sp}, \tau_\theta$

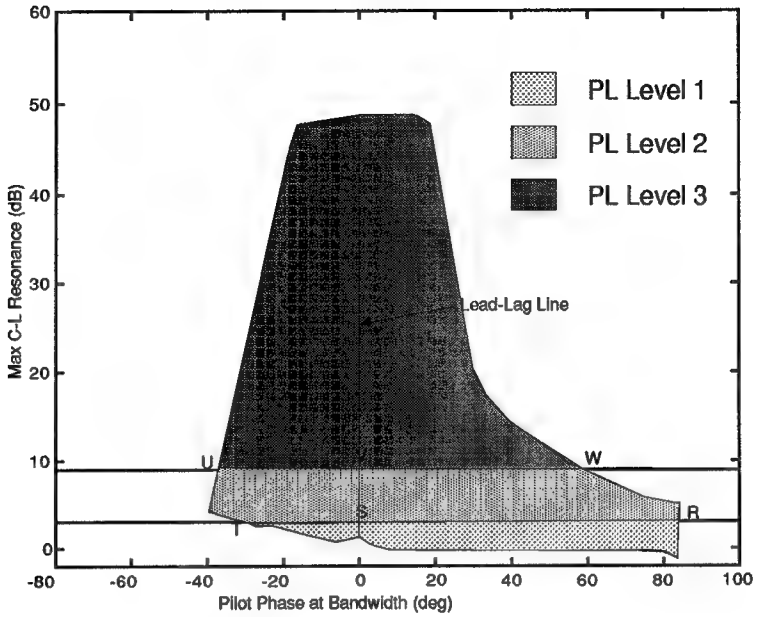

Figure H.5 (Case 8) Pilot-in-the-Loop Regions (PL)

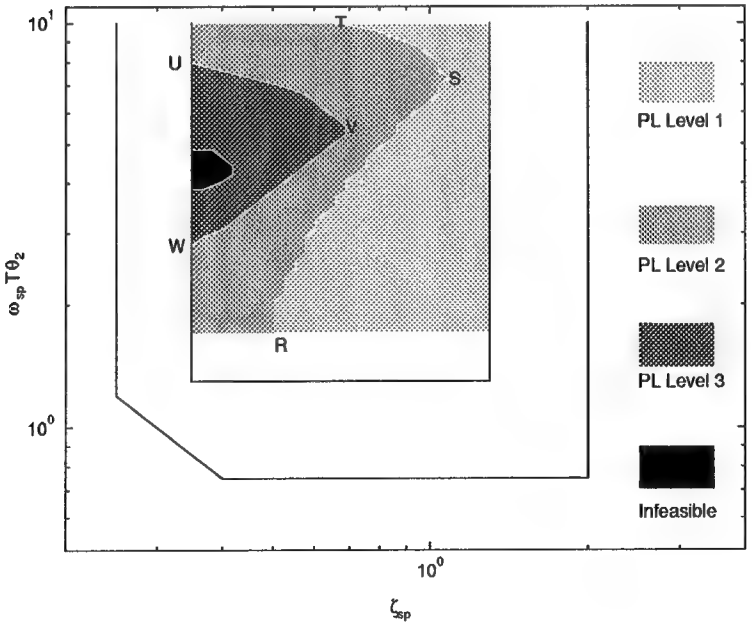

Figure H.6 (Case 8) Pilot-in-the-Loop Mapped into the $\omega_{sp}T_{\theta_2}, \zeta_{sp}, \tau_\theta$

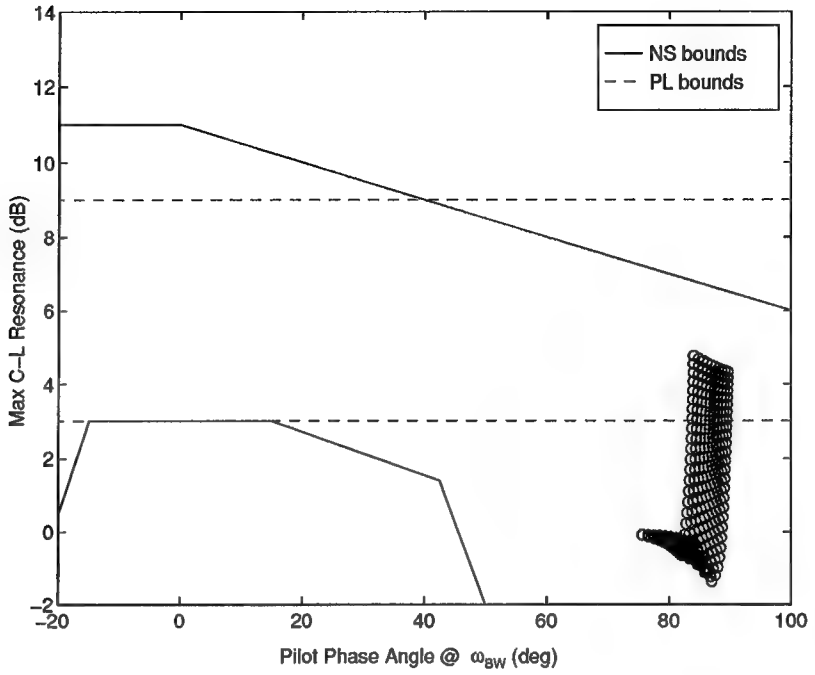

Figure H.7 (Case 8x) Mapping of Excluded Region from $\omega_{sp}T_{\theta_2}, \zeta_{sp}, \tau_\theta$

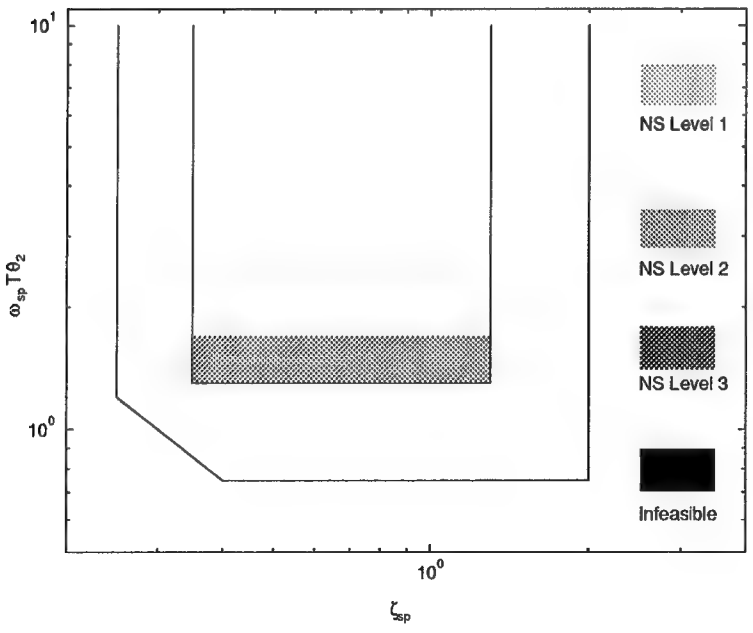

Figure H.8 (Case 8x) Neal-Smith Regions Mapped into $\omega_{sp}T_{\theta_2}, \zeta_{sp}, \tau_\theta$

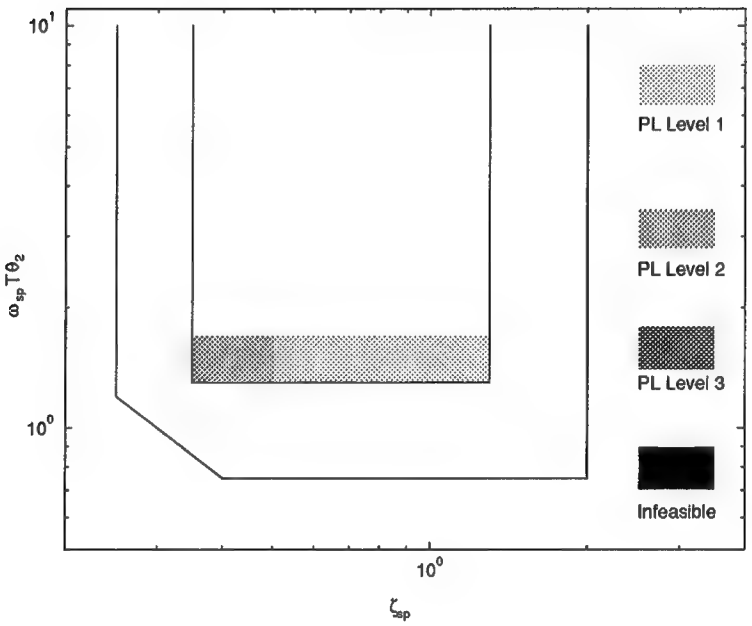

Figure H.9 (Case 8x) Pilot-in-the-Loop Mapped into the $\omega_{sp}T_{\theta_2}, \zeta_{sp}, \tau_\theta$

Appendix I. Case 9

Case	*Level*	ω_{BW}	τ_θ	T_{θ_2}
9	2	1.50	0.10	1.96

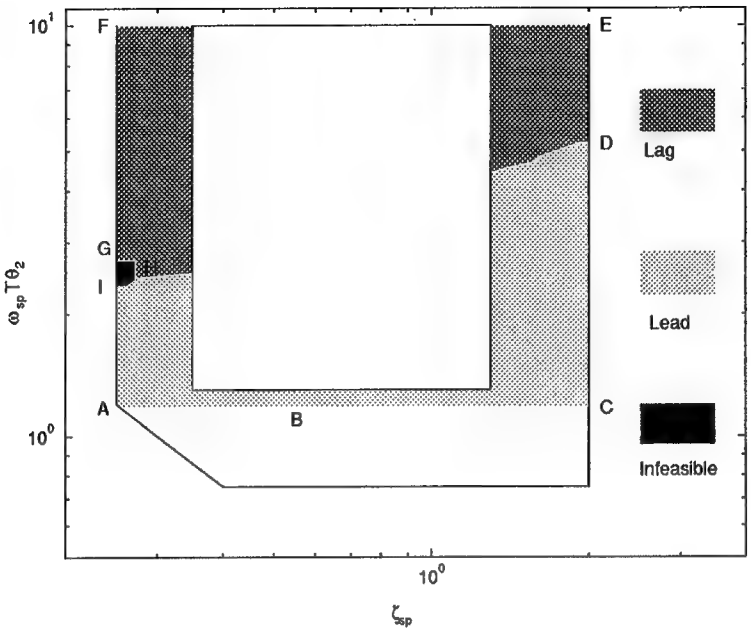

Figure I.1 (Case 9) Lead, Lag, and Infeasible Regions on $\omega_{sp}T_{\theta_2}, \zeta_{sp}, \tau_\theta$

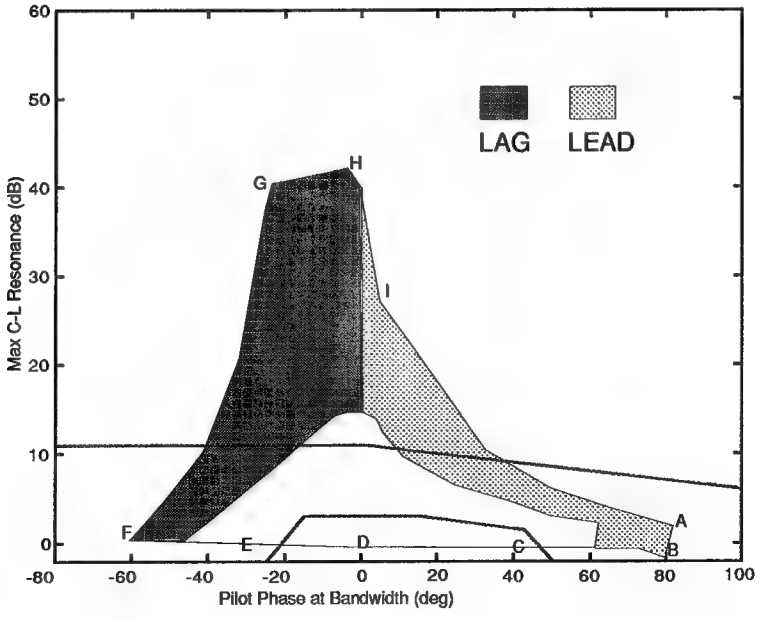

Figure I.2 (Case 9) $\omega_{sp}T_{\theta_2}, \zeta_{sp}, \tau_\theta$ Mapped into Neal-Smith

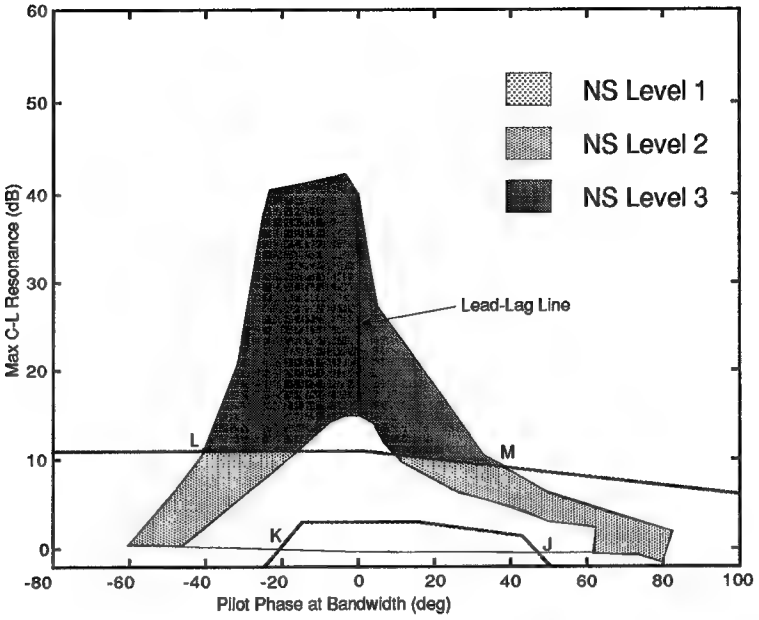

Figure I.3 (Case 9) Neal-Smith Regions (NS)

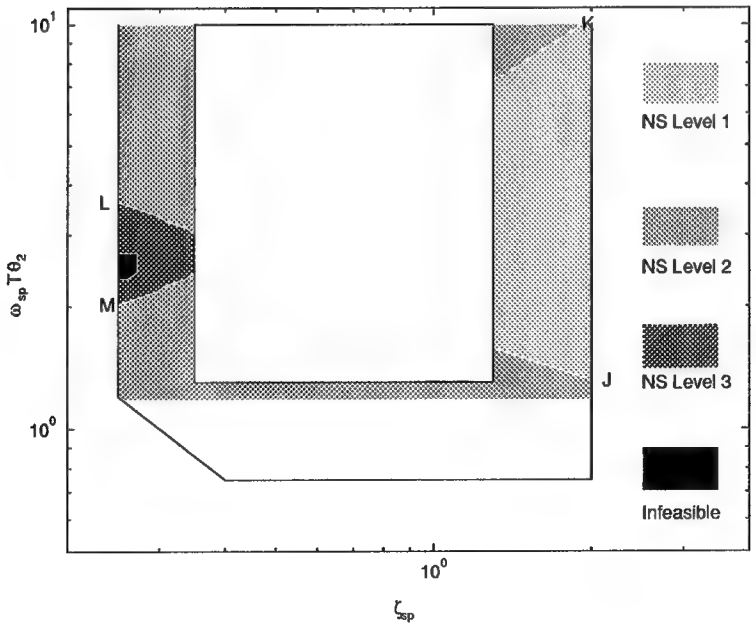

Figure I.4 (Case 9) Neal-Smith Regions Mapped into $\omega_{sp}T_{\theta_2}, \zeta_{sp}, \tau_\theta$

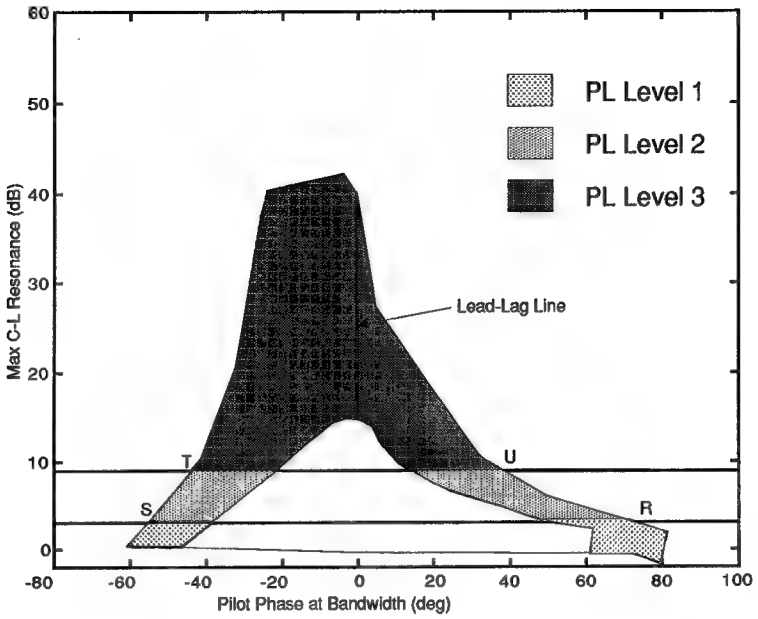

Figure I.5 (Case 9) Pilot-in-the-Loop Regions (PL)

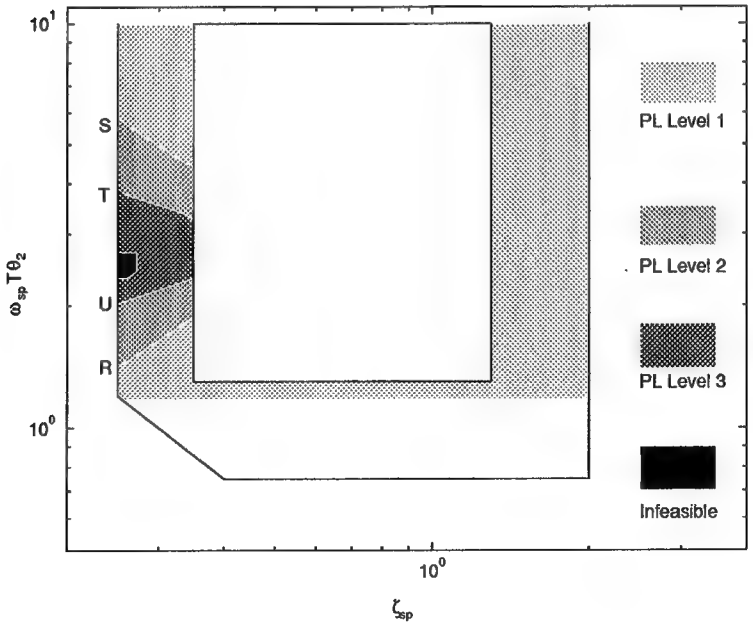

Figure I.6 (Case 9) Pilot-in-the-Loop Mapped into the $\omega_{sp}T_{\theta_2}, \zeta_{sp}, \tau_\theta$

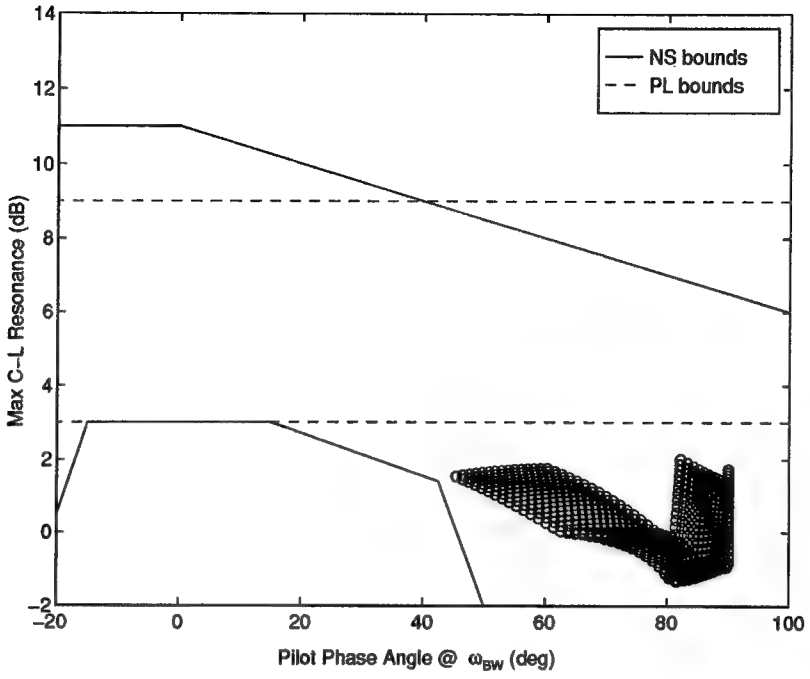

Figure I.7 (Case 9x) Mapping of Excluded Region from $\omega_{sp} T_{\theta_2}, \zeta_{sp}, \tau_\theta$

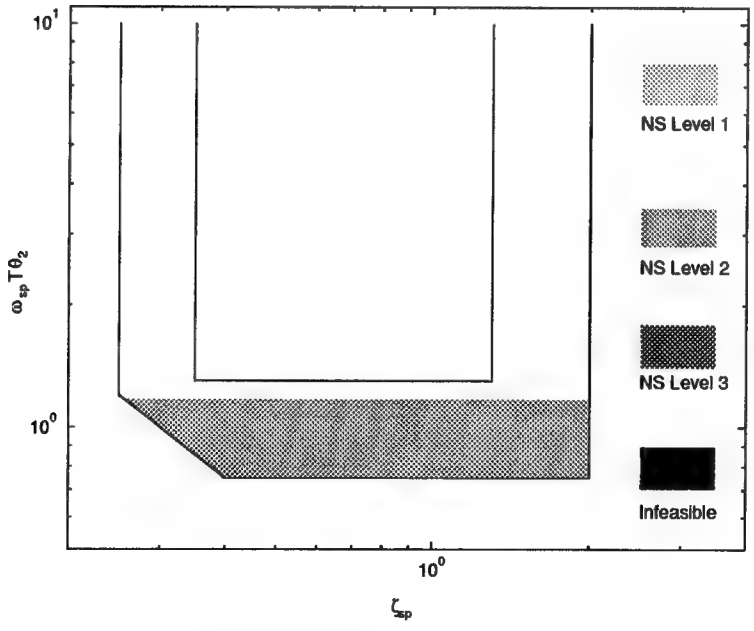

Figure I.8 (Case 9x) Neal-Smith Regions Mapped into $\omega_{sp} T_{\theta_2}, \zeta_{sp}, \tau_\theta$

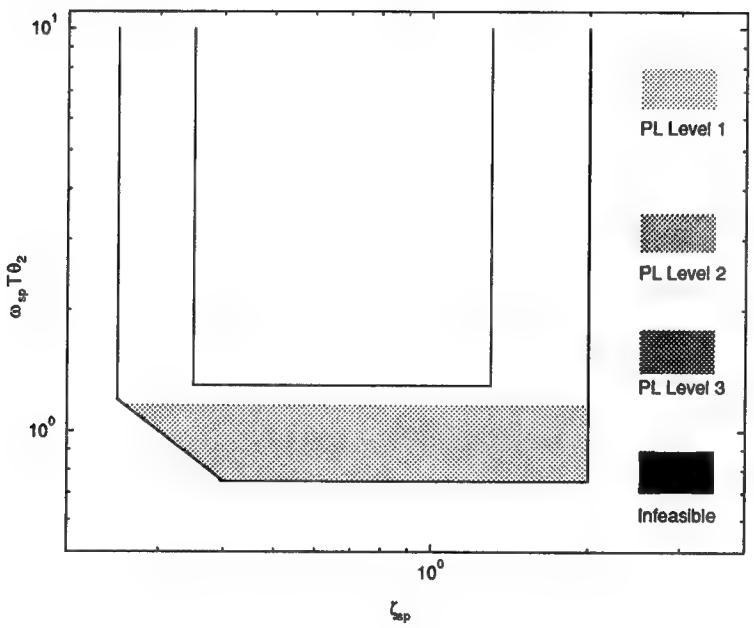

Figure I.9 (Case 9x) Pilot-in-the-Loop Mapped into the $\omega_{sp}T_{\theta_2}, \zeta_{sp}, \tau_\theta$

Appendix J. Case 10

Case	*Level*	ω_{BW}	τ_θ	T_{θ_2}
10	2	2.50	0.10	1.96

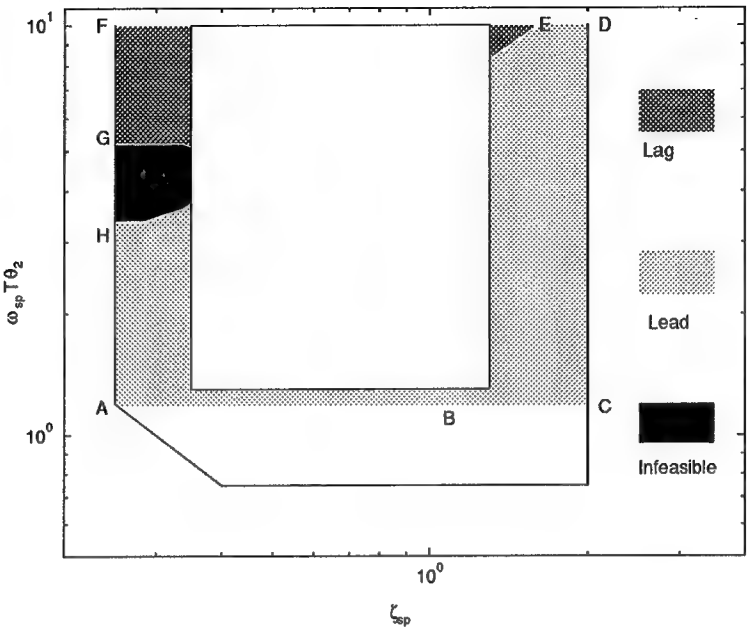

Figure J.1 (Case 10) Lead, Lag, and Infeasible Regions on $\omega_{sp}T_{\theta_2}, \zeta_{sp}, \tau_\theta$

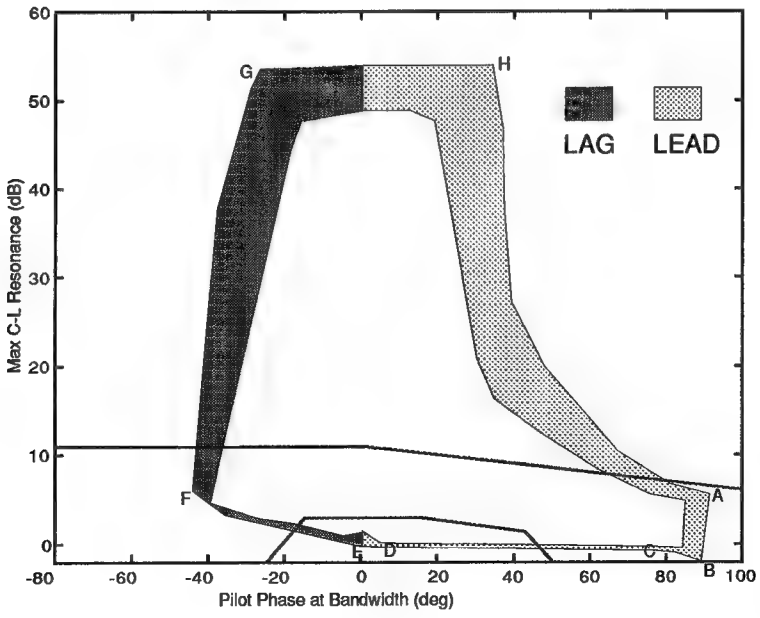

Figure J.2 (Case 10) $\omega_{sp}T_{\theta_2}, \zeta_{sp}, \tau_\theta$ Mapped into Neal-Smith

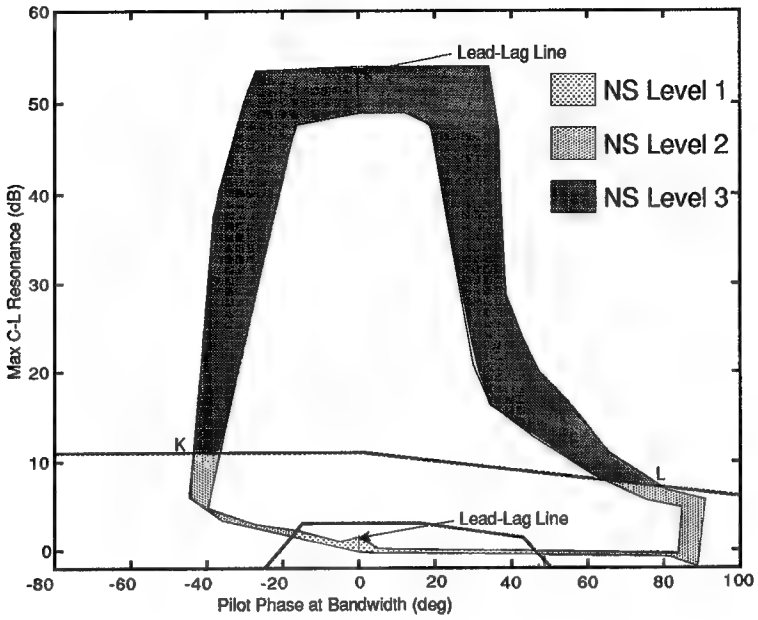

Figure J.3 (Case 10) Neal-Smith Regions (NS)

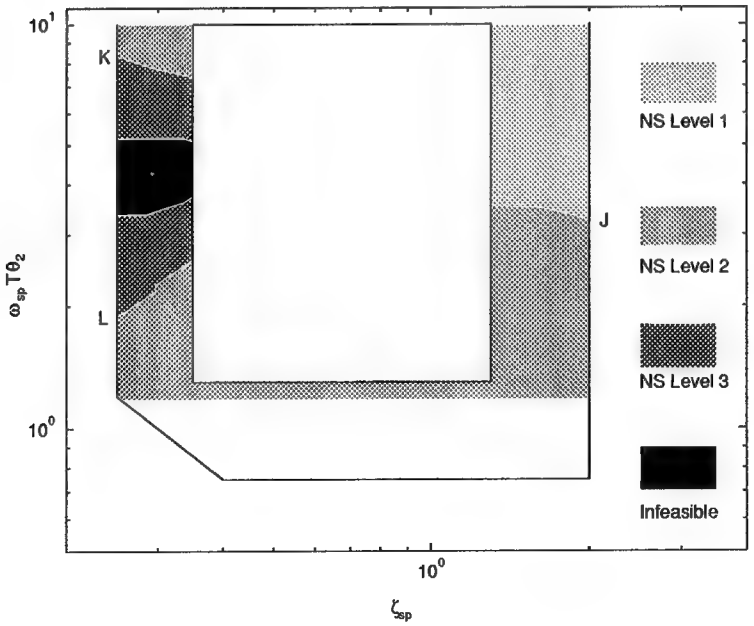

Figure J.4 (Case 10) Neal-Smith Regions Mapped into $\omega_{sp}T_{\theta_2}, \zeta_{sp}, \tau_\theta$

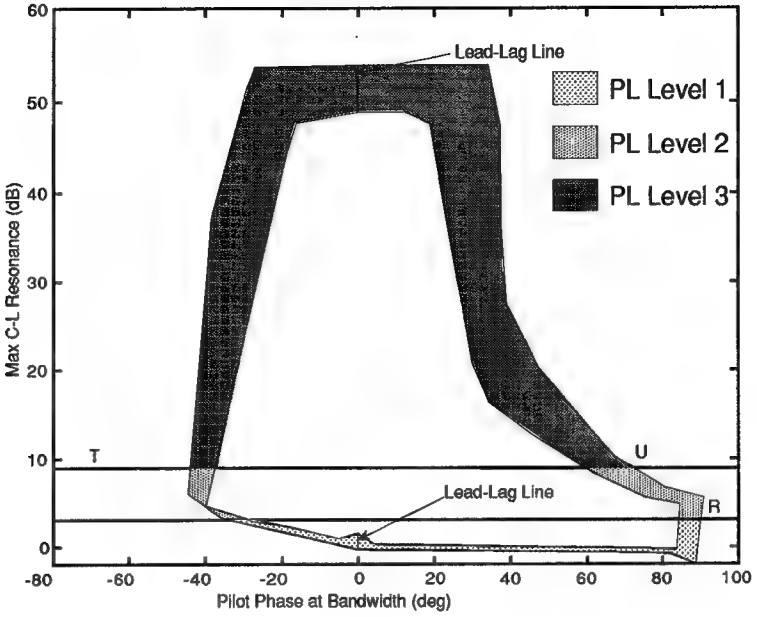

Figure J.5 (Case 10) Pilot-in-the-Loop Regions (PL)

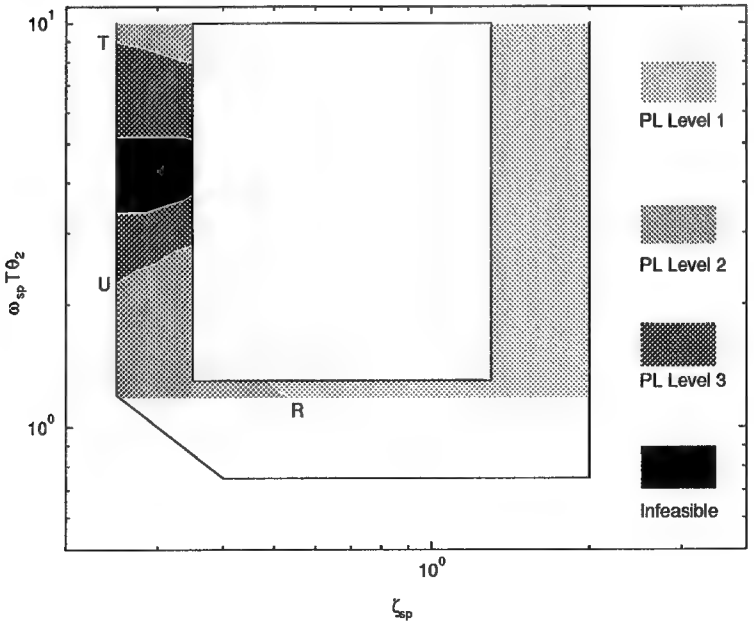

Figure J.6 (Case 10) Pilot-in-the-Loop Mapped into the $\omega_{sp}T_{\theta_2}, \zeta_{sp}, \tau_\theta$

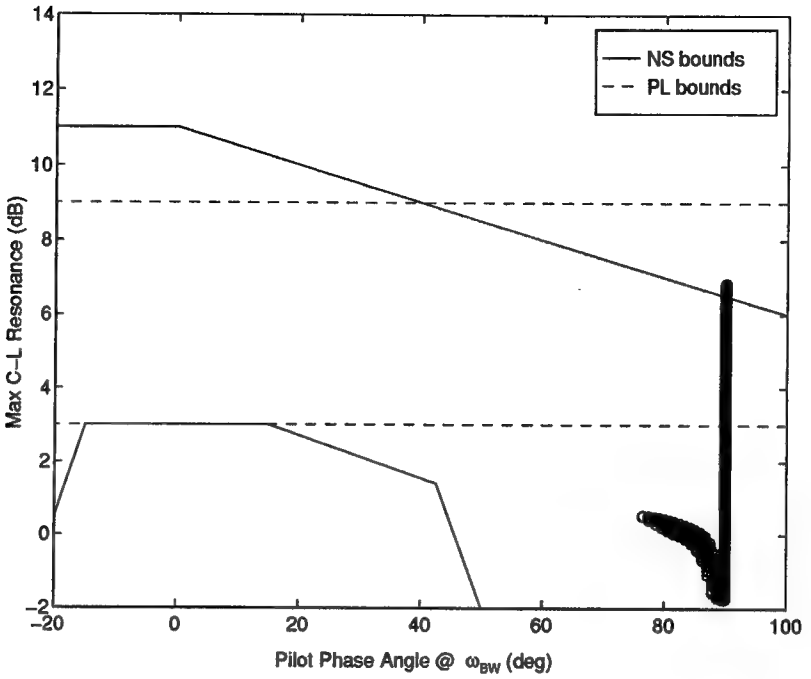

Figure J.7 (Case 10x) Mapping of Excluded Region from $\omega_{sp} T_{\theta_2}, \zeta_{sp}, \tau_\theta$

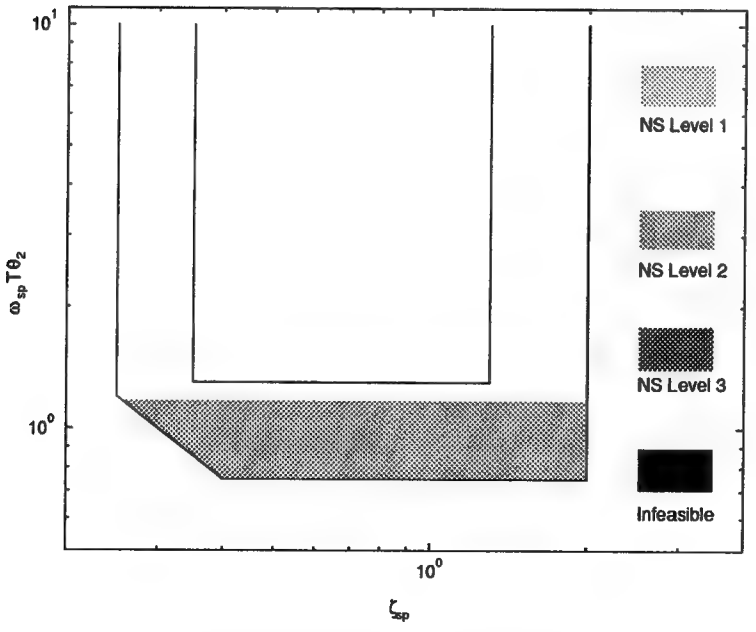

Figure J.8 (Case 10x) Neal-Smith Regions Mapped into $\omega_{sp} T_{\theta_2}, \zeta_{sp}, \tau_\theta$

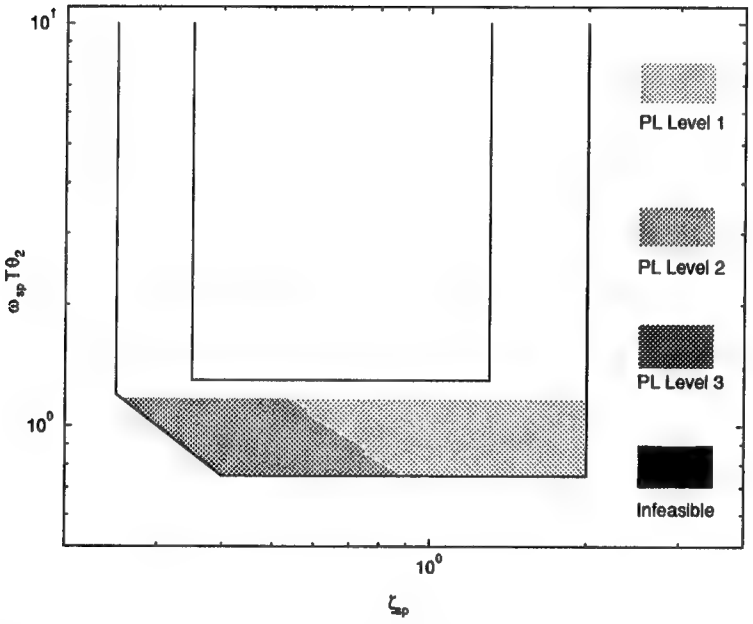

Figure J.9 (Case 10x) Pilot-in-the-Loop Mapped into the $\omega_{sp}T_{\theta_2}, \zeta_{sp}, \tau_\theta$

Appendix K. Case 11

Case	*Level*	ω_{BW}	τ_θ	T_{θ_2}
11	2	1.50	0.20	1.96

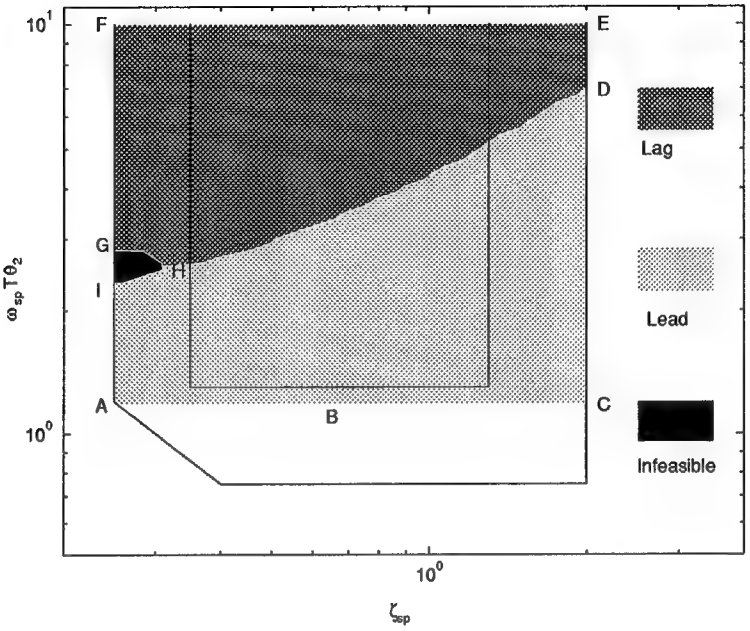

Figure K.1 (Case 11) Lead, Lag, and Infeasible Regions on $\omega_{sp}T_{\theta_2}, \zeta_{sp}, \tau_\theta$

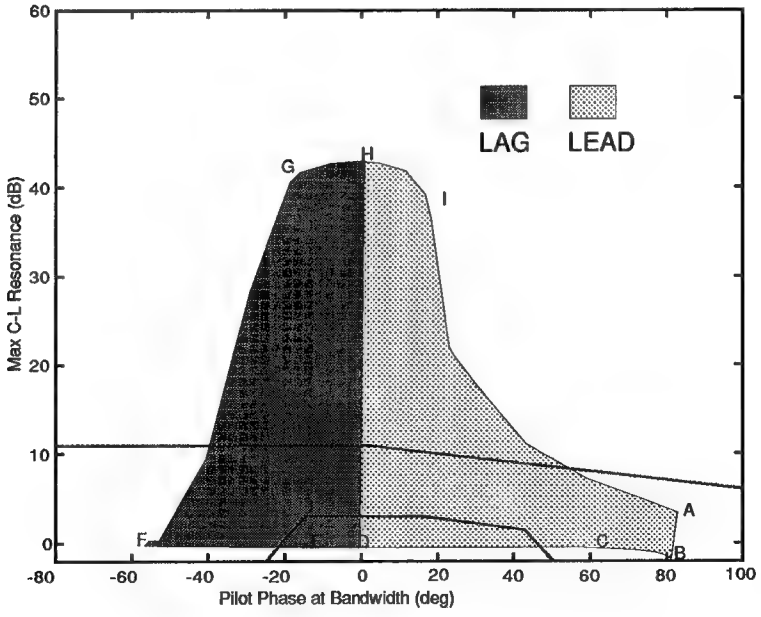

Figure K.2 (Case 11) $\omega_{sp}T_{\theta_2}, \zeta_{sp}, \tau_\theta$ Mapped into Neal-Smith

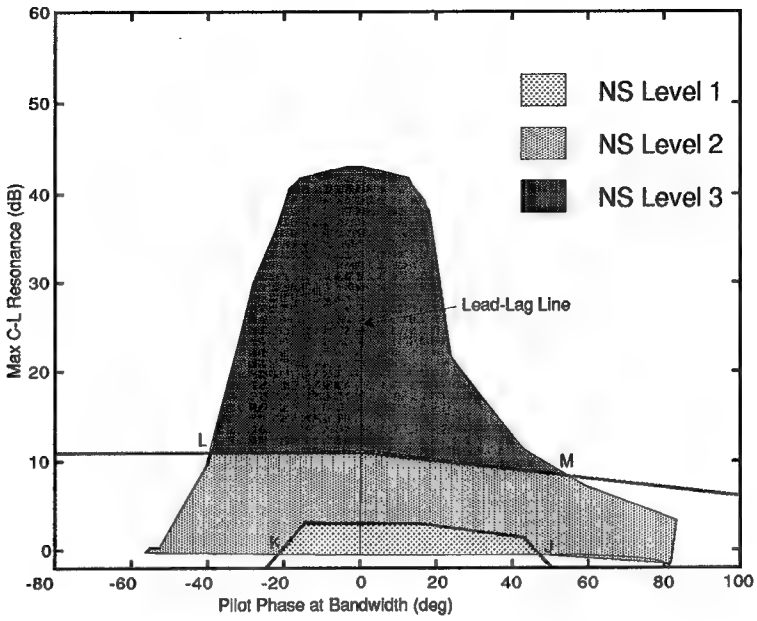

Figure K.3 (Case 11) Neal-Smith Regions (NS)

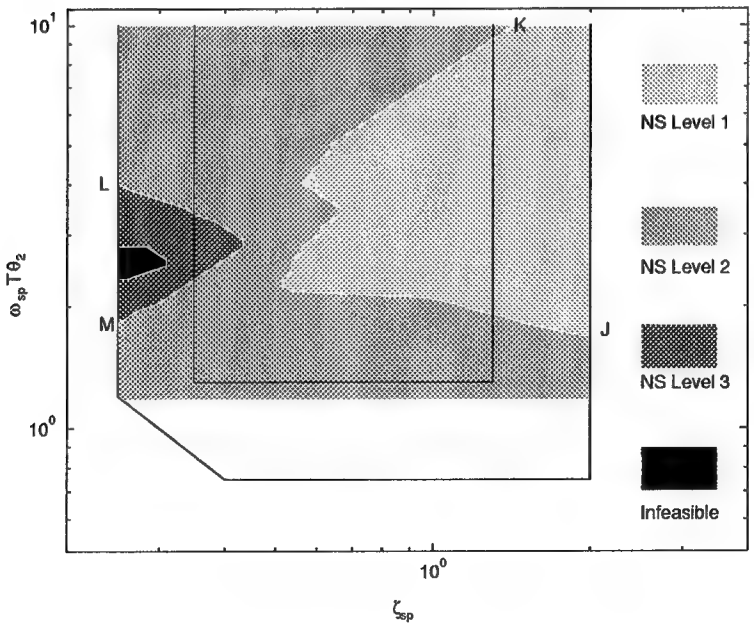

Figure K.4 (Case 11) Neal-Smith Regions Mapped into $\omega_{sp}T_{\theta_2}, \zeta_{sp}, \tau_\theta$

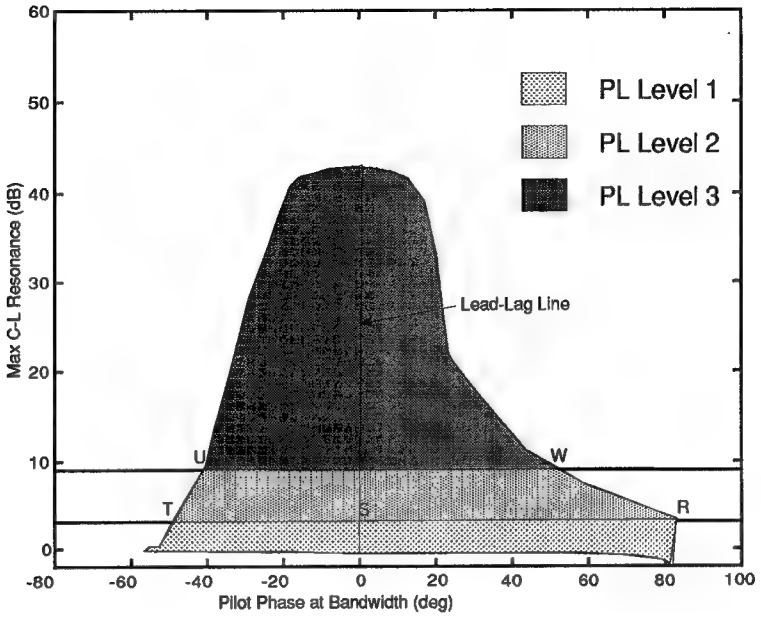

Figure K.5 (Case 11) Pilot-in-the-Loop Regions (PL)

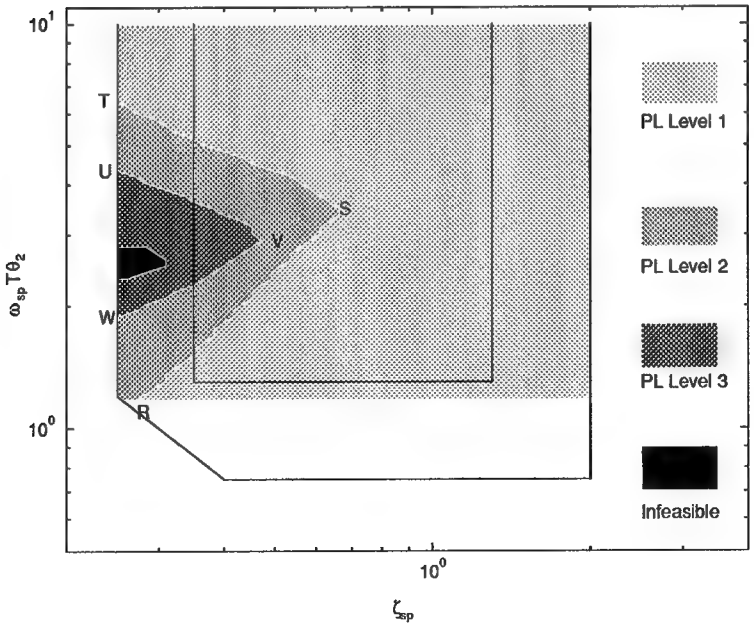

Figure K.6 (Case 11) Pilot-in-the-Loop Mapped into the $\omega_{sp}T_{\theta_2}, \zeta_{sp}, \tau_\theta$

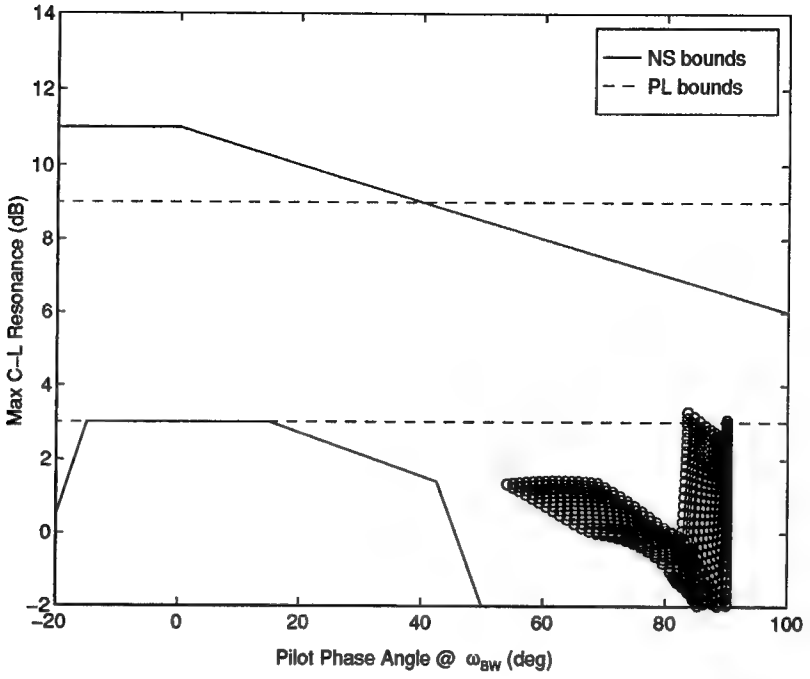

Figure K.7 (Case 11x) Mapping of Excluded Region from $\omega_{sp}T_{\theta_2}, \zeta_{sp}, \tau_\theta$

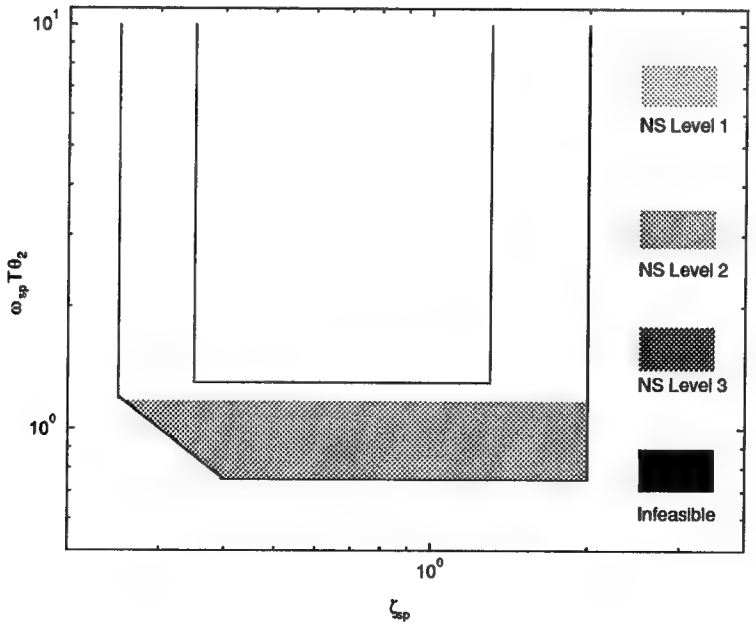

Figure K.8 (Case 11x) Neal-Smith Regions Mapped into $\omega_{sp}T_{\theta_2}, \zeta_{sp}, \tau_\theta$

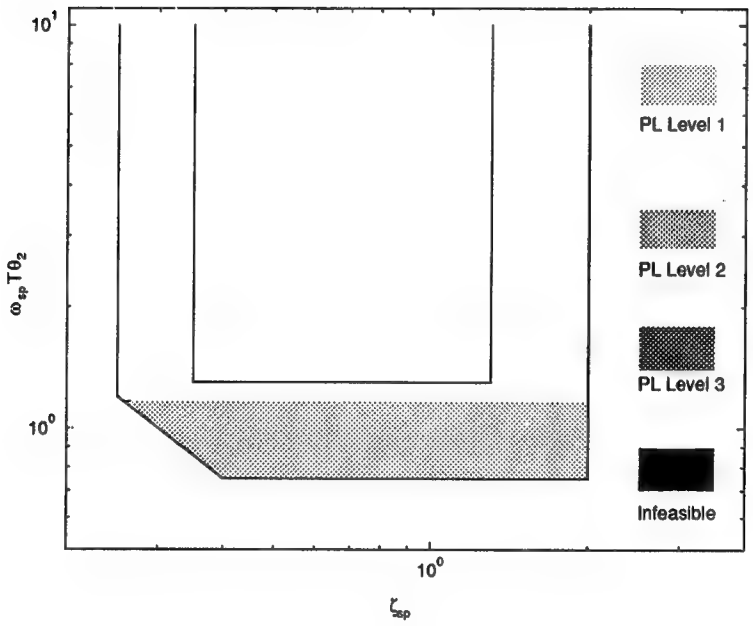

Figure K.9 (Case 11x) Pilot-in-the-Loop Mapped into the $\omega_{sp}T_{\theta_2}, \zeta_{sp}, \tau_\theta$

Appendix L. Case 12

Case	*Level*	ω_{BW}	τ_θ	T_{θ_2}
12	2	2.50	0.20	1.96

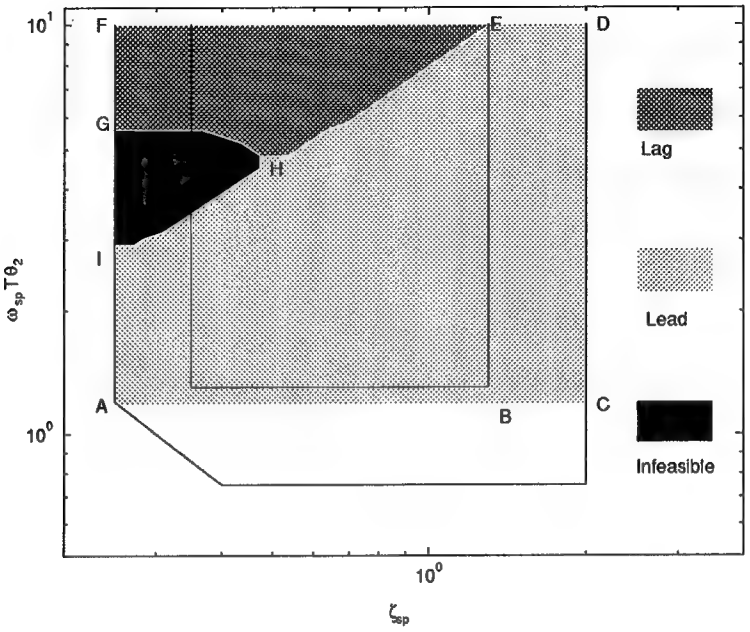

Figure L.1 (Case 12) Lead, Lag, and Infeasible Regions on $\omega_{sp}T_{\theta_2}, \zeta_{sp}, \tau_\theta$

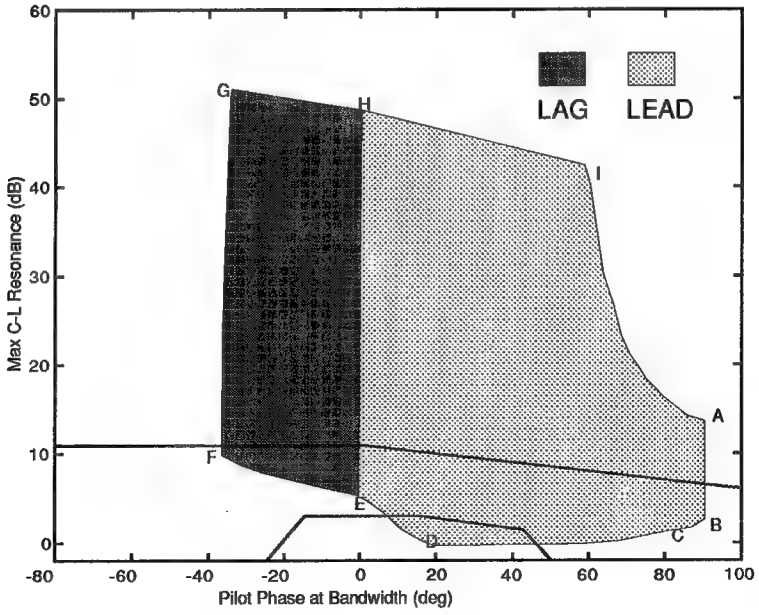

Figure L.2 (Case 12) $\omega_{sp}T_{\theta_2}, \zeta_{sp}, \tau_\theta$ Mapped into Neal-Smith

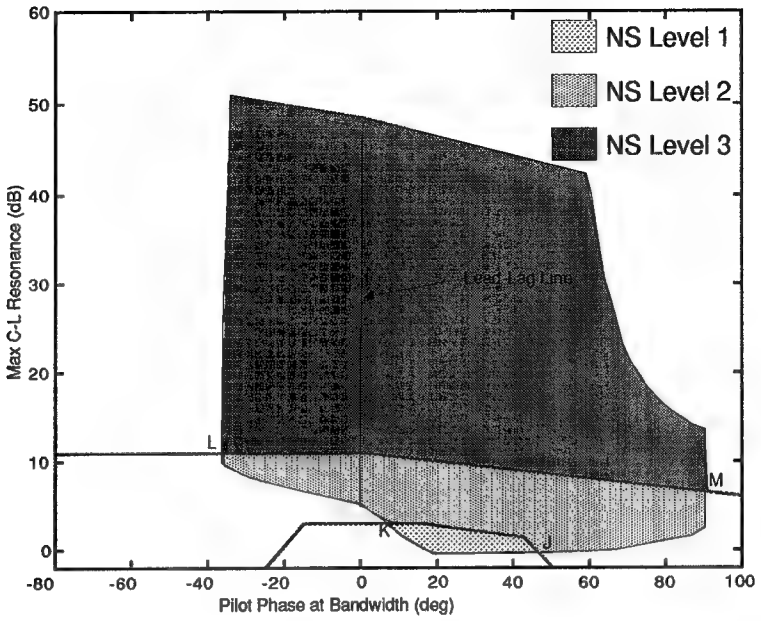

Figure L.3 (Case 12) Neal-Smith Regions (NS)

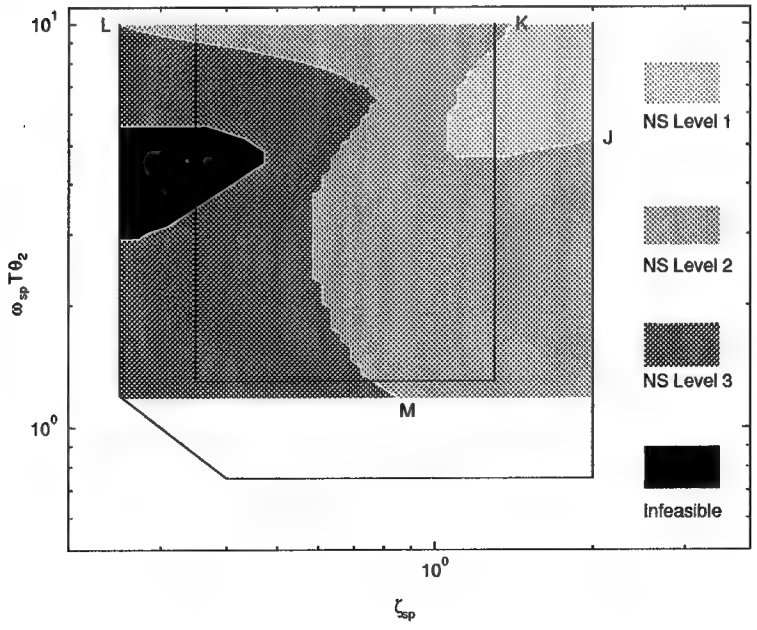

Figure L.4 (Case 12) Neal-Smith Regions Mapped into $\omega_{sp}T_{\theta_2}, \zeta_{sp}, \tau_\theta$

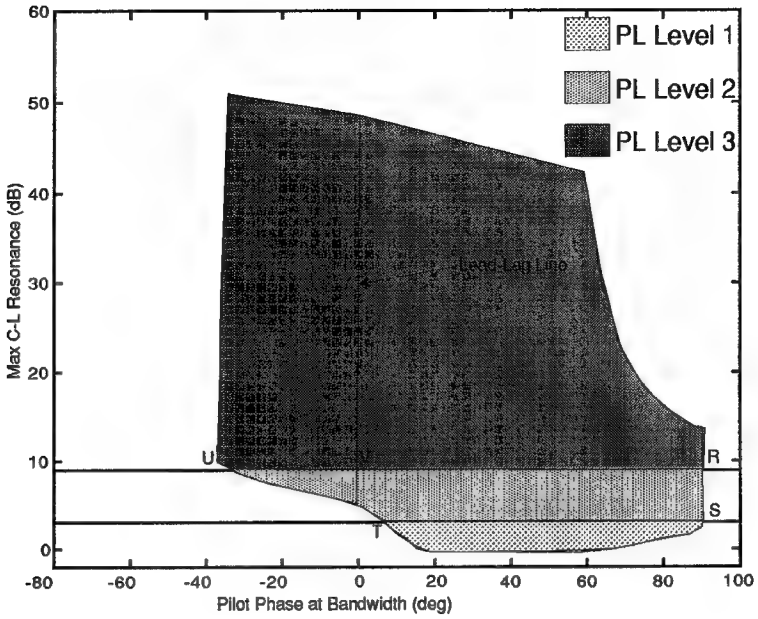

Figure L.5 (Case 12) Pilot-in-the-Loop Regions (PL)

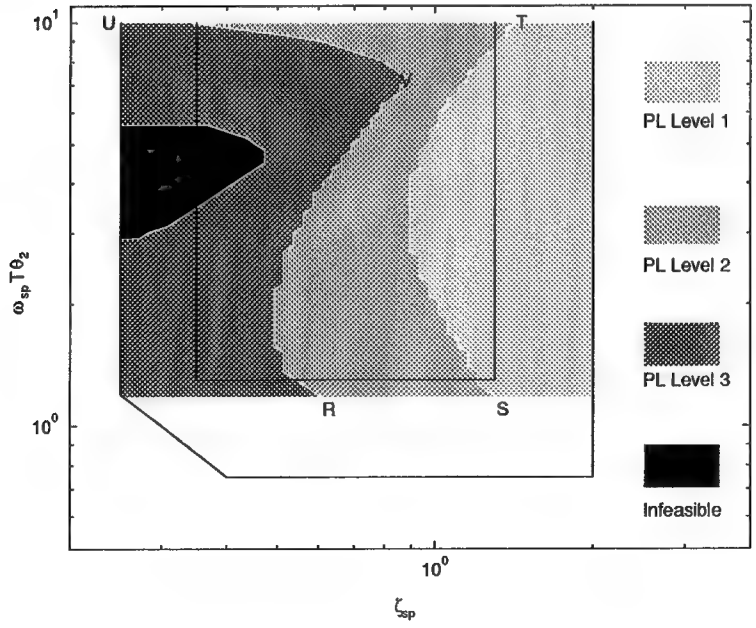

Figure L.6 (Case 12) Pilot-in-the-Loop Mapped into the $\omega_{sp}T_{\theta_2}, \zeta_{sp}, \tau_\theta$

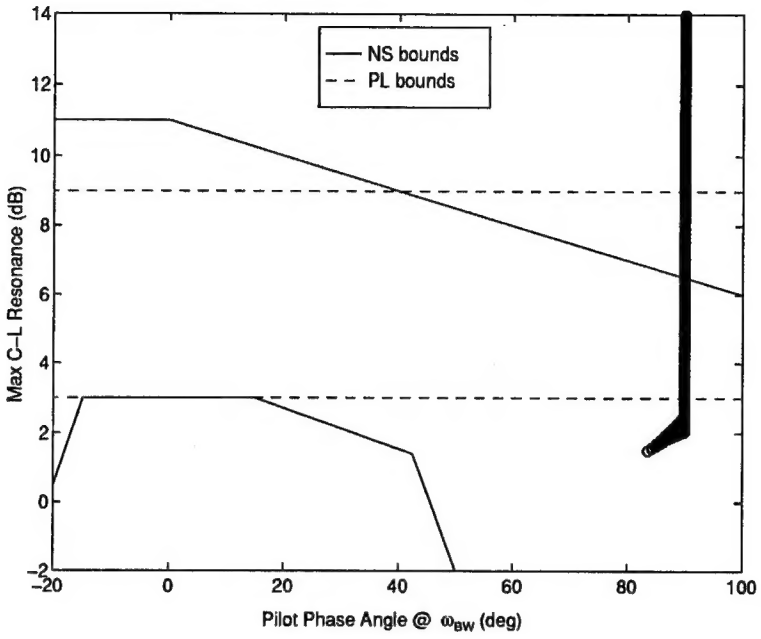

Figure L.7 (Case 12x) Mapping of Excluded Region from $\omega_{sp}T_{\theta_2}, \zeta_{sp}, \tau_\theta$

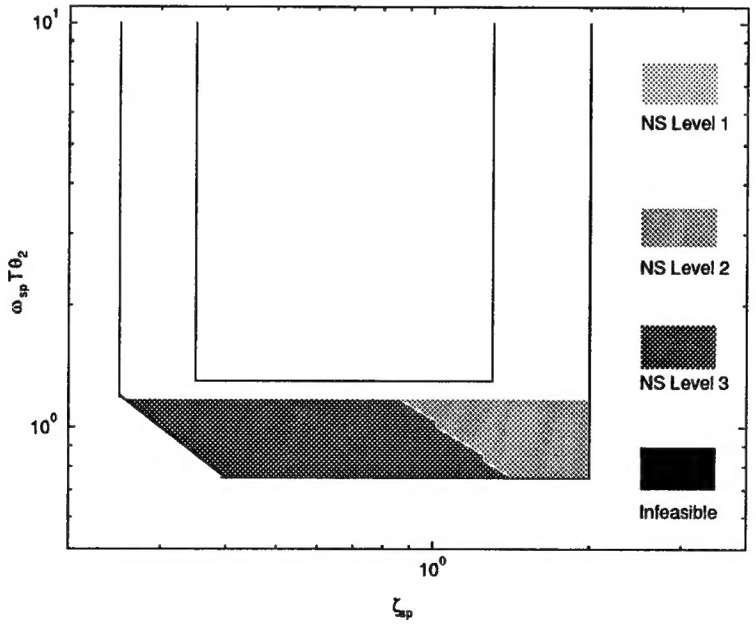

Figure L.8 (Case 12x) Neal-Smith Regions Mapped into $\omega_{sp}T_{\theta_2}, \zeta_{sp}, \tau_\theta$

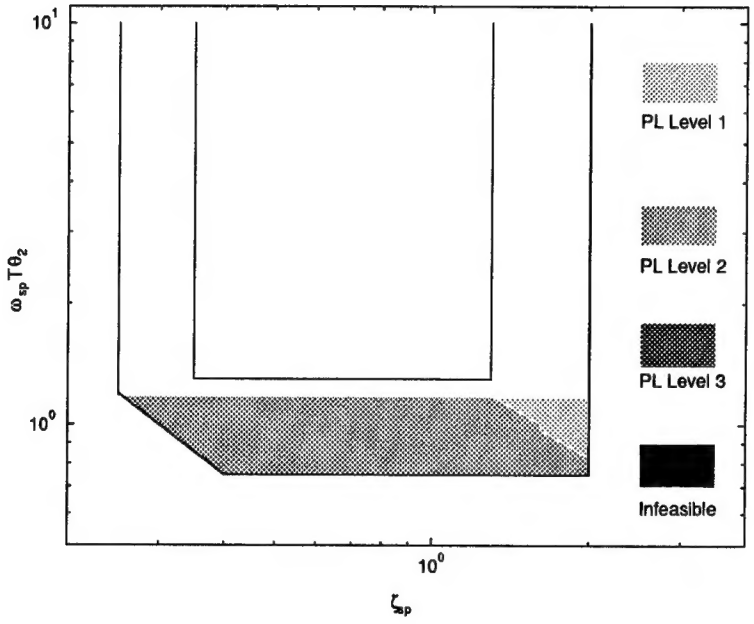

Figure L.9 (Case 12x) Pilot-in-the-Loop Mapped into the $\omega_{sp}T_{\theta_2}, \zeta_{sp}, \tau_\theta$

Bibliography

1. Chalk, Charles R. *Flight Evaluation of Various Short Period Dynamics at Four Drag Configurations for the Landing Approach Task.* Technical Report FDL-TDR-64-60, Wright Patterson AFB, OH: Flight Dynamics Laboratory, October 1964.
2. Cooper, G. E. and R. P. Harper Jr. *The Use of Pilot Rating in the Evaluation of Aircraft Handling Qualities.* Technical Report NASA-TN-D-5153, Washington D.C.: National Aeronautics and Space Administration, April 1969.
3. Department of Defense. *USAF Test Pilot School Flying Qualities Textbook, Volume II, Part 1.* Technical Report USAF-TPS-CUR-86-02. April 1986.
4. Department of Defense. *Flying Qualities of Piloted Aircraft.* Military Standard 1797A. Washington D.C.: Government Printing Office, 30 January 1990.
5. Edkin, B. *Dynamics of Flight.* New York: John Wiley and Sons, Inc., 1959.
6. Edkins, Capt Craig. "Handling Qualities Toolbox, Version 1.3." July 1993.
7. Franklin, Gene F., et al. *Feedback Control of Dynamic Systems, 2nd Edition.* Reading, MA: Addison-Wesley, 1991.
8. Grace, Andrew. *Optimization Toolbox.* Massuchusetts: MathWorks, 1993.
9. Jex, Henry R. and Charles H. Cromwell III. *Theoretical and Experimental Invetsigation of Some New Longitudinal Handling Qualities Parameters.* Technical Report ASD-TR-61-26, Washington D.C.: National Aeronautics and Space Administration, June 1962.
10. Langdon, S. D., et al. *Fixed Wing Stability and Control Theory and Flight Test Techniques.* Technical Report USNTPS-FTM-No. 103, Patuxent River, MD: US Naval Test Pilot School, Naval Air Test Center, January 1975.
11. McRuer, D. T., et al. *A Systems Analysis View of Longitudinal Flying Qualities.* Technical Report WADD TR 60-43, USAF: National Aeronautics and Space Administration, January 1960.
12. Neal, P.T. and Rogers E. Smith. *An In-Flight Investigation to Develop Control System Design Criteria for Fighter Airplanes.* Technical Report AFFDL-TR-70-74, Wright Patterson AFB, OH: Air Force Flight Dynamics Laboratory, December 1970.
13. Performance and Flying Qualities Branch, Flight Test Engineering Division, 6510th Test Wing,Air Force Flight Test Center. *Engineer's Handbook for Aircraft Performance and Flying Qualities Flight Testing.* Technical Report. May 1971.
14. Roskam, Jan. *Airplane Flight Dynamics and Automatic Flight Controls, Part 1.* Ottawa, KS: Roskam Aviation and Engineering Corporation, 1982.
15. Schittowski, K. "NLQPL: A FORTRAN-subroutine Solving Constrained Nonlinear Programming Problems," *Operations Research, 5*(4):485–500 (1985).
16. Vanderplaats, Garret N. *Numerical Optimization Techniques for Engineering Design.* New York: McGraw-Hill, 1984.

17. WL/FIGXF. *VISTA/NF-16D Technical Data for Customer Usage*. Technical Report. August 1991.

18. WRDC/FIGX. *VISTA, The Premier High Performance In-Flight Simulator*. Pamphlet. Wright Patterson AFB, OH.